12-2014

Development of a Forward/Adjoint Hybrid Monte Carlo Absorbed Dose Calculational Method for Use in Radiation Therapy

Mat M. Tamimi

University of Tennessee - Knoxville, mtamimi@vols.utk.edu

To the Graduate Council:

I am submitting herewith a dissertation written by Mat M. Tamimi entitled "Development of a Forward/ Adjoint Hybrid Monte Carlo Absorbed Dose Calculational Method for Use in Radiation Therapy." I have examined the final electronic copy of this dissertation for form and content and recommend that it be accepted in partial fulfillment of the requirements for the degree of Doctor of Philosophy, with a major in Nuclear Engineering.

Ronald E. Pevey, Major Professor

We have read this dissertation and recommend its acceptance:

Laurence F. Miller, Lawrence W. Townsend, Aly Fathy

Accepted for the Council:
Carolyn R. Hodges

Vice Provost and Dean of the Graduate School

(Original signatures are on file with official student records.)

Development of a Forward/Adjoint Hybrid Monte Carlo Absorbed Dose Calculational Method for Use in Radiation Therapy

A Dissertation Presented for the

Doctor of Philosophy

Degree

The University of Tennessee, Knoxville

Mat M. Tamimi

December 2014

DEDICATION

This dissertation is dedicated to

    The two people that brought me to this life, my parents Abdel Jawad and Khawla;

    The anchors of my being, my brothers and sisters Aminah, Imad, Rula, Mobeen and Tasneem;

    The love of my life, my wife Cristina;

    The light in my life, my girls Nancy, Samira and Ayat;

    and the hope for my future my grandchildren, my boys Nabeel and Yasser.

ACKNOWLEDGEMENTS

ABSTRACT

A successful radiation therapy treatment aims at conforming (i.e., concentrating) radiation dose to the entire tumor volume (i.e., diseased area) while avoiding surrounding normal tissue (i.e., healthy non-diseased areas). This objective is achieved clinically by finding a set of radiation beam parameters that successfully deliver the desired dose distribution.

In this project, a hybrid forward/adjoint Monte Carlo based absorbed dose computation method is developed and tested, aimed at eventual implementation in a radiation therapy external beam treatment planning system to predict the absorbed dose produced by a medical linear accelerator. This absorbed dose calculational engine was designed to be:

1. **Efficient.** This is achieved by incorporating several Monte Carlo techniques used in the Nuclear Engineering field for deep penetration and reactor analysis problem.

2. **Flexible.** This is achieved by using a Cartesian grid and a voxelized material map.

Currently most of the absorbed dose calculation algorithms in radiotherapy are 3-D based predictive models. The use of such algorithms results in treatment planning quality that depends tremendously on the planner's experience and knowledge base. This dependence, along with inaccuracy in predicting absorbed dose due to the assumptions and simplifications used in these algorithms, can result in a predicted absorbed dose that under- or over-predicts the delivered dose.

As an alternative, forward and adjoint Monte Carlo absorbed dose computation methods have been used and validated by several authors (Difilippo, 1998; Goldstein & Regev, 1999; Jeraj & Keall, 1999). However, in the "pure" forward or adjoint methods, each change in the radiation beam parameters requires its own time-consuming 3D calculation; for the hybrid technique developed in this research, a single 3D calculation for each desired dose region (tumor or healthy organ) is all that is required.

This project also improves the Monte Carlo methodology by incorporating the use of voxelized fictitious scattering and surface forward/adjoint coupling. The accuracy is demonstrated through comparison with forward and adjoint MCNP calculations of a simple beam/patient sample problem.

TABLE OF CONTENT

LIST OF TABLES

LIST OF FIGURES

LIST OF ABBREVIATIONS

MC	Monte Carlo.
PTV	Planning Target Volume.
OAR	Organs at risk.
CAT Scan	Computed axial tomography.
MRI	Magnetic resonance imaging.
PET	Positron emission tomography.
Linac	Medical linear accelerator.
Gy	Gray – SI unit for absorbed dose = 1 joule / kg
3DCRT	Three dimensional conformal radiation therapy.
MLC	Multi-leaf collimator.
IMRT	Intensity – Modulated radiation therapy.
IGRT	Image-guided radiation therapy.
DVH	Dose Volume Histogram.
TPS	Treatment Planning System.
OBI	On board imaging.
NTCP	Normal tissue complications probability.
TCP	Tumor control probability.
TAR	Tissue air ratio.
rTAR	Ratio of tissue air ratio.
eTAR	Equivalent tissue air ratio.
FFT	Fast Fourier transform.
DSAR	Differential scatter air ratio.
EGS	Electron Gamma Shower
MCNP	Monte Carlo N-Particle.
VMC & VMC++	Voxel Monte Carlo.
ITS	Integrated tiger series.
NIST	National institute of standards and technology.
DPM	Dose Planning method.
ENDF	Evaluated nuclear data formats.

Chapter 1
Background and Introduction

1.1. History of Radiation therapy

The possibilities for therapeutic use of radiation were immediately recognized soon after the discovery of x-rays in 1895 (Dowsett, Kenny, & Johnston, 1998). Clinicians started to use x-rays to treat cancers while researchers investigated different x-ray production and delivery methods. Soon after consequences of radiation misuse were observed, the medical community realized the need to control treatment outcome and the "Radiation Therapy" field was born. Radiation therapy is the branch of medicine that deals with the use of radiation as a method to treat cancer. Due to the large amount of radiation and radiobiology research, a lot of accomplishments in radiation therapy have been realized since that time.

Figure 1-1 summarizes in a pictorial format these historical accomplishments chronologically, beginning with the discovery of x-rays by Wilhelm Conrad Roentgen in 1895 and continuing to the most recent advancements in medical linear accelerator design and imaging methods. The field is constantly advancing and evolving due to the continual need to have better control on treatment outcomes (Hall, 1988).

Radiotherapy is the treatment of cancer by means of ionizing radiation. The purpose of radiotherapy is to eradicate the tumor and spare the surrounding normal tissues as much as possible (Colvett, 2006). To achieve this objective, clinicians need to have both x-ray delivery systems (e.g., medical linear accelerator (Linac)) and absorbed dose prediction systems (e.g., treatment planning systems (TPS)). The Linac should be able to produce several types of radiation (e.g., x-ray or charged particle beams (electrons)) and employ several delivery methods (e.g., static versus dynamic methods). At the same time, the TPS should have the ability to account for the patient anatomy to predict delivered dose with high accuracy (Metcalfe, Kron, & Hoban, 1997).

1895	• Wilhelm Conrad Roentgen discovered X-rays and demonstrated X-ray properties by producing first radiograph.
1896	• Antoine-Henri Becquerel discovered radioactivity.
1897	• Professor Freund demonstrated the first therapeutic use when a hairy mole disappeared after treating it with x-rays.
1901	• Pierre Curie produced radium "burn" on his forearm that took several weeks to heal. Advantages of radiation was realized as a diagnostic tool by making X-ray images and a treatment method to treat cancerous cells.
1913	• W.D. Coolidge produced the first electrically heated cathode tube (140 kV). • GE developed first X-ray tubes with high energy (200 kV). used to treat chronic tumors located in areas such as the lungs, abdomen and pelvis.
WWI	• The development of Radiological Equipment that aided in diagnosing and locating foreign objects in injured soldier's bodies.
1937	• Higher energy X-Ray machines (one MV) was developed that had execellent outcomes when used to treat superficial and shallow cancer. The only pitfall was the excessive skin reactions and poor local control when treating deeply seated tumors.
After WWII	• Cyclotrons and nuclear reactors available and production of synthetic radium started. Clinians used other radioactive elements in cancer treatment.
1951	• Cobalt-60 (1.25 MV) machine produced using synthetic radium . Its popularity was due to its reliability and relatively simple design. Further it provide reasonable skin sparing properties, (maximum dose is achieved at 0.5 cm depth).
1953	• Radar research produced microwave generators Magnetrons and Klystrons. New Linac design offer two photon and five electrons energies, shorter treatment time due to higher dose rate and the sharper dose fall out at the radiation field edges.
1970's &1980's	• Computer advancement led to computerized treatment planning systems, newer imaging technologies such as CAT Scans, MRI and PET, and improved beam shaping devices such as Multi - leaf Collimator (MLC) and tissue compensators.

Figure 1-1 Time line for radiation therapy advancements

1.2. Radiobiology background

It is the aim of radiotherapy to minimize the damage to healthy tissue while administering a killing dose to the tumor. The amount of dose required to achieve a particular level of cell killing is extremely variable because cells have different radiosensitivites (Williams & Thwaites, 2000). The killing of individual cells using radiation is statistical in nature, depending on the occurrence of individual ionizing events. However, when the effect of radiation on a large collection of cells is considered, whether it is a tumor mass or an organ, the effect is largely deterministic; there is a dose threshold below which no clinical effect will be observed and a dose above which the effect will be observed in every individual.

The biological response of a cell to the amount of dose received can be illustrated in dose-response curves, examples of which are given in the Figure 1-2. As delivered dose increases, more cells are destroyed; these curves show that a sigmoidal relationship exists between radiation dose and the probability of achieving tumor control. This principle also applies to normal tissue and cells. As a result, the probability of normal tissue complications (NTCP) and tumor control (TCP) are similar. The relationship between the NTCP and the TCP is known as the therapeutic ratio, also illustrated in Figure 1-2.
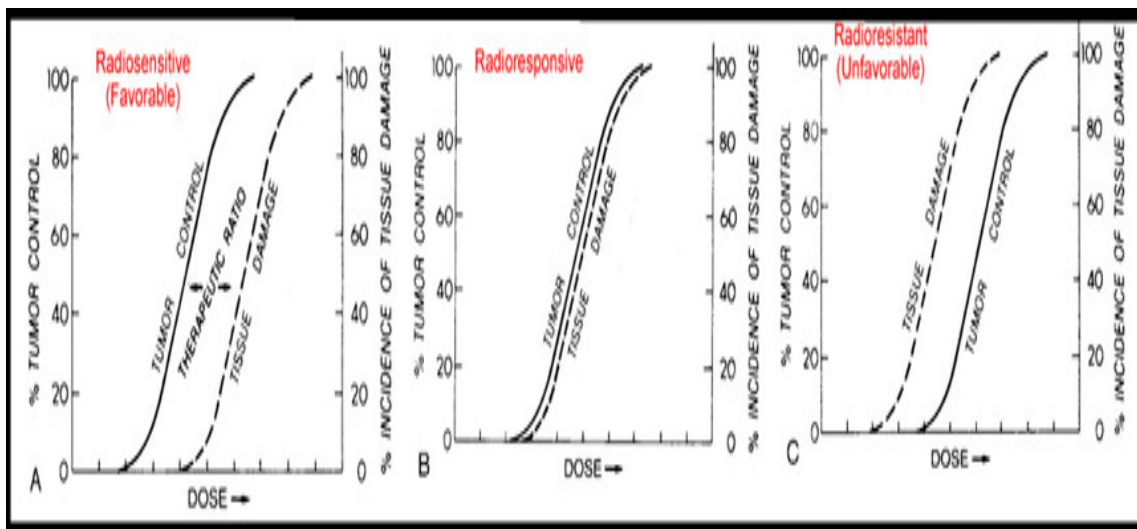
Figure 1-2 Therapeutic ratio concept from cell response curve

The probability of a favorable outcome is good when the TCP curve is to the left of the NTCP curve. An increase in delivery and computation accuracy is required when the TCP and

NTCP curves are very close to each other, requiring very accurate delivery methods. When the TCP curve is to the right of the NTCP curve, combined modality approaches are needed (e.g., chemo-radiation or interstitial/intracavitary implants). The tumors treated successfully by radiotherapy are those in which the tumor curve lies to the left of the curve for the limiting normal tissue. For those types of tumors, the dose required to achieve a high probability of complete regression of the tumor is lower than the dose that produces a significant number of complications in normal tissue. In these situations, treatment plans are desired to assure that the high dose region conforms to the shape of the target volume as much as possible—sparing normal tissue—by applying beams with conformal shapes from several directions (Williams & Thwaites, 2000).

The next few sections will review the evolution of both radiation therapy techniques, treatment planning techniques, and the corresponding absorbed dose prediction methods.

1.3. Radiation therapy treatment techniques

The control of delivered absorbed dose is achieved using radiation therapy techniques, which have evolved over time. Figure 1-3 summarizes this development.

Initial treatment techniques were simple to plan and to deliver due to limitations in first generation medical linear accelerators. With the advancements in computer technology, improved designs and features of the medical linear accelerators led to developments of newer treatment techniques (Thwaites & Tuohy, 2006).

Parallel opposed fields (high doses is delivered to large volumes of normal tissue).

4-field technique (less high dose delivered to normal tissue)

Isocentric rotation (similar to bicycle wheel spokes, dose to normal tissue reduced).

3D conformal (conforming the shape of the beam to the tumor volume which confines the dose almost exclusively to the target).
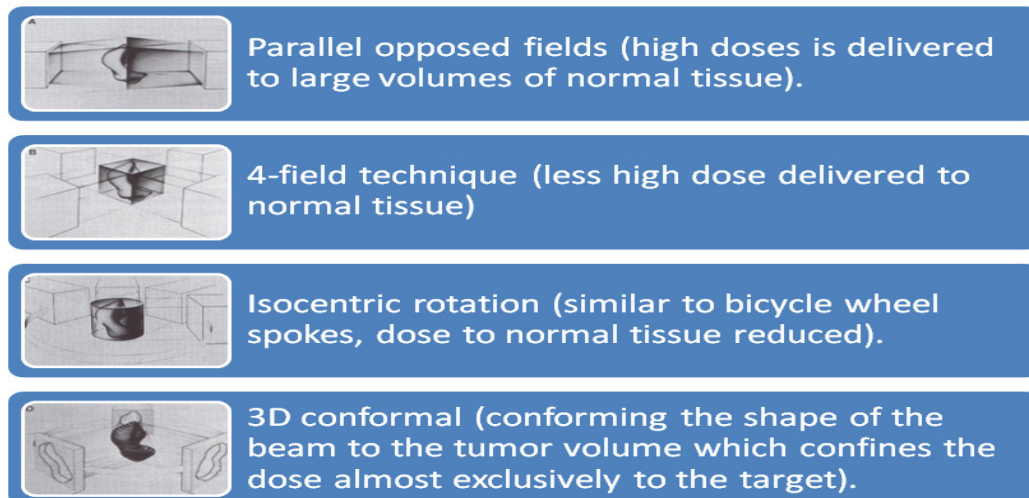
Figure 1-3 Evolution of radiotherapy techniques (Bentel, Nelson, & Noell, 1982)

4

The three-dimensional conformal radiotherapy (3DCRT) was introduced in the early 1980's (Colvett, 2006). Initially this treatment method used shielding blocks made manually from low melting point metal (e.g., Cerrobend). With the most recent advancement in computer-controlled Linacs, manufacturers have developed mechanical blocking systems referred to as multi-leaf collimators (MLCs). These devices replace the need to fabricate shielding blocks and give planners the ability to vary beam intensity and shape across a radiation field; this has given birth to the latest treatment technique, intensity modulated radiation therapy (IMRT). Furthermore, the recent development of digital imaging receptors have led to the introduction of the image guided radiation therapy (IGRT) technique by adding on board imaging (OBI) systems to the accelerators (see Figure 1-4). Clinicians are able to localize tumor position with more precision using this technique, by imaging the patient before the initiation of treatment and by monitoring the treatment progress through imaging during the treatment (Colvett, 2006; Thwaites & Tuohy, 2006).
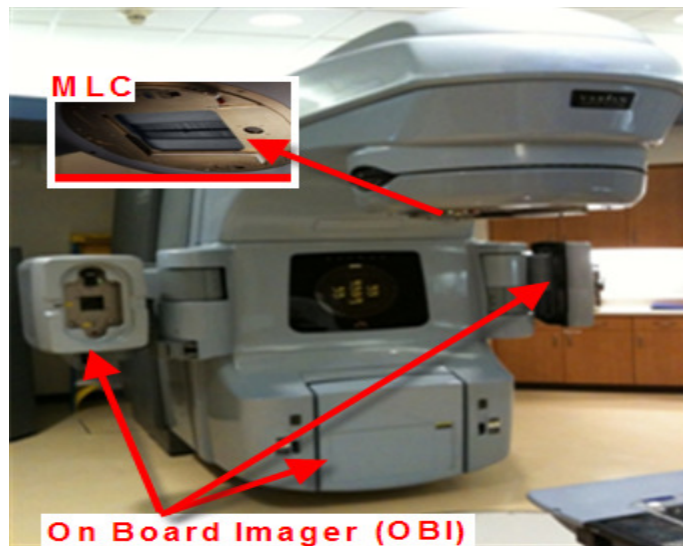
Figure 1-4 Medical linear accelerator equipped with MLC and OBI

1.4. Treatment planning techniques

1.4.1. 3DCRT process versus IMRT process

Using the 3DCRT planning methods requires the planner to compute a dose distribution and evaluate the resulting volumetric dose using a Dose Volume Histogram (DVH) (Armstrong et al., 1993) to see if the treatment objectives are achieved. On the other hand, IMRT uses a

computerized algorithm that searches for the solution and evaluates the results until a suitable solution is found.

The optimization parameters and structure "*penalty weights*" are the primary variables used to control the IMRT search for optimal dose distributions, as opposed to the beam weight or shape optimization in the 3DCRT treatment planning search. Specification of the optimization parameters and beam placement requires detailed knowledge of the dose calculation algorithms and anatomical features of the patient, such as the proximity of the normal tissue to the target.

As a result, the combination of beams, optimization parameters, and beam shaping structures needed to achieve the best plan are planning system and patient specific. Planners must develop an intuition as to how these factors affect distributions, so the plan can be optimized.

1.4.2. Manual optimization

The processes of creating IMRT or 3DCRT treatment plans are quite similar, but the bases of the plan designs are significantly different. The conventional 3DCRT treatment planning is forward based and optimization is done manually.

The process starts when the treatment planner chooses initial beam parameters (i.e., number of beams, beam energy, weighting, direction, and beam modifying devices such as blocks and wedges). The computer then calculates the resulting dose distribution, which is evaluated by the planner. At this point, the planner can chose to accept or reject the plan based on the physician's defined criterion. If the distribution is not satisfactory, the planner designs another plan by adjusting the various beam parameters. The new dose distribution is computed and evaluated and the process is repeated until the planner arrives at a satisfactory absorbed dose distribution. Therefore in conventional 3DCRT treatment planning the planner arrives at the optimized dose distribution without having to explicitly define the optimum or desired dose distribution.

1.4.3. Computer-aided optimization

Researchers have attempted to improve on the tedious trial and error nature of the manual process by automating it using computer-driven parameter optimization.

1.4.3.1. <u>3DCRT process planning</u>

In one early method the "*beam's eye view*" was used for accurate delineation of treatment volumes to avoid real or dosimetric geographic misses. This was especially useful for oblique fields because it "facilitated the design of accurate customized blocking and avoided inadvertent blocking of the tumor or unnecessary irradiation of normal tissues" (Vijayakumar et al., 1991). Another method proposed by Soderstrom and Brahme used two different measures for the selection of advantageous beam directions: "lowest entropy" and "low frequency part of the Fourier transform" of the optimal beam profiles (Soderstrom & Brahme, 1992). Langer and Leong described a method for "formulating and solving this optimization problem as a combinatorial linear program" (Langer & Leong, 1987).

A method by Mageras and Mohan utilizes the simulated annealing approach to optimize radiation treatment plans; in this method, a set of beam weights are iteratively adjusted so as to minimize a cost function. This method was motivated by its potential for finding the global or near-global minimum among multiple minima. This method was found to be slow, requiring several tens of thousands of iterations to optimize 50 to 100 variables." (Mageras & Mohan, 1993)

1.4.3.2. <u>IMRT process planning</u>

Treatment goals are best achieved using IMRT. The IMRT process is made of three integral parts—an inverse treatment planning process, plan delivery design (static or dynamic delivery), and quality assurance of the produced plans.

In the inverse planning step, the planner aims at finding the radiation beam parameters that will produce the desired absorbed dose distribution, as shown in Figure 1-5. The IMRT planner accomplishes this task by searching iteratively for a set of beam parameters for an optimal fluence that will deliver the desired dose distribution. First, the planner evaluates and stops the optimization when the optimized plan produces dose distribution that meets criterion defined at the start of optimization. Second, the accepted optimal dose distribution is converted to a machine deliverable treatment plan by producing a multi leaf collimator (MLC) motion sequence that will produce this dose distribution. Lastly, the treatment plan is verified to assure that the produced leaf motion sequence will produce the optimal calculated dose distribution in the patient.
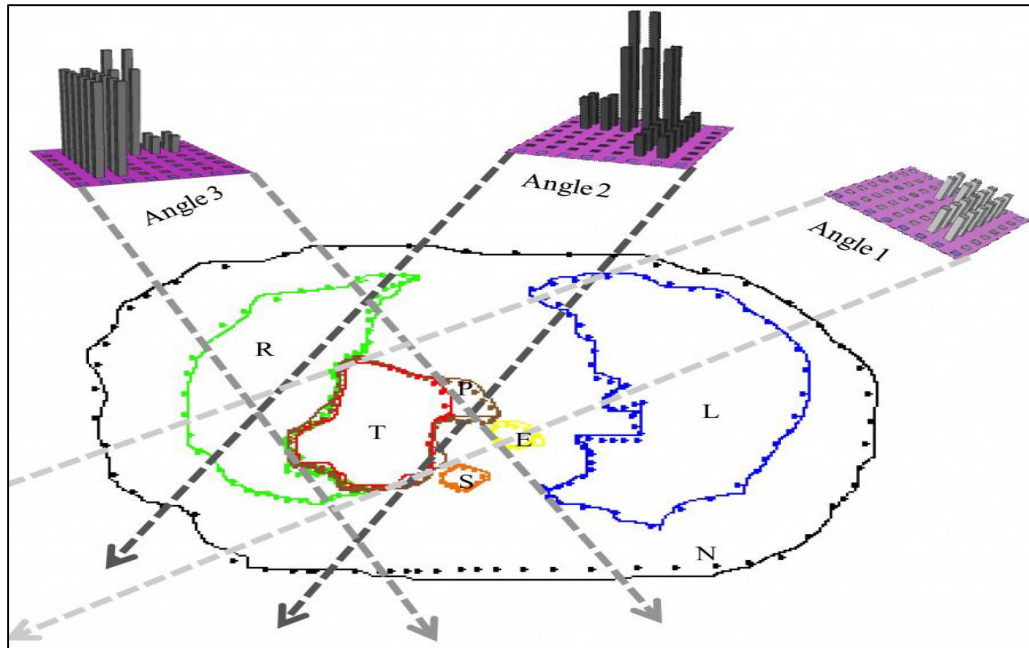
Figure 1-5 IMRT solution for tumor dose

During the IMRT optimization process, the planner defines the desired absorbed doses for the following structure volumes as described in ICRU reports 29, 50 & 71 (Morgan-Fletcher, 2001; Units & Measurements, 1978):

1. **CTV** (clinical target volume). This normally is the gross tumor volume and subclinical extensions.

2. **PTV** (planning target volume). This is the **CTV** plus added margins to account for variations in tissue positions, sizes, and shapes, as well as for variations in patient position and beam geometries, both intrafractionally (i.e., during the treatment) and interfractionally (from one treatment to another).

3. **OAR** (organs at risk). Radiosensitive normal tissues, whose radiation sensitivity may significantly affect treatment planning (i.e., spinal cord, heart, parotids, etc.). Dose-volume (DVH) constraints are determined by the planner through the definition of maximum allowable doses for these organs, along with a set of penalty weights to indicate the relative importance of the organ.

1.5. Treatment plan delivery design

Once an IMRT plan is designed, it can be delivered via several methods:

1. Physical compensators (Purdy, 1997). These are used to modify the dose distribution to conform to irregular target shapes due to missing tissue or irregular patient contours; the fabrication is time consuming and their use is cumbersome. A picture of an actual compensator is shown in Figure 1-6.
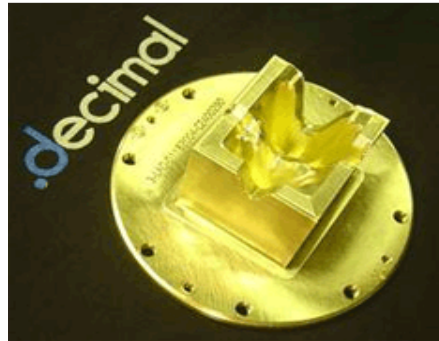
Figure 1-6 IMRT Physical compensator delivery solution

2. Computer-controlled slit and multi-leaf collimators (MLCs) (Carol, 1994) sequences as shown in Figure 1-7.
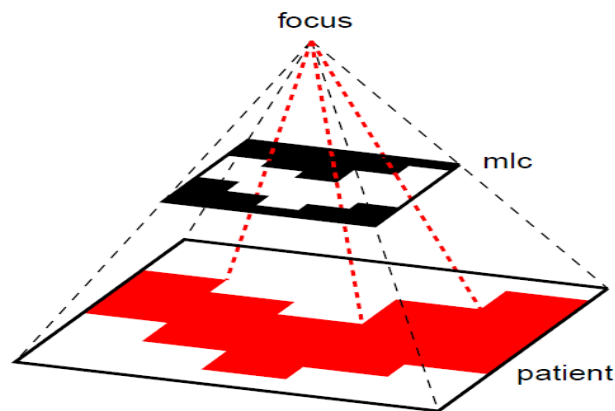
Figure 1-7 IMRT MLC delivery solution

These have made the delivery of intensity-modulated fields more practical by allowing delivery of the IMRT plan using either multiple static fields or one dynamic field with dynamic multi-leaf collimator (DMLC) as described in (Spirou & Chui, 1994). The static method is commonly referred to as "Step-and-Shoot" method while the dynamic method is referred to as the "Sliding window" method. Each delivery method has its advantages and limitations. In the literature there exist some studies comparing delivery methods (Chui, Chan, Yorke, Spirou, &

Ling, 2001), but there are really no available data that permit a true head-to-head comparison between the currently available various IMRT delivery techniques.

1.6. Absorbed dose calculation techniques

Accurate knowledge of delivered absorbed dose is critical for predicting the clinical outcomes of the prescribed radiation treatments. This goal dictates dose assessment tools that are able to predict delivered dose with high precision and accuracy.

1.6.1. Evolution of absorbed dose calculations techniques

In the early algorithms, absorbed dose in the patient was estimated using simplifications such as assuming that the patient was totally composed of water, ignoring all internal organs and only using the external patient contour (Nikos Papanikolaou et al., 2004). These simplifications introduced errors when computing the final absorbed dose distribution, due to the fact that absorbed dose distributions are highly dependent on the differing material densities and atomic compositions in the human body.

Advances in imaging led to the development of CT-based dose corrections methods. A full map of the patient's internal anatomy can be constructed from electron density map generated by CT's (Nath et al., 1994). This electron density map is converted into a material map through a conversion process allowing planners to predict dose distribution that is close to the actual dose distribution for the internal anatomy (Sontag & Cunningham, 1978). The initial calculational methods employing CTs were one dimensional correction methods while the most recent methods are three dimensional and aim at achieving better absorbed dose prediction accuracy (Nikos Papanikolaou et al., 2004). Table 1-1 summarizes these calculation methods.

Table 1-1 Absorbed dose calculations method that uses CT data

Absorbed dose calculation methods that uses CT data	
1-D	1. Ratio of tissue Air Ratio factors (rTAR)
2-D	1. Equivalent Tissue Air Ratio factors (eTAR). 2. Fast Fourier Transform method (FFT).
3-D	1. Differential scatter air ratio (DSAR). 2. Delta volume. 3. Dose spread array. 4. Differential pencil beam.

These advances led to the development of the convolution superposition techniques. The convolution superposition techniques are predictive models that simulate particle transport and energy deposition in human tissues. The models use a database of deposition kernels calculated using Monte Carlo techniques and mathematical expression to predict the absorbed dose distribution. Some of the most common algorithms that use the superposition convolution techniques are the Point Kernel model (Pencil Beam algorithm), the direct summation method, and the collapsed cone method (Ahnesjö, 1999 #92, Papanikolaou, 2004 #68). The difference between these models is the way they deal with the changes in the primary fluence and changes in the spread of deposited energy when computing absorbed dose distributions.

In general, treatment planning systems algorithms are divided into two major types:

1. **Lookup-based algorithms.** These algorithms provide point doses estimates in patients based on conversion factors of the doses derived from a look-up table.
2. **Model-based algorithms.** The collected clinical data are fitted into mathematical physical models, which are used to predict the dose distribution in the entire volume in question based on a superposition convolution dose algorithm.

1.6.2. Shortcomings of the predictive methods

Existing clinical practice favors model-based algorithms because they offer fast computation speed. In general, there are two methods to calculate absorbed dose: simplified and detailed. The simplified method is called the analytical (deterministic) method, which calculates absorbed dose based on several assumptions (e.g., ignoring patient internal anatomy and assuming the patient is homogenous medium). The detailed methods are Monte Carlo simulations of the actual physical phenomenon, with the computed absorbed dose based on simulated particles transported in a geometrically accurate model of a phantom or patient (Metcalfe et al., 1997).

When computing absorbed dose using a predictive model, dose from primary photons is explicitly calculated and simplifications (e.g., tissue heterogeneities) are applied to compute the dose deposited by scattered radiation. This approach is not desirable because it leads to under- or over-estimating of the predicted absorbed dose; its accuracy needs to be increased in order for us to be able to use these algorithms clinically. Currently, this is accomplished by collecting an extensive set of beam data for every possible beam combination. As a result, an accurate beam

model is created and used in the treatment planning system to compute absorbed dose (Nikos Papanikolaou & Klein, 2008).

1.7. Monte Carlo: The best dose calculation method

The Monte Carlo simulation methods are very accurate and are considered to be the gold standard for dose calculation (Rogers, 2006) in medical physics, since accurate knowledge of the delivered absorbed dose is crucial in predicting the clinical outcomes of the prescribed treatments. Currently, any deterministic method developed is benchmarked against Monte Carlo simulations.

The primary pitfalls of the direct use of Monte Carlo in treatment planning are the large amount of computer time and data storage required and the extreme effort needed to validate the results. The best solution is to improve the efficiency of Monte Carlo through improved methodology development, as represented by this project.

Chapter 2
Monte Carlo method background

2.1. Monte Carlo history

Use of Monte Carlo (MC) methods has increased in radiation therapy planning in recent years due to the large gains in computer power per unit cost and the availability of many powerful software tools. The Monte Carlo methods use statistical sampling for performing numerical integrations and system simulations. The MC method in its form today was first developed and named at the end of the Second World War. The main motivation behind developing MC techniques was radiation transport for nuclear weapons design; Stanislaw Ulam and John von Neumann saw an opportunity to develop this new statistical sampling application because of the availability of ENIAC, the first electronic computer (Chetty et al., 2007).

The development of MC techniques has continued to parallel the exponential increase in the power of digital computers, as they became widely available to universities, research laboratories, and other large institutions in the 1950s and 1960s (Chetty et al., 2007). The attention in the medical physics field was directed to Monte Carlo methods as the need for better and more accurate dose calculation algorithms increased.

2.2. Monte Carlo as a radiation transport tool and absorbed dose calculator

Monte Carlo methods simulate radiation particle histories as random walks. In its simplest form, each simulated particle is followed from its inception until its death, with decisions at each particle event made based on basic physics laws to mimic actual radiation interactions in media; the resulting measurable outcomes (e.g., dose in desired regions) are collected from the sampled histories and statistically analyzed to estimate the expected outcomes from real particles.

This technique for calculating dose in patients is favored due to the simplicity of the underlying physical basis when compared to the analytic (deterministic) algorithms. In addition, this method only requires knowledge of the relative probability and outcomes of various physical interactions that have been understood since the mid-20th century; even though the interactions may be complex to simulate in detail, the basic ideas of each interaction are well understood. Hence, the overall process is easy to comprehend and implement in a computer code. Furthermore, dose computation is straight forward and can be performed during the simulation

13

without complex approximations or models of dose deposition. This manner of computing doses from first principles makes it superior to conventional dose calculation methods.

2.3. Modes of Monte Carlo radiation transport

We can simulate a radiation particle's random walk using Monte Carlo methods from an actual source to all regions of interest in a patient and then compute the expected dose to these regions. This mode of calculation is referred to as the <u>forward</u> mode. Alternatively, we can think of radiation particles starting in a region of interest and traveling backwards in time and space towards a source. This mode of transport is referred to as the <u>adjoint</u> mode. Or, finally, we can devise a hybrid mixture of the forward and adjoint calculations which combines the advantages of each. The following subsections provide a brief description of each of these approaches.

2.3.1. Forward Monte Carlo radiation transport

In forward Monte Carlo radiation transport, photons interactions with matter are described by the forward Boltzmann transport equation (Bell & Glasstone, 1970). The transport process starts with the initial position, direction, and energy determined from the particular statistical distributions characterizing the photon beam source. The photons undergo interactions, such as photoelectric effect, Compton scattering and pair production, as they travel through the system. By keeping track of interaction rates in regions of interest, we can estimate average fluxes in those regions. Other flux-based quantities can be estimated by multiplying flux contributions by pre-calculated conversion factors (e.g., for absorbed dose, a flux-to dose response function (ANSI/ANS-6.1.1, 1977)). In the field of medical physics, forward Monte Carlo radiation transport is used to compute the dose rate in all voxels inside a region of interest, for a given set of source parameters and these voxel dose rates are converted into an expected average dose in the region. This dose rate is usually normalized to the dose delivered per source particle. For this project the Voxel8 computer code was developed to solve the forward problem; its detailed algorithm and description is presented in Chapter 5.

It is often stated in the medical physics literature that the forward Monte Carlo dose calculations are too time consuming for regular clinical use. The primary reason for this is that separate long-running forward Monte Carlo calculations through the 3D patient geometry are

required for each of the many sets of radiation parameters considered by the planner; this makes each step of the planning process take an inordinate amount of time to evaluate.

2.3.2. Adjoint Monte Carlo radiation transport

The adjoint transport equation (Bell & Glasstone, 1970) describes the transport of adjoint photons emerging from a region of interest and travelling toward the source. The adjoint photons are transported in a fashion similar to the forward photons, with the following exceptions:

- Instead of starting in the source beam (with initial position, direction, and space chosen according to the characteristic beam distributions), the adjoint particles start in the region of interest (particular to a calculation) uniformly, isotropic in direction, and with an energy distribution corresponding to the groupwise flux-to-dose conversion factors.

- Instead of starting with a particle weight that is the sum of the groupwise sources (i.e., total source strength), the adjoint particles begin with a weight equal to the sum of the groupwise flux-to-dose conversion factors.

- When a scattering event occurs, the group-to-group scattering matrix is inverted (i.e., adjointed) so that particles scatter from the original group to a final group according to the physical cross section appropriate to scattering the other way. For example, the normal scattering cross section from group 1 to group 3 is used to find the probability of scattering from group 3 to group 1.

- To properly normalize the previous energy group reversal, the traditional "absorption weighting" multiplicative weight correction of:

$$\frac{\sum_{g'=1}^{G} \Sigma_s^{g \to g'}}{\Sigma_{tg}} = \frac{\Sigma_{sg}}{\Sigma_{tg}}$$

used in the forward mode after each scatter is replaced in adjoint calculations with:

$$\frac{\sum_{g'=1}^{G} \Sigma_s^{g' \to g}}{\Sigma_{tg}}$$

(With the superscripts reversed like this, there is no physical interpretation of the numerator.)

The calculated adjoint flux at a particular point, direction, and energy can be interpreted as the expected contribution of an emerging photon with those parameters to the dose at the ROI used as the adjoint source. As a result, the total dose to the ROI can be calculated rapidly by multiplying the source (as a function of space, energy, and direction) times the adjoint flux and integrating over all independent variables (convolution of the external source function with the adjoint flux). Therefore, for a known and unchanging set of source parameters, a single adjoint calculation for each region of interest could be calculated; specifically for each unique patient geometry. For this project the Pixel8 computer code was developed to solve the adjoint problem; its detailed algorithm and description is presented in Chapter 5.

2.3.3. Hybrid forward/adjoint Monte Carlo radiation transport

Direct use of the adjoint method would require that the calculation geometry include the location of the source point, which for our application is outside the patient. Therefore, efficiencies can be gained by performing an adjoint calculation from the region of interest to the patient surface, a forward calculation from the source to the patient surface, and combining the results.

The hybrid forward/adjoint Monte Carlo transport method restricts the adjoint calculation to the patient geometry and computes the surface adjoint flux by particle type, location, direction and energy. The resulting surface fluxes serve as surface sensitivity functions, equal to the dose contribution that would occur to the region of interest (i.e., region that served as the adjoint source) of a forward particle impinging on the surface at the indicated surface position, direction, and energy group.

The advantage of this hybrid approach is that the long-running adjoint calculation is independent of the source beam parameters, so can be precalculated for the patient's regions of interest as a preliminary step of the treatment planning process. Then, each source beam arrangement that the planner wants to consider can be evaluated very quickly with a fast-running forward transport of the beam to the patient surface - often ignoring air attenuation - using the

precalculated adjoint surface fluxes as multiplicative flux-to-dose conversions factors to determine the contribution to the dose in the region of interest.

The basic approach was first developed for general radiation shielding analysis in the "Monte Carlo Adjoint Shield" (MASH) code system at the University of Tennessee (in collaboration with the Oak Ridge National Laboratory) as part of J.O. Johnson's PhD dissertation (Johnson, 1992). MASH performs the forward phase of the calculation with a discrete ordinates code that "determines the fluence on a coupling surface surrounding the shielding geometry due to an external neutron/gamma-ray source. The Monte Carlo [adjoint] calculation determines the effectiveness of the fluence at that surface in causing a response in a detector within the shielding geometry, i.e., the "***dose importance***" of the coupling surface fluence. A coupling code folds the fluence together with the dose importance, giving the desired dose response. The coupling code can determine the dose response as a function of the shielding geometry orientation relative to the source, distance from the source, and energy response of the detector." (Johnson, Emmett, Rhoades, & Childs, 1992).

2.4. Fictitious scattering (Woodcock hole tracking) concept

Besides the use of the hybrid forward/adjoint MASH-like surface coupling, this project also incorporates an improved particle tracking algorithm in the Monte Carlo calculations. This is an improvement over traditional tracking approaches. For both forward and adjoint Monte Carlo traditional tracking algorithms, the computational performance of the simulation is poor for heterogeneous voxelized phantoms because the particle mean free path lengths (i.e., the average distance travelled between collisions) vary between regions forcing the particle tracking algorithm to spend time locating intersections of the particle track with region boundaries. We can reduce the computer time spent on particle tracking for photons in a voxelized phantom by using ***fictitious interaction*** *tracking* (also known as Woodcock tracking). *Fictitious interaction tracking* is a sampling technique useful when the transported particles have a relatively large mean free path length in comparison to the dimensions of the problem geometry (Brown & Martin, 2003). This technique is also called *Woodcock tracking* (Carter, Cashwell, & Taylor, 1972; Cramer, 1977; Kawrakow & Fippel, 2000; Woodcock, Murphy, Hemmings, & Longworth, 1965) or *delta scattering* (Ljungberg, Larsson, & Johansson, 2005; Tenney, Bowsher, &

Jaszczak, 2004). This sampling technique is expected to lead to more efficient means of transporting beam photons through a voxelized phantom (in both forward and adjoint modes).

2.4.1. Why fictitious scattering works

In a heterogeneous medium the mean free path is not constant. As a result boundary tracking is necessary and it will consume a lot of computer time. Reduction in computer time can be achieved using the fictitious scattering tracking method. The fictitious scattering method make the mean free path within a multi material region constant eliminating the boundary tracking step from the calculation. Fictitious scattering is implemented by using the problem largest total linear attenuation cross section Σ_{Tmax} when transporting the particles between interaction sites. This is equivalent to adding extra linear attenuation cross section artificially to the actual total linear attenuation cross section for all region materials. For a problem with several materials the maximum total linear attenuation cross section is given by:

$$\Sigma_{Tmax} = Max(\Sigma_{T1}, \Sigma_{T2}, \Sigma_{T3}, \cdots, \Sigma_{Tn}) \, or$$

$$\Sigma_{Tmax} = \Sigma_{T1} + \Sigma_{T1`} = \Sigma_{T2} + \Sigma_{T2`} = \Sigma_{T3} + \Sigma_{T3`} = \cdots = \Sigma_{Tn} + \Sigma_{Tn`}$$

In the formula above $\Sigma_{T1`}, \Sigma_{T2`}, \Sigma_{T3`}, \cdots, \Sigma_{Tn`}$ are artificial cross-sections added to achieve the constant linear attenuation cross section. As a result the total number of particle collisions is increased but the distribution of real particle collisions remains unchanged.

Define $I(x)$ as the intensity of particles at a point x along an axis, and Σ_{Ti} is the total attenuation cross section of region. The amount of particles removed due to collisions in dx from the beam is:

$$\# \, particles \, removed \, due \, to \, real \, collisions = \, I(x)\{\Sigma_{Ti}dx\}.$$

The particles intensity after traversing dx along the axis is:

$$I(x + dx) = I(x) - \, I(x)\{\Sigma_{Ti}dx\} = \, I(x)(1 - \, \Sigma_{Ti}dx)$$

Using the maximum total attenuation cross section of the problem fictitious cross section is:

$$\Sigma_{Fictitious} \, = (\Sigma_{Tmax} - \Sigma_{Ti})$$

The amount of particles removed fictitiously at same location is:

$$\# \, particles \, removed \, due \, to \, fictitious \, collisions = \, I(x)\{(\Sigma_{Tmax} - \Sigma_{Ti})dx\}$$

Then the accurate particles intensity after traversing dx along the axis is using the maximum total attenuation cross section of the problem is:

$$I(x + dx) = I(x) - I(x)\{\Sigma_{Tmax}dx\} + I(x)\{(\Sigma_{Tmax} - \Sigma_{Ti})dx\}$$

$$I(x + dx) = I(x)[1 - \Sigma_{Tmax}dx + \Sigma_{Tmax}dx - \Sigma_{Ti}dx]$$

$$I(x + dx) = I(x)[1 - \Sigma_{Ti}dx]$$

We can also derive the first equation from the above equation. Therefore, both equations are equivalent and hence the distribution of real collisions is conserved.

Chapter 3
Project objective

Due to the increased use of Monte Carlo methods in medical physics as an absorbed dose evaluator, this research aims at building software to aid in more efficient planning of cancer patient treatments. Because the traditional use of the Monte Carlo method is too slow for clinical use, our objective is to demonstrate the viability of a hybrid forward/adjoint Monte Carlo technique for faster absorbed dose computations.

Our objective was to build a set of Monte Carlo codes capable of calculating forward and adjoint Monte Carlo problems and to adapt them to hybrid forward/adjoint use; this will aid in the design of optimized patient treatment plans. For validation, we set out to demonstrate that the forward and hybrid approach yields the same results (within statistical error).

For increased efficiency, this objective was accomplished by implementing several Monte Carlo techniques that have been shown useful in deep penetration and reactor analysis, but have not yet been applied to radiation therapy. These techniques are:

1. Replacing the conventional ray tracing method used to track adjoint particles with the "Fictitious Scattering" (commonly known as "Woodcock Tracking") method on a dedicated regular Cartesian grid. This has been shown to be effective for problem geometries with material cells smaller than particle mean free paths, which should make it an efficient technique to use with spatial geometries described by CT-image-based Cartesian voxels.

2. Implementing the hybrid forward/adjoint capability by interfacing the external conical beam source with a calculated adjoint surface sensitivity through an integration procedure to predict absorbed dose in specified internal structures. The adjoint method, commonly used in the reactor physics and radiation shielding design, are used to produce the surface adjoint fluxes (which serve as flux-to-dose response functions for the region of interest used as the adjoint source.

In order to harvest the usefulness of the adjoint method for a specific geometry (patient) we will:

1. Calculate (starting from the tumor volume) an adjoint flux $\varphi^*_{Tumor}(r, \Omega, E)$ on each external surface of the patient body (or a box containing the patient body) as a function of surface, pixel, direction and energy.

2. Similarly calculate the adjoint flux $\varphi^*_{OAR}(r, \Omega, E)$ on each external surface for each other region of interest (e.g., organ at risk).

3. Fold the computed adjoint fluxes $\varphi^*_{Tumor}(r, \Omega, E)$ and $\varphi^*_{OAR}(r, \Omega, E)$ with the result of a forward transport of source particles to each visible patient surface to compute an estimate of the delivered absorbed dose to the regions of interest.

This will represent the first time that either of these techniques have been used in a medical physics application. Our objective is to demonstrate the viability of the approach and prepare the way for future optimization and application in the field.

Chapter 4

Methodology used in the Project

In this chapter, descriptions and derivations will be provided for the techniques that we use in this project:

1. A general derivation of the multigroup Boltzmann equation with a description of Monte Carlo algorithms used to simulate photon transport.
2. Application of fictitious scattering to particle tracking.
3. Application of the hybrid forward/adjoint coupling for dose determination.

4.1. Boltzmann transport equation for non-multiplying media

As a radiation particle traverses a medium, it interacts via different mechanisms with the medium. As a result and depending on the particle energy, the particle releases some or all of its energy as it is either absorbed or scattered to a new energy and direction. The amount of energy in joules that a kilogram of the medium absorbs from the released energy at interaction sites is defined as absorbed dose. Absorbed dose can be computed from an estimate of radiation fluxes in the interaction multiplied by a flux-to-dose conversion factor. Therefore, estimation of fluxes in different regions in space will enable us to predict absorbed dose at those locations.

The Boltzmann transport equation provides the mathematical relationship between radiation particles and the medium they are interacting with. The transport equation describes the balance of particles entering and leaving a differential volume in space, energy, and direction. As a result, it relates mathematically medium radiological properties to radiation particle interaction mechanisms. Our research is focused on "photon systems where no fissionable isotopes are present" hence non-multiplying media (Lewis & Miller, 1984).

4.1.1. Continuous form of the time dependent Boltzmann transport equation

The continuous time-dependent form of the transport equation is:

$$\frac{1}{v}\frac{\partial\varphi(\vec{r},\hat{\Omega},E,t)}{dt} + \hat{\Omega}\cdot\vec{\nabla}\,\varphi(\vec{r},\hat{\Omega},E,t) + \Sigma_{Total}^{medium}(\vec{r},E)\,\varphi(\vec{r},\hat{\Omega},E,t) = S(\vec{r},\hat{\Omega},E,t) \qquad (4\text{-}1)$$

The term $S(\vec{r}, \hat{\Omega}, E, t)$ is the source term and it accounts for all particle sources in the medium. $S(\vec{r}, \hat{\Omega}, E, t)$ is the sum of all particle sources such as sources embedded in the medium (external sources), scattering events and fission reactions within the system. Mathematically this is written as:

$$S(\vec{r}, \hat{\Omega}, E, t) = S^{Ext}(\vec{r}, \hat{\Omega}, E, t)$$

$$+ \int_0^\infty dE' \int_{4\pi} d\hat{\Omega}' \, \Sigma_{Scatt}^{medium}(\vec{r}, \hat{\Omega}' \to \hat{\Omega}, E' \to E) \varphi(\vec{r}, \hat{\Omega}', E', t)$$

$$+ \chi(E) \int_0^\infty dE' \int_{4\pi} d\hat{\Omega}' \, v \, \Sigma_{fission}(\vec{r}, E') \, \varphi(\vec{r}, E', t)$$

The term $\hat{\Omega} \cdot \bar{\nabla}\varphi(\vec{r})$ is the streaming operator defined by:

$$\hat{\Omega} \cdot \bar{\nabla}\varphi(\vec{r}) \equiv \hat{\Omega} \cdot \hat{i} \frac{\partial \varphi(\vec{r})}{\partial x} + \hat{\Omega} \cdot \hat{j} \frac{\partial \varphi(\vec{r})}{\partial y} + \hat{\Omega} \cdot \hat{k} \frac{\partial \varphi(\vec{r})}{\partial z}$$

with

$$
\begin{aligned}
\boldsymbol{v} &= \quad \text{Particle velocity.} \\
\vec{\boldsymbol{r}} &= \quad \text{Particle position vector.} \\
\boldsymbol{\varphi(\vec{r}, \hat{\Omega}, E, t)} &= \quad \text{Particle angular flux.} \\
\boldsymbol{dt} &= \quad \text{Differential time.} \\
\hat{\boldsymbol{\Omega}} &= \quad \text{Direction of particle.} \\
\bar{\boldsymbol{\nabla}} &= \quad \text{Del operator.} \\
\boldsymbol{\Sigma_{Total}^{medium}(\vec{r}, E)} &= \quad \text{Medium total cross section (attenuation coefficient).} \\
\boldsymbol{S(\vec{r}, \hat{\Omega}, E, t)} &= \quad \text{The combined source term.} \\
\boldsymbol{S^{Ext}(\vec{r}, \hat{\Omega}, E, t)} &= \quad \text{External fixed source.} \\
\boldsymbol{\Sigma_{Scatt}^{medium}(\vec{r}, \hat{\Omega}' \to \hat{\Omega}, E' \to E)} &= \quad \text{Scattering cross section.} \\
\boldsymbol{\chi(E)} &= \quad \text{Fission neutrons energy spectrum.} \\
\boldsymbol{v} &= \quad \text{Average number of neutrons released per fission.} \\
\boldsymbol{\Sigma_{fission}(\vec{r}, E')} &= \quad \text{Fission cross section.}
\end{aligned}
$$

Our project deals with steady-state dose production from a fixed, unchanging source, so we can remove time dependent terms from Equation (4-1) giving us the steady state transport equation:

$$\hat{\Omega} \cdot \bar{\nabla} \varphi(\vec{r}) \ + \ \Sigma_{Total}^{medium}(\vec{r}, E) \, \varphi(\vec{r}, \hat{\Omega}, E) \ = \ S(\vec{r}, \hat{\Omega}, E, t)$$

where

$$S(\vec{r}, \hat{\Omega}, E) \ = \ S^{Ext}(\vec{r}, \hat{\Omega}, E) \ + \int_0^\infty dE' \int_{4\pi} d\hat{\Omega}' \ \Sigma_{Scatt}^{medium}(\vec{r}, \hat{\Omega}' \rightarrow \hat{\Omega}, E' \rightarrow E) \varphi(\vec{r}, \hat{\Omega}', E')$$

Or, in expanded form:

$$\hat{\Omega} \cdot \bar{\nabla} \varphi(\vec{r}) \ + \ \Sigma_{Total}^{medium}(\vec{r}, E) \, \varphi(\vec{r}, \hat{\Omega}, E) \ = \ S^{Ext}(\vec{r}, \hat{\Omega}, E) \ +$$
$$\int_0^\infty dE' \int_{4\pi} d\hat{\Omega}' \ \Sigma_{Scatt}^{medium}(\vec{r}, \hat{\Omega}' \rightarrow \hat{\Omega}, E' \rightarrow E) \varphi(\vec{r}, \hat{\Omega}', E')$$

(4-2)

We need to specify a boundary condition to solve this equation. For our project, an escaping particle cannot re-enter the problem geometry; therefore, the boundary flux is zero for all incoming directions. If we define the boundary surface normal as $\hat{n}$ and pointing outward, then the boundary condition is written mathematically as:

$$\varphi(\vec{r}_{surface}, \hat{\Omega}, E) = 0 \ \ for \ \hat{n} \cdot \hat{\Omega} \ < \ 0$$

(4-3)

The $\hat{n} \cdot \hat{\Omega} \ < \ 0$ condition indicates that the source particles are incoming with respect to the boundary surface normal $\hat{n}$. This translates to an angle of $90° < \theta < 180°$ with surface normal.

4.1.2. Multigroup form of the transport equation

An exact solution of the time-independent energy dependent transport Equation (4-2) can be obtained by using the multigroup approximation (Duderstadt, 1976; Lewis & Miller, 1984). In this approximation the particle energy is divided into G finite number of intervals, ΔE_g called "energy groups"; where $E_G \ = \ 0$ and E_0 is sufficiently large that the number of particles at

higher energies is negligible. The particles in group g are taken to be just the particles with energies between E_g and E_{g-1}. Normally the group number increases as the energy decreases.

The group angular flux is defined as:

$$\varphi_g(\vec{r},\widehat{\Omega}) \;=\; \int_{E_g}^{E_{g-1}} dE\,\varphi(\vec{r},\widehat{\Omega},E) \;=\; \int_g dE\,\varphi(\vec{r},\widehat{\Omega},E)$$

We proceed by dividing the nonmultiplying and time-independent transport equation (4-2) into contributions from each group:

$$\int_0^\infty dE' \;=\; \sum_{g'=1}^{G} \int_{g'} dE'$$

Integrating between E_g and E_{g-1}, we get g coupled groupwise balance equations:

$$\widehat{\Omega}\cdot\vec{\nabla}\int_g dE\,\varphi(\vec{r},\widehat{\Omega},E) \;+\; \int_g dE\,\Sigma_{Total}^{medium}(\vec{r},E)\varphi(\vec{r},\widehat{\Omega},E) \;=\; \int_g dE\,S^{Ext}(\vec{r},\widehat{\Omega},E)$$

$$+\; \sum_{g'=1}^{G} \int_g dE \int_{g'} dE' \int_{4\pi} d\Omega'\,\Sigma_{Scatt}^{medium}(\vec{r},E'\rightarrow E,\widehat{\Omega}'\cdot\widehat{\Omega})\varphi(\vec{r},\widehat{\Omega}',E')$$

We need to assume that angular flux is separable in energy to express this equation in terms of the group fluxes. We start by assuming that the angular flux can be approximated as the product of a known function of energy $f(E)$ and group flux $\varphi_g(\vec{r},\widehat{\Omega})$ as follow:

$$\varphi(\vec{r},\widehat{\Omega},E) \;=\; f(E)\,\varphi_g(\vec{r},\widehat{\Omega}), \qquad for\ E_g\ <\ E\ \leq\ E_{g-1}$$

Substituting this equation into the above equation, we get:

$$\widehat{\Omega}\cdot\vec{\nabla}\left(\int_g dE\,f(E)\right)\varphi_g(\vec{r},\widehat{\Omega}) \;+\; \int_g dE\,\Sigma_{Total}^{medium}(\vec{r},E)f(E)\,\varphi_g(\vec{r},\widehat{\Omega}) \;=\; \int_g dE\,S^{Ext}(\vec{r},\widehat{\Omega},E)$$

$$+\; \sum_{g'=1}^{G} \int_g dE \int_{g'} dE' \int_{4\pi} d\Omega'\,\Sigma_{Scatt}^{medium}(\vec{r},E'\rightarrow E,\widehat{\Omega}'\cdot\widehat{\Omega})f(E')\,\varphi_{g'}(\vec{r},\widehat{\Omega}')$$

If we utilize the fact that the energy dependent weighting function $f(E)$ is normalized by the definition of the group flux as follow:

$$\int_g dE f(E) = 1,$$

the above formula simplifies to:

$$\hat{\Omega} \cdot \vec{\nabla} \varphi_g(\vec{r}, \hat{\Omega}) + \int_g dE \, \Sigma_{Total}^{medium}(\vec{r}, E) f(E) \, \varphi_g(\vec{r}, \hat{\Omega}) = \int_g dE S^{Ext}(\vec{r}, \hat{\Omega}, E)$$

$$+ \sum_{g'=1}^{G} \int_g dE \int dE' \int_{4\pi} d\Omega' \, \Sigma_{Scatt}^{medium}(\vec{r}, E' \to E, \hat{\Omega}' \cdot \hat{\Omega}) f(E') \, \varphi_{g'}(\vec{r}, \hat{\Omega}')$$

If we define the group total cross sections as:

$$\Sigma_{Total,g}^{medium}(\vec{r}) = \int_g dE \Sigma_{Total}^{medium}(\vec{r}, E) f(E) , \qquad (4\text{-}4)$$

the scattering cross section to group g from all other groups g' as:

$$\Sigma_{Scatt\,gg'}^{medium}(\vec{r}, \hat{\Omega}' \cdot \hat{\Omega}) = \int_g dE \int_{g'} dE' \int_{4\pi} d\Omega' \Sigma_{Scatt}^{medium}(\vec{r}, E' \to E, \hat{\Omega}' \cdot \hat{\Omega}) f(E'), \qquad (4\text{-}5)$$

and the g group external source as:

$$S_g^{Ext}(\vec{r}, \hat{\Omega}) = \int_g dE S^{Ext}(\vec{r}, \hat{\Omega}, E), \qquad (4\text{-}6)$$

then the nonmultiplying and time-independent multigroup transport equation becomes:

$$\left[\hat{\Omega} \cdot \vec{\nabla} + \Sigma_{Total,g}^{medium}(\vec{r}) \right] \varphi_g(\vec{r}, \hat{\Omega})$$
$$= S_g^{Ext}(\vec{r}, \hat{\Omega}) + \sum_{g'=1}^{G} \int_{4\pi} d\Omega' \Sigma_{Scatt\,gg'}^{medium}(\vec{r}, \hat{\Omega}' \cdot \hat{\Omega}) \varphi_{g'}(\vec{r}, \hat{\Omega}') \qquad (4\text{-}7)$$

4.1.3. Monte Carlo simulation of the Boltzmann equation

The following is a simplified outline of the algorithm followed to complete a Monte Carlo history (Irving, 1971):

1. Starting with the given source distribution, select the initial position $\vec{r}'$ and initial group g', and set initial weight to:

$$Weight = \sum_{g'=1}^{G} \int_{0}^{\infty} ds S_{g'}(\vec{s})$$

2. Choose distance, R, to next interaction site from the PDF:

$$p(R) = \Sigma_{Total,g'}^{medium}\left(\vec{r}' + R\widehat{\Omega}'\right) e^{-\int_{0}^{R} \Sigma_{Total,g'}^{medium}\left(\vec{r}' + R' \widehat{\Omega}'\right) dR'}$$

3. Set $\vec{r} = \vec{r}' + R\widehat{\Omega}'$

a. If $\vec{r}$ is outside the system, particle escapes and history terminated.

4. Adjust the particle weight for non-absorption weighting

$$Weight = \binom{Previous}{Weight} \frac{\Sigma_{Scatt,g'}^{medium}(\vec{r})}{\Sigma_{Total,g'}^{medium}(\vec{r})}$$

and contribute to your tallies.

5. Decide on new energy group and new direction

a. Choose new group g from group to group scattering ratios

b. Choose new direction from tabulated μ value for the selected new group.

6. If new weight is below cutoff weight terminate history, otherwise

a. Set $\vec{r}' = \vec{r}$

b. Set $g' = g$

7. Go to step 2.

4.2. Applying fictitious scattering to the Boltzmann transport equation

4.2.1. Derivation of Boltzmann transport equation with fictitious scattering

The fictitious scattering (Woodcock Tracking) general model is developed by finding the distance to the next collision site assuming that the entire system is homogenous with one total

cross section $\Sigma_{Total,g}^{System}$ per group for all the system materials at all spatial points. It is "implemented by requiring $\Sigma_{Total,g}^{System}$ to be spatially independent and when practical, to be greater than or equal to the largest cross section in the system" Σ_{Maximum} (Cramer, 1977). We start with the conventional nonmultiplying and time-independent multigroup transport equation (4-7) and add the fictitious collision term $\Sigma_{Total,g}^{System}(\vec{r})\,\varphi_g(\vec{r},\widehat{\Omega})$ to both sides of the equation:

$$\widehat{\Omega}\cdot\vec{\nabla}\,\varphi_g(\vec{r},\widehat{\Omega}) + \Sigma_{Total,g}^{medium}(\vec{r})\varphi_g(\vec{r},\widehat{\Omega}) + \Sigma_{Total,g}^{System}(\vec{r})\,\varphi_g(\vec{r},\widehat{\Omega}) = S_g^{Ext}(\vec{r},\widehat{\Omega})$$

$$\Sigma_{Total,g}^{System}(\vec{r})\,\varphi_g(\vec{r},\widehat{\Omega}) + \sum_{g'=1}^{G}\int_{4\pi}d\Omega'\,\Sigma_{Scatt\,gg'}^{medium}(\vec{r},\widehat{\Omega}'\cdot\widehat{\Omega})\varphi_{g'}(\vec{r},\widehat{\Omega}')$$

If we move the term $\Sigma_{Total,g}^{medium}(\vec{r})\varphi_g(\vec{r},\widehat{\Omega})$ to the right side and collect terms, this becomes:

$$\widehat{\Omega}\cdot\vec{\nabla}\,\varphi_g(\vec{r},\widehat{\Omega}) + \Sigma_{Total,g}^{System}(\vec{r})\,\varphi_g(\vec{r},\widehat{\Omega}) = S_g^{Ext}(\vec{r},\widehat{\Omega})$$

$$+\{\Sigma_{Total,g}^{System}(\vec{r}) - \Sigma_{Total,g}^{medium}(\vec{r})\}\varphi_g(\vec{r},\widehat{\Omega})$$

$$+\sum_{g'=1}^{G}\int_{4\pi}d\widehat{\Omega}'\,\Sigma_{Scatt\,gg'}^{medium}(\vec{r},\widehat{\Omega}'\cdot\widehat{\Omega})\varphi_{g'}(\vec{r},\widehat{\Omega}')$$

(4-8)

We next rewrite the second term on the right hand side of the equation as:

$$\{\Sigma_{Total,g}^{System}(\vec{r}) - \Sigma_{Total,g}^{medium}(\vec{r})\}\varphi_g(\vec{r},\widehat{\Omega}) = \Sigma_{Total,g}^{System}(\vec{r})\varphi_g(\vec{r},\widehat{\Omega})\left\{1 - \frac{\Sigma_{Total,g}^{medium}(\vec{r})}{\Sigma_{Total,g}^{System}(\vec{r})}\right\}$$

Using the definition of the Dirac delta function, the last term of (4-8) can be written as:

$$\sum_{g'=1}^{G}\int_{4\pi}d\widehat{\Omega}'\left[\Sigma_{Total,g'}^{System}(\vec{r})\left\{1 - \frac{\Sigma_{Total,g'}^{medium}(\vec{r})}{\Sigma_{Total,g'}^{System}(\vec{r})}\right\}\delta(\widehat{\Omega}'\to\widehat{\Omega})\right]\varphi_{g'}(\vec{r},\widehat{\Omega}')$$

And for the scattering cross section we can separate out the angular redistribution PDF to get:

$$\Sigma_{Scatt\,gg'}^{medium}(\vec{r},\widehat{\Omega}'\cdot\widehat{\Omega}) = \Sigma_{Scatt\,gg'}^{medium}(\vec{r})\,f(\widehat{\Omega}'\cdot\widehat{\Omega})$$

Substituting all of this back into (4-8) and collecting the terms yields:

$$\hat{\Omega} \cdot \vec{\nabla}\, \varphi_g(\vec{r},\hat{\Omega}) \;+\; \Sigma_{Total,g}^{System}(\vec{r})\, \varphi_g(\vec{r},\hat{\Omega}) \;=\; S_g^{Ext}(\vec{r},\hat{\Omega})$$

$$+ \sum_{g'=1}^{G} \int_{4\pi} d\Omega' \Big[\Sigma_{Scatt,gg'}^{medium}(\vec{r})\; f(\hat{\Omega}' \cdot \hat{\Omega})$$

$$+\, \Sigma_{Total,g'}^{System}(\vec{r}) \left\{ 1 - \frac{\Sigma_{Total,g'}^{medium}(\vec{r})}{\Sigma_{Total,g'}^{System}(\vec{r})} \right\} \delta(\hat{\Omega}\,' \to \hat{\Omega}) \Big]\; \varphi_{g'}(\vec{r},\hat{\Omega}') \tag{4-9}$$

Factoring out the $\Sigma_{Total,g}^{System}(\vec{r})$ term from the square bracket to the right of equation (4-9) will result in the following:

$$\hat{\Omega} \cdot \vec{\nabla}\, \varphi_g(\vec{r},\hat{\Omega}) \;+\; \Sigma_{Total,g}^{System}(\vec{r})\, \varphi_g(\vec{r},\hat{\Omega}) = S_g^{Ext}(\vec{r},\hat{\Omega})$$

$$+ \sum_{g'=1}^{G} \int_{4\pi} d\Omega' \left[\frac{\Sigma_{Scatt,gg'}^{medium}(\vec{r})}{\Sigma_{Total,g'}^{System}(\vec{r})}\; f(\hat{\Omega}' \cdot \hat{\Omega}) \right.$$

$$\left. +\, \left\{ 1 - \frac{\Sigma_{Total,g'}^{medium}(\vec{r})}{\Sigma_{Total,g'}^{System}(\vec{r})} \right\} \delta(\hat{\Omega}\,' \to \hat{\Omega}) \right] \Sigma_{Total,g'}^{System}(\vec{r})\varphi_{g'}(\vec{r},\hat{\Omega}') \tag{4-10}$$

Rewrite the term $\dfrac{\Sigma_{Scatt,gg'}^{medium}(\vec{r})}{\Sigma_{Total,g}^{System}(\vec{r})}$ as follow:

$$\frac{\Sigma_{Scatt,gg'}^{medium}(\vec{r})}{\Sigma_{Total,g'}^{System}(\vec{r})} = \frac{\Sigma_{Total,g'}^{medium}(\vec{r})}{\Sigma_{Total,g'}^{System}(\vec{r})} \times \frac{\Sigma_{Scatt,gg'}^{medium}(\vec{r})}{\Sigma_{Total,g'}^{medium}(\vec{r})} \tag{4-11}$$

And define the fictitious collision density term $\psi_{g'}^{System}(\vec{r},\hat{\Omega}')$ as:

$$\psi_{g'}^{System}(\vec{r},\hat{\Omega}') = \Sigma_{Total,g'}^{System}(\vec{r})\varphi_{g'}(\vec{r},\hat{\Omega}') \tag{4-12}$$

Similar to equation (4-12), the real collision density term $\psi_{g'}^{Real}(\vec{r},\hat{\Omega}')$ is:

$$\psi_{g'}^{Real}(\vec{r},\hat{\Omega}') = \Sigma_{Total,g'}^{medium}(\vec{r})\varphi_{g'}(\vec{r},\hat{\Omega}') \tag{4-13}$$

Then the ratio of the real collision rate to the fictitious collision rate becomes:

$$\frac{\psi_{g'}^{Real}(\vec{r},\widehat{\Omega}')}{\psi_{g'}^{System}(\vec{r},\widehat{\Omega}')} = \frac{\Sigma_{Total,g'}^{medium}(\vec{r})}{\Sigma_{Total,g'}^{System}(\vec{r})} \tag{4-14}$$

and the real collision rate in terms of the fictitious collision rate is:

$$\psi_{g'}^{Real}\left(\vec{r},\widehat{\Omega}'\right) = \frac{\Sigma_{Total,g'}^{medium}(\vec{r})}{\Sigma_{Total,g'}^{System}(\vec{r})}\, \psi_{g'}^{System}\left(\vec{r},\widehat{\Omega}'\right) \tag{4-15}$$

Substituting (4-11) and (4-12) back into (4-10) we get:

$$\widehat{\Omega}\cdot\vec{\nabla}\,\varphi_g(\vec{r},\widehat{\Omega}) + \Sigma_{Total,g}^{System}(\vec{r})\,\varphi_g(\vec{r},\widehat{\Omega}) = S_g^{Ext}(\vec{r},\widehat{\Omega})$$

$$+ \sum_{g'=1}^{G}\int_{4\pi} d\Omega'\left[\frac{\Sigma_{Total,g'}^{medium}(\vec{r})}{\Sigma_{Total,g'}^{System}(\vec{r})} \times \frac{\Sigma_{Scatt,gg'}^{medium}(\vec{r})}{\Sigma_{Total,g'}^{medium}(\vec{r})}\, f(\widehat{\Omega}'\cdot\widehat{\Omega})\right.$$

$$\left. + \left\{1 - \frac{\Sigma_{Total,g'}^{medium}(\vec{r})}{\Sigma_{Total,g'}^{System}(\vec{r})}\right\}\delta(\widehat{\Omega}' \to \widehat{\Omega})\right]\psi_{g'}^{System}(\vec{r},\widehat{\Omega}') \tag{4-16}$$

Multiplying $\psi_{g'}^{System}(\vec{r},\widehat{\Omega}')$ into the right hand bracket and using (4-15), becomes equation (4-17):

$$\widehat{\Omega}\cdot\vec{\nabla}\,\varphi_g(\vec{r},\widehat{\Omega}) + \Sigma_{Total,g}^{System}(\vec{r})\,\varphi_g(\vec{r},\widehat{\Omega}) = S_g^{Ext}(\vec{r},\widehat{\Omega})$$

$$+ \sum_{g'=1}^{G}\int_{4\pi} d\Omega'\left[\frac{\Sigma_{Scatt,gg'}^{medium}(\vec{r})}{\Sigma_{Total,g'}^{medium}(\vec{r})} \times \psi_{g'}^{Real}(\vec{r},\widehat{\Omega}') \times f(\widehat{\Omega}'\cdot\widehat{\Omega})\right.$$

$$\left. + \left\{1 - \frac{\Sigma_{Total,g'}^{medium}(\vec{r})}{\Sigma_{Total,g'}^{System}(\vec{r})}\right\}\delta(\widehat{\Omega}' \to \widehat{\Omega})\psi_{g'}^{System}(\vec{r},\widehat{\Omega}')\right] \tag{4-17}$$

The right hand side of equation (4-17) at $\widehat{\Omega}' \to \widehat{\Omega}$ is the emergent particle density for all events (source real collisions, and fictitious collisions), which we can designate as q_g^{System}:

$$q_g^{System}(\vec{r},\widehat{\Omega}') = \sum_{g'=1}^{G}\left[\frac{\Sigma_{Scatt,gg'}^{medium}(\vec{r})}{\Sigma_{Total,g'}^{medium}(\vec{r})} \times \psi_{g'}^{Real}(\vec{r},\widehat{\Omega}')\right] \tag{4-18}$$

$$+ \left\{1 - \frac{\Sigma_{Total,g'}^{medium}(\vec{r})}{\Sigma_{Total,g'}^{System}(\vec{r})}\right\} \psi_{g'}^{System}(\vec{r},\hat{\Omega}')\Bigg]$$

Since, the emergent particle density for source real collisions is q_g :

$$q_g\left(\vec{r},\hat{\Omega}'\right) = \sum_{g'=1}^{G} \frac{\Sigma_{Scatt,gg'}^{medium}(\vec{r})}{\Sigma_{Total,g'}^{medium}(\vec{r})} \psi_{g'}^{Real}(\vec{r},\hat{\Omega}') \qquad (4\text{-}19)$$

Or, as shown in equation (4-10), is also equal to:

$$q_g\left(\vec{r},\hat{\Omega}'\right) = \sum_{g'=1}^{G} \frac{\Sigma_{Scatt,gg'}^{medium}(\vec{r})}{\Sigma_{Total,g'}^{System}(\vec{r})} \psi_{g'}^{System}(\vec{r},\hat{\Omega}') \qquad (4\text{-}20)$$

Substitute equation (4-19) into equation (4-18) to get

$$q_g^{System}(\vec{r},\hat{\Omega}') = q_g\left(\vec{r},\hat{\Omega}'\right) + \sum_{g'=1}^{G} \left\{1 - \frac{\Sigma_{Total,g'}^{medium}(\vec{r})}{\Sigma_{Total,g'}^{System}(\vec{r})}\right\} \psi_{g'}^{System}(\vec{r},\hat{\Omega}') \qquad (4\text{-}21)$$

The angular flux is computed from equations (4-12) and (4-13):

$$\varphi_g(\vec{r},\hat{\Omega}') = \sum_{g'=1}^{G} \frac{\psi_{g'}^{System}(\vec{r},\hat{\Omega}')}{\Sigma_{Total,g'}^{System}(\vec{r})} = \sum_{g'=1}^{G} \frac{\psi_{g'}^{Real}(\vec{r},\hat{\Omega}')}{\Sigma_{Total,g'}^{medium}(\vec{r})} \qquad (4\text{-}22)$$

All of the above equations are valid when the absorption weighting Monte Carlo method is used to find a solution. Further, for this type of transport (absorption weighting) the real emergent density $q_g\left(\vec{r},\hat{\Omega}'\right)$ is given by:

$$q_g\left(\vec{r},\hat{\Omega}'\right) = \sum_{g'=1}^{G} \frac{\Sigma_{Scatt,gg'}^{medium}(\vec{r})}{\Sigma_{Total,g'}^{medium}(\vec{r})} \psi_{g'}^{Real}(\vec{r},\hat{\Omega}')$$

$$\qquad (4\text{-}23)$$

$$= \sum_{g'=1}^{G} \frac{\Sigma_{Scatt,gg'}^{medium}(\vec{r})}{\Sigma_{Total,g'}^{System}(\vec{r})} \psi_{g'}^{System}(\vec{r},\hat{\Omega}')$$

And the fictitious emergent density is:

$$q_g^{System}(\vec{r}, \hat{\Omega}') = \sum_{g'=1}^{G} \left[\frac{\Sigma_{Scatt,gg'}^{medium}(\vec{r})}{\Sigma_{Total,g'}^{System}(\vec{r})} + \left\{ 1 - \frac{\Sigma_{Total,g'}^{medium}(\vec{r})}{\Sigma_{Total,g'}^{System}(\vec{r})} \right\} \right] \psi_{g'}^{System}(\vec{r}, \hat{\Omega}') \quad (4\text{-}24)$$

And using (4-23) and (4-24) the flux is:

$$\varphi_g(\vec{r}, \hat{\Omega}') = \sum_{g'=1}^{G} \frac{q_{g'}(\vec{r}, \hat{\Omega}')}{\Sigma_{Scatt,gg'}^{medium}(\vec{r})}$$

$$= \frac{q_g^{System}(\vec{r}, \hat{\Omega}')}{\sum_{g'=1}^{G} \left[\Sigma_{Scatt,gg'}^{medium}(\vec{r}) + \Sigma_{Total,g'}^{System}(\vec{r}) \left\{ 1 - \frac{\Sigma_{Total,g'}^{medium}(\vec{r})}{\Sigma_{Total,g'}^{System}(\vec{r})} \right\} \right]} \qquad (4\text{-}25)$$

4.2.2. Use of fictitious scattering in Monte Carlo algorithms

When implementing the fictitious scattering method, the distance to the next interaction site is computed using fictitious cross section $\Sigma_{Total,g}^{System}(\vec{r})$. If the interaction site is within the problem boundary, we determine if the interaction is real or fictitious based on the ratio between the true site attenuation coefficient and the fictitious cross section. A true scattering interaction occurs with a probability of $\frac{\Sigma_{Total,g}^{medium}(\vec{r})}{\Sigma_{Total,g}^{System}(\vec{r})}$, which indicates that a real scattering event has taken place with an absorption weighting correction applied. Otherwise, with probability of $\left\{ 1 - \frac{\Sigma_{Total,g}^{medium}(\vec{r})}{\Sigma_{Total,g}^{System}(\vec{r})} \right\}$ a fictitious interaction occurred and the particle continues on the same path without any change of direction, energy and weight.

The fictitious scattering method is implemented using a random number to determine if each collision is real or fictitious (random number RN are uniformly distribution in the interval $0 \leq RN \leq 1$). The algorithm is:

1. Choose a fictitious cross-section $\Sigma_{Total,g}^{System}(\vec{r})$. This is normally chosen to be the largest expected cross section value during any particle flight.
2. Sample trial flight distance using :

$$p(R) = \Sigma_{Total,g'}^{System}(\vec{r}' + R\hat{\Omega}')\, e^{-\int_0^R \Sigma_{Total,g'}^{System}(\vec{r}' - R'\,\hat{\Omega}')\, dR'}$$

3. Move the particle that distance and find $\Sigma_{Total,g}^{medium}(\vec{r})$ at the new location.

4. Compute $P = \dfrac{\Sigma_{Total,g}^{medium}(\vec{r})}{\Sigma_{Total,g}^{System}(\vec{r})}$.

5. Draw a random number *RN* and test for type of collision:

    a. A real collision occurs if $RN \leq \dfrac{\Sigma_{Total,g}^{medium}(\vec{r})}{\Sigma_{Total,g}^{System}(\vec{r})}$ and ordinary collision

        mechanisms are used to determine post collision parameters:

        i.   New photon Energy;

        ii.   New particle direction.

    b. A fictitious collision occurs if $> \dfrac{\Sigma_{Total,g}^{medium}(\vec{r})}{\Sigma_{Total,g}^{System}(\vec{r})}$, and the particle continues with

        the same direction, energy, and particle weight.

The fictitious scattering tracking becomes inefficient if $\Sigma_{Total,g}^{System}(\vec{r})$ is much larger than the typical cross-section; otherwise it is a very powerful Monte Carlo technique.

For adjoint transport, the fictitious scattering algorithm is the same.

4.3. Hybrid forward/adjoint technique

The hybrid forward/adjoint technique is best described using operator notation for the forward and adjoint transport. We start by defining the traditional forward solution of the transport equation as a groupwise solution of the forward operator:

$$L_g\, \varphi_g(\vec{r},\hat{\Omega}) \;=\; S_g(\vec{r},\hat{\Omega})$$

where:

$$L_g \equiv \hat{\Omega} \cdot \vec{\nabla} \;+\; \Sigma_{Total,g}^{Medium}(\vec{r}) \;-\; \sum_{g'=1}^{G} \int_{4\pi} d\Omega'\, \Sigma_{Scatt,gg'}^{medium}(\vec{r},\hat{\Omega} \cdot \hat{\Omega}')$$

For a standard shielding problem with both sources and detectors located inside the system boundary and non-reentrant boundaries, the forward flux solution is found for zero inward boundary flux:

$$\varphi_g(\vec{r}_{surface}, \widehat{\Omega}) = 0 \ \ for \ \hat{n} \cdot \widehat{\Omega} < 0 \ \ for \ all \ \vec{r} \in \ Surface$$

Once we have an estimate of $\varphi_g(\vec{r}, \widehat{\Omega})$ we then fold it into the detector response function $R_g(\vec{r}, \widehat{\Omega})$, to get the desired response in the volume (i.e., Absorbed Dose D) using:

$$D = \int_V dV \sum_{g=0}^{G} \int_{4\pi} d\widehat{\Omega} \ \varphi_g(\vec{r}, \widehat{\Omega}) \ R_g(\vec{r}, \widehat{\Omega}) = \langle \varphi_g, R_g \rangle \qquad (4\text{-}26)$$

The "bra-ket" notation used in equation (4-26) is a simple way to express full integration (or summation) over all independent variables.

Similarly, we can define a solution of the adjoint transport equation as a groupwise solution of the adjoint operator:

$$L_g^* \ \varphi_g^*(\vec{r}, \widehat{\Omega}) = R_g(\vec{r}, \widehat{\Omega})$$

where

$$L_g^* \equiv -\widehat{\Omega} \cdot \vec{\nabla} + \Sigma_{Total,g}^{Medium}(\vec{r}) - \sum_{g'=1}^{G} \int_{4\pi} d\Omega' \Sigma_{Scatt,g'g}^{medium}(\vec{r}, \widehat{\Omega} \cdot \widehat{\Omega}')$$

The reason for the use of the response function for the adjoint source becomes apparent when we consider that the mathematical relation between the forward and adjoint operators is given by:

$$\langle \varphi_g^*, L_g \ \varphi_g \rangle = \langle \varphi_g, L_g^* \varphi_g^* \rangle + \int_V dV \sum_{g=0}^{G} \int_{4\pi} d\widehat{\Omega} \ \widehat{\Omega} \cdot \vec{\nabla} \{ \varphi_g(\vec{r}, \widehat{\Omega}) \varphi_g^*(\vec{r}, \widehat{\Omega}) \} \qquad (4\text{-}27)$$

The last term can be put in a more convenient form using the divergence theorem, which transforms a volume integral into a surface integral as follow:

$$\int_V dV \bar{\nabla} f_g(\vec{r}, \hat{\Omega}) = \int_S dS \hat{n} f_g(\vec{r}, \hat{\Omega}) \tag{4-28}$$

Using the divergence theorem, Equation (4-27) can be written as:

$$\langle \varphi_g^*, L_g \, \varphi_g \rangle = \langle \varphi_g, L_g^* \varphi_g^* \rangle + \langle \hat{\Omega} \cdot \hat{n} \, \varphi_g, \varphi_g^*, \rangle_S \tag{4-29}$$

where

$$\langle \hat{\Omega} \cdot \hat{n} \, \varphi_g, \varphi_g^*, \rangle_S \equiv \int_S dS \sum_{g=0}^{G} \int_{4\pi} d\hat{\Omega} \, \hat{\Omega} \cdot \hat{n} \, \varphi_g(\vec{r}, \hat{\Omega}) \varphi_g^*(\vec{r}, \hat{\Omega}) \tag{4-30}$$

The usefulness of this can be shown when we expand the definition of the dose rate (4-26):

$$
\begin{aligned}
D &= \langle \varphi \, , R \rangle \\
&= \langle \varphi \, , L^* \varphi^* \rangle & (from \; adjoint \; solution \; is \; L^* \varphi^* = R) \\
&= \langle \varphi^*, L\varphi \rangle - \langle \hat{n} \cdot \hat{\Omega} \, \varphi \, , \varphi^* \rangle_S & (from \; operators \; relationship) \\
&= \langle \varphi^* , S \rangle - \langle \hat{n} \cdot \hat{\Omega} \, \varphi \, , \varphi^* \rangle_S & (from \; forward \; solution \; is \; L\varphi = S)
\end{aligned}
\tag{4-31}
$$

This terse but useful derivation shows that the dose rate in a region, which is normally calculated using the first line (i.e., by determining the flux with a forward calculation and then folding the flux with a response function in the region of interest), can also be found in two other ways, using the last line:

1. If an adjoint-only calculation is performed with both the source region and response region within the boundary of the calculation and void boundary conditions used on a non-reentrant outer boundary, then the response rate is given by:

$$D = \langle \varphi^*, S \rangle$$

since the second term in the bottom line of Equation (4-31) goes to zero due to:

$$\varphi_g(\vec{r}_{surface}, \hat{\Omega}) = 0 \; for \; \hat{n} \cdot \hat{\Omega} < 0 \; for \; all \; \vec{r} \in Surface$$

and

$$\varphi_g^*(\vec{r}_{surface}, \hat{\Omega}) = 0 \; for \; \hat{n} \cdot \hat{\Omega} \geq 0 \; for \; all \; \vec{r} \in Surface$$

35

which means that their product is zero for all directions.

2. If an adjoint calculation is performed which contains the detector, but not the source (i.e., the source particles arrive from outside by impinging on the boundary in an incoming direction), then the response rate is given by:

$$D = -\left\langle \hat{n} \cdot \hat{\Omega} \, \varphi, \varphi^* \right\rangle_S$$

(which will be positive since the directions are incoming).

The second case above is the basis for the hybrid forward/adjoint technique.

Chapter 5

Voxel8 and Pixel8 Code Algorithms

The purpose of this chapter is to explain in detail the algorithms within the FORTRAN computer codes developed for this project. The first three sections of this chapter give general outlines and flowcharts of the three modes developed: forward, adjoint, and hybrid forward/adjoint. The last section covers the details of how the decisions are made at each of the decisions points of the Monte Carlo random walk.

5.1. Forward mode

5.1.1. Outline of the forward Monte Carlo code(Voxel8)

Find the maximum total cross sections for each group

For n = 1 to desired number of histories (NPS).

1. Starting from initial source position, pick initial particle direction   within the primary collimator specified cone apex angle and set initial weight to the sum of the group sources (or to one and correct later).

2. Compute intersection point   between the picked particle direction & plane defining adjustable field size.

3. Test if   within adjustable field size or not

   - If NO, **END THE HISTORY**.

4. Sample source energy group.

5. Sample distance to collision site using the maximum total cross section.

6. Compute collision site location   .

7. Test if the collision site is within the problem geometry:

   - If NO, **END THE HISTORY**

8. Score flux-based tallies based on current energy group, weight, and the maximum total cross section as follow:

$$\varphi = \left(\frac{Weight}{\Sigma_{Total,g}^{System}(\vec{r}) \, V} \right) \, in \, units \, \left(\frac{1}{cm^2} \right)$$

9. Lookup the material at this collision site

10. Compute Fictitious scattering probability

11. Determine type of collision

- If fictitious, continue the particle path unchanged (GOTO bullet 5).

12. Lookup the following for the location site material and particle energy group:

- Scattering probability.
- Group to group CDF for scattering
- Group to group cosine scattering angle data.

13. Compute:

- New particle weight based on scattering probability using

$$Weight = \binom{Previous}{Weight} \frac{\Sigma_{Scatt,g'}^{medium}(\vec{r})}{\Sigma_{Total,g'}^{medium}(\vec{r})}$$

- New energy group after scatter.
- New direction of travel after scatter for this group-to-group transfer.

(**GOTO bullet 5**).

End

Perform post-processing and output the results

5.1.2. Flow chart of the forward Monte Carlo code (Voxel8)

FORWARD TRANSPORT ALGORITHM

Pick source direction within a max cone angle
$(\Omega_{x0}, \Omega_{y0}, \Omega_{z0})$

Find intersection point top of patient box
$(x_{Field}, y_{Field}, z_{Field}) = (x_{BoxSurface}, y_{BoxSurface}, z_{BoxSurface})$

TRY AGAIN

FALSE

Test if within field window

TRUE

Set initial particle weight based max cone angle (ConeMU)
$W_0 = (1.0 - ConeMU) / 2$

Start In patient Transport:
1) Position: (x_0, y_0, z_0)
2) Group: g
3) Direction: $\Omega_{x0}, \Omega_{y0}, \Omega_{z0}$

Pick g

Set $(x_0, y_0, z_0) =$
$(x_{BoxSurface}, y_{BoxSurface}, z_{BoxSurface})$

Pick distance to interaction site:
$s = -\ln(\xi) / \Sigma_{tmax,g}$

Find new position:
$x = x_0 + \Omega_{x0} s$
$y = y_0 + \Omega_{y0} s$
$z = z_0 + \Omega_{z0} s$

Position in phantom

FALSE
OUTSIDE PHANTOM

TRUE WITHIN PHANTOM

Lookup cell parameters:
1) $\Sigma_{t,g} = \Sigma_t(i, j, k, g)$
2) $CDF_{s,g} = CDF_s(i, j, k, g)$
3) Dose conversion factor

Find: Cell number (i,j,k) given
Cell Dimension: $\Delta x, \Delta y, \Delta z$
$i = x / \Delta x + 1$
$j = y / \Delta y + 1$
$k = z / \Delta z + 1$

Score $\delta\phi = \{ W / [\Sigma_{tmax,g} \bullet V_{cell}] \} \times [$ Flux to dose conversion factor $]$

Pick ξ

KILL

Play Russian Roulette

$W = W_0 \Sigma_{scat,g} / \Sigma_{t,g}$

Compute $\Sigma_{t,g} / \Sigma_{tmax,g}$

SURVIVE

TRUE REAL COLLISION

$\xi < \Sigma_{t,g} / \Sigma_{tmax,g}$

From XS files find
1) New Group g
2) New Direction $\Omega_x, \Omega_y, \Omega_z$
3) Set $x_0 = x; y_0 = y; z_0 = z$

FALSE   (*FICTITIOUS SCATTERING*)

Set $x_0 = x; y_0 = y; z_0 = z$
Keep same group g &Direction $\Omega_{x0}, \Omega_{y0}, \Omega_{z0}$

Figure 5-1 Flow chart of forward Monte Carlo code (Voxel8)

5.2. Adjoint mode

5.2.1. Outline of the Adjoint Monte Carlo code (Pixel8) steps

Find the maximum total cross sections for each group

For For n = 1 to desired number of histories (NPS).

1. Sample initial position within ROI voxel from set boundaries (x_0, y_0, z_0).
2. Sample source energy group from the dose response function.
3. Sample direction isotropically $(\widehat{\Omega}_{x0}, \widehat{\Omega}_{y0}, \widehat{\Omega}_{z0})$.
4. Set particle initial weight to the sum of the group response function values (or to one and correct later).
5. Sample distance to collision site using the maximum total cross section for the group.
6. Compute the new location $(x_{new}, y_{new}, z_{new})$.
7. Test if collision site $(x_{new}, y_{new}, z_{new})$ is within the problem geometry:

    - If NO, Figure out the following about the exited particle:
        - ➢ Which boundary surface the particle crossed.
        - ➢ Particle energy.
        - ➢ The surface pixel indexes at the point of exit.
        - ➢ The "igloo" zone according to particle direction.
    - Score to appropriate tally according to the parameters determined above
    - terminate history (GOTO bullet 15).

8. Find the collision site voxel and look up:

    - Material.
    - Total cross section (given material and energy group).

9. Compute fictitious scattering probability
10. Determine type of collision

    - Fictitious, keep particle group, direction and weight (GOTO bullet 6).

11. Lookup the following for the voxel material and particle energy group:

- Scattering probability.
- Group to group CDF.
- Group to group cosine scattering angle data.

12. Compute:

- New particle weight based on (sum of group-to-group Scattering cross sections for the current group)/Total cross section. If the weight is below the Russian Roulette lower weight, then play Russian Roulette, ENDING the history if the particle fails.
- New group after scatter.
- New direction of travel after scatter.

13. Set the new particle parameter values found in step 13. (**GOTO bullet 6**.)

14. Figure out the following:

- Which boundary surface the particle crossed.
- Particle energy.
- The surface pixel indexes at the point of exit.
- The "igloo" zone according to particle direction.

15. Contribute to the appropriate tally according to parameters determine from previous steps (surface, pixel index, energy group, igloo zone) the following (adjoint flux):

$$\varphi^* = \left(\frac{Weight}{Cos\theta \; dA}\right) \; units \; \left(\frac{cGy}{cm^2}\right)$$

END

Perform post-processing and output the results.

5.2.2. Flow chart of the Adjoint Monte Carlo code (Pixel8)

ADJOINT TRANSPORT ALGORITHM
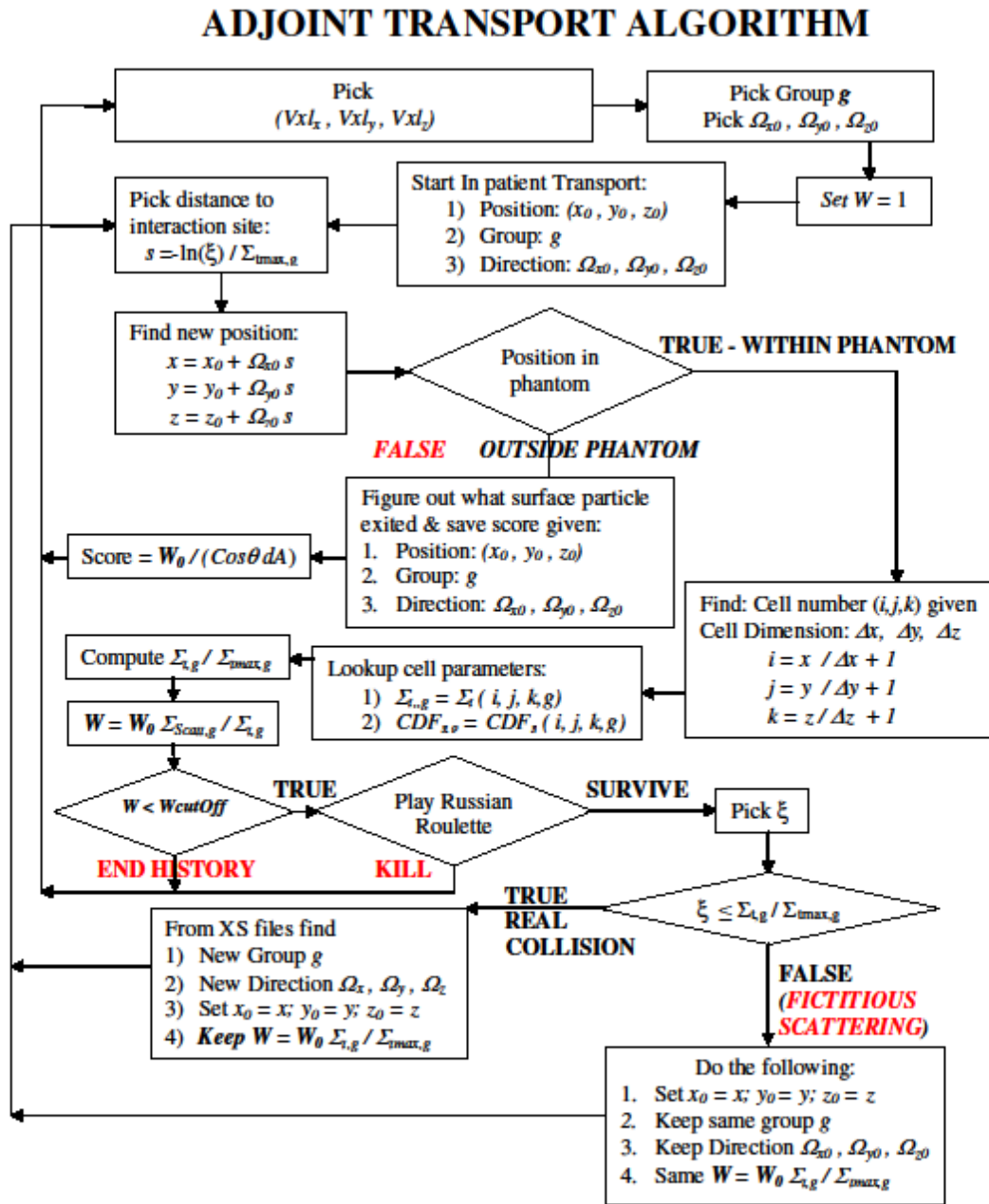
Figure 5-2 Flow chart of adjoint Monte Carlo code (Pixel8)

5.3. Hybrid forward/adjoint mode

5.3.1. Procedural steps for the surface integration

Read the Adjoint Monte Carlo code results (Adjoint surface flux by (surface, pixel, energy group, directional bin).

For $n = 1$ to $desired$ $number$ of $histories$ (NPS).

1. Starting from initial source position pick initial particle direction Ω_0 within the primary collimator specified cone apex angle – set initial weight to sum of group source rates, $w_{forward.}$

2. Compute intersection point $(x_{intersect}, y_{intersect}, z_{intersect})$ on the patient surface.

3. Test if $(x_{intersect}, y_{intersect}, z_{intersect})$ is within the adjustable field size

    - If NO, discard this direction and choose another one (**GOTO bullet 1**).

4. Sample source energy group.

5. Locate appropriate (surface, energy, igloo direction) bin and retrieve the saved adjoint flux for the bin, w_{bin}.

6. Add contribution to the dose from this intersection as:

$$\Delta D = \int_S dS \sum_{g=1}^{G} \int_{\hat{n}\cdot\widehat{\Omega}<0} d\widehat{\Omega} \, |\hat{n}\cdot\widehat{\Omega}| \varphi_g^*(\vec{r},\widehat{\Omega}) \, \varphi_g(\vec{r},\widehat{\Omega}) \cong w_{forward} \cdot w_{bin}$$

END

Perform post-processing and output the results

5.4. Details of the decisions made in the random walks
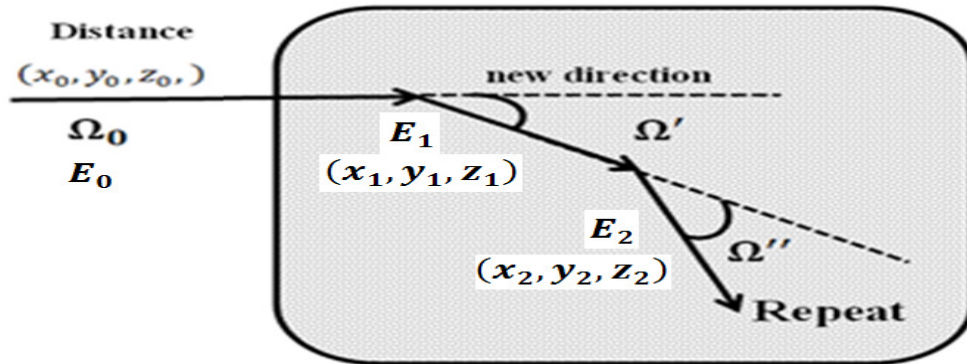
Figure 5-3 Random walk / history steps

Figure 5-3 illustrates the events occurring during particle random walk in a medium (E. D. Cashwell & Everett, 1959) and are the bases of Monte Carlo simulation of radiation transport in a medium. For the purpose of our project, this random walk is essentially the same in forward and adjoint Monte Carlo mode except at the start of the random walk and for the energy group determination after a scattering event.

5.4.1. Selection of initial particle parameters

5.4.1.1. Initial direction

In forward mode, we start our transport by selecting an initial particle direction in the cone illustrated in Figure 5-4 (chosen so that it completely covers the adjustable field size window), with the particle immediately killed if it is not inside the adjustable field size window. The result is an initial direction choice within the adjustable field size window. The passing particle will have an initial weight of:

$$Wght_0 = \frac{(1 - Cos(\theta))}{2}$$
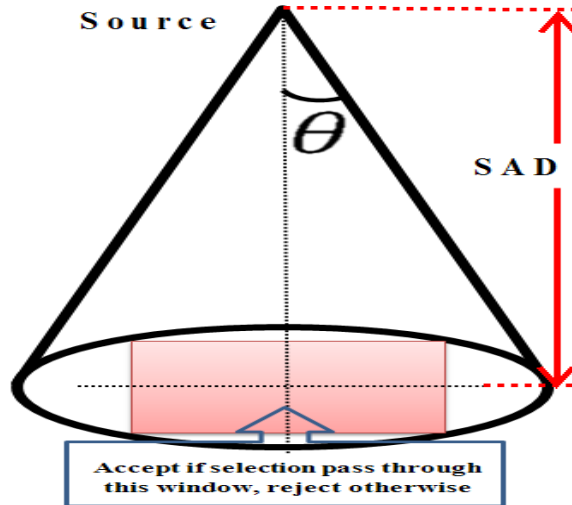
Figure 5-4 Photon direction selection

In adjoint mode, we start from a region of interest voxel (i.e., selecting a voxel index) where all voxels have the same probability. Then a starting point (x, y, z) is selected inside the given geometrical boundary as follow:

1. *Select random number ξ_x then compute*

$$x_i = x_{min} + dx \times \xi_x.$$

2. *Select random number ξ_y then compute*

$$y_i = y_{min} + dy \times \xi_y.$$

3. *Select random number ξ_z then compute*

$$z_i = z_{min} + dz \times \xi_z.$$

Then we test if these coordinates are within the region of interest or not. If they are we proceed if not we sample for another point. Then an initial direction is selected by selecting the cosine of a polar angle and an azimuthal angle. Then these two values are converted to Cartesian coordinates. The steps are as follow:

1. *Select random number ξ_μ then compute*

$$\Omega_z = \mu = -1.0 + 2.0 \times \xi_\mu$$

2. *Select random number ξ_ϕ then compute*

$$\phi = 2.0 \times \pi \times \xi_\phi$$

3. *Then compute*:

$$\sqrt{1 - \mu^2}$$

4. *x & y direction component*:

$$\Omega_x = \sqrt{1 - \mu^2} \, Cos(\phi)$$
$$\Omega_y = \sqrt{1 - \mu^2} \, Sin(\phi)$$

5.4.1.2. *Initial energy*

Our research interest is the poly-energetic photon spectrum generated by a medical linear accelerator. Description of this spectrum can be found in papers published by Mohan, Chui, and Lidofsky in 1985 and the paper by Sheikh-Bagheri and Roger in 2002 (Mohan, Chui, & Lidofsky, 1985; Sheikh-Bagheri & Rogers, 2002). The latest paper by Sheikh Bagheri & Rogers (Mohan et al., 1985; Sheikh-Bagheri & Rogers, 2002) calculates and tabulates the photon spectrum using Monte Carlo simulation for nine beams from three major manufacturers of commercial medical linear accelerators with energies ranging from 4-25 MV at the source location. The data is separated into two categories according to the linear accelerator maximum energy as high energy (energy between 15-25 MV) and low energy (4-10 MV). Figure 5-5 is a plot of the computed photon spectrum for a low energy Linac while Figure 5-6 is a plot of the computed photon spectrum for a high energy Linac.

In forward transport mode, the desired photon spectrum is selected. The probability distribution function PDF and the cumulative probability distribution CDF are calculated and a search array is built. The initial particle energy is selected from the CDF.
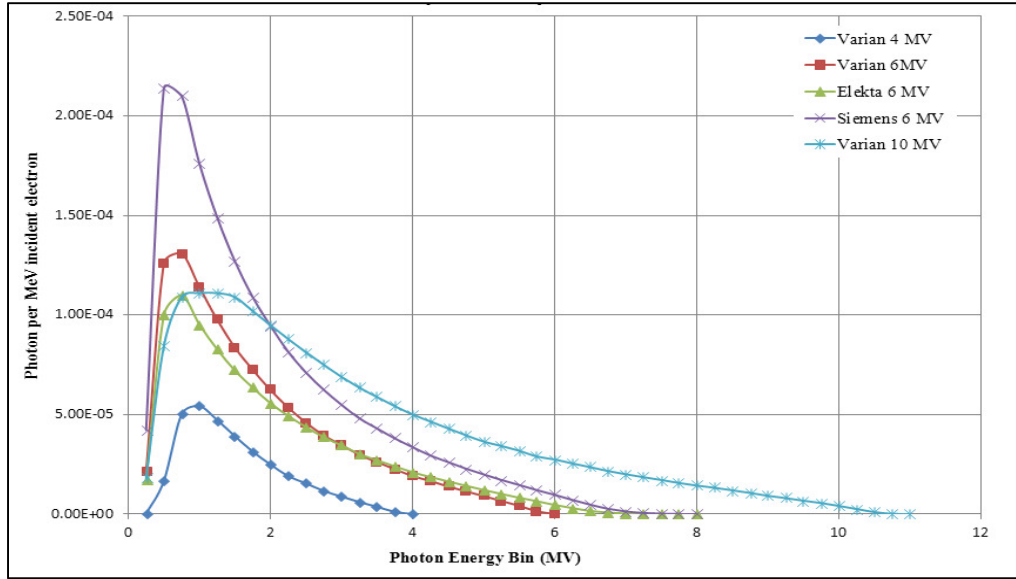
Figure 5-5 Low energy spectrum (4-10 MV) from Medical Linear Accelerator
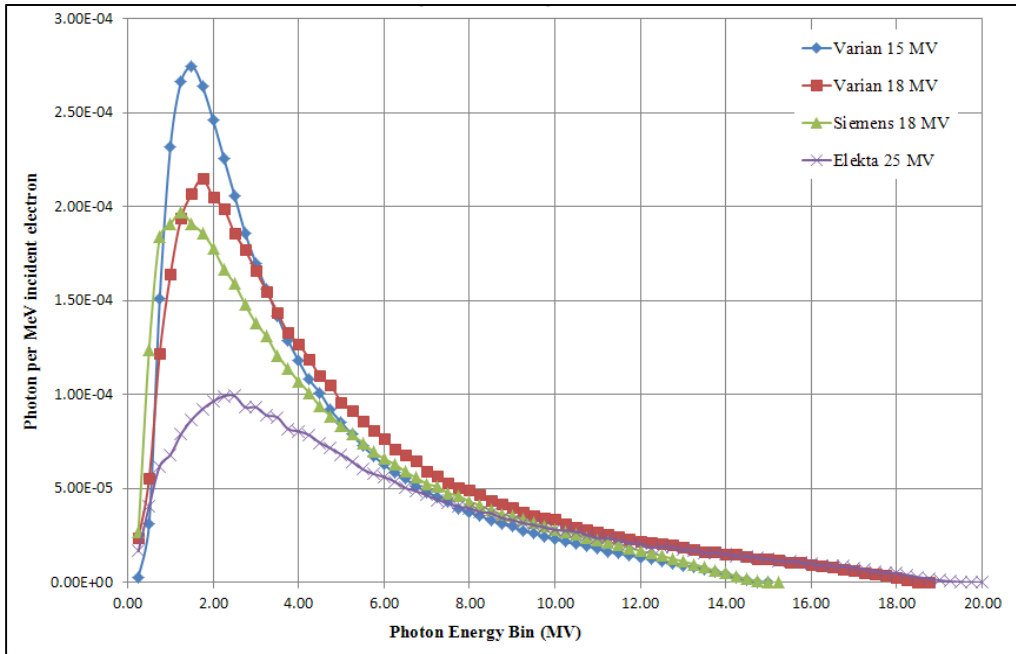
Figure 5-6 High energy spectrum (15-25 MV) from Medical Linear Accelerator

To speed up the initial energy selection process, a search array was built that bins the photon spectrum CDF into a known number of bins. The number of search array bins reflects the desired search precision. The current implementation uses a search array size of a 1000. Therefore, the search array bins index reflects the photon group CDF values multiplied by a 1000. The array itself holds the corresponding energy group value. Once a group is selected it is verified against the actual photon CDF and adjusted accordingly. Using the search array will eliminate the need to loop through the entire photon spectrum CDF every time we start a new history.

Similarly in adjoint transport mode, the best guess about the adjoint source probability distribution is built from the response function before the start of transport. The probability distribution function PDF and the cumulative probability distribution CDF are calculated and a search array is built. During transport the initial adjoint particle energy is sampled from the search array then verified with the CDF.

5.4.1.3. Sampling the distance to interaction / collision site Sampling
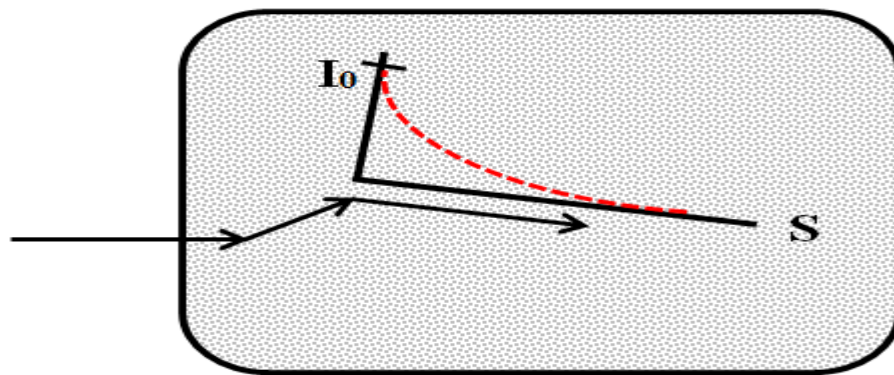
Figure 5-7 Distance to collision site sampling

Both the forward and adjoint transport use the same process to sample distance to collision site. This process is illustrated in Figure 5-7. Define the optical depth, $\beta(x)$, as the expected number of mean free paths traversed by a particle traveling a distance x through a medium with

arbitrarily specified macroscopic cross-section $\Sigma(x)$ (Carter & Cashwell, 1975; Carter et al., 1972; E. Cashwell, Neergaard, Taylor, & Turner, 1972; E. D. Cashwell & Everett, 1959):

$$\beta(x) = \int_0^x \Sigma(x') \, dx'$$

Assuming that $\Sigma(x)$ is finite and $\Sigma(x) \geq 0$, the probability of traversing a distance x in a medium without collision event when x is $0 \leq x < \infty$ is:

$$probability \ of \ traversing \ a \ distance \ x \ = \ e^{-\beta(x)}$$

The independent interaction probability per distance traveled event is:

$$\frac{d\beta}{dx} = \Sigma(x)$$

which leads to $0 \leq \frac{d\beta}{dx} < \infty$.

The probability density function (PDF) for a collision occurring after a particle travels a distance x through a medium is given by the product of the above two probabilities:

$$PDF(x) = \frac{d\beta}{dx} \cdot e^{-\beta(x)}$$

Normalizing the result by integrating the equation yield the normalization constant :

$$G = \int_0^\infty \frac{d\beta}{dx} \cdot e^{-\beta(x)} \, dx = 1 - e^{-\beta(\infty)}$$

To allow for particles that have no collisions (i.e., exit the problem geometry without interaction), we define the "**no collision probability**" P_{NC} as:

$$P_{NC} = e^{-\beta(\infty)}$$

The normalization constant G becomes:

$$G = \int_0^\infty \frac{d\beta}{dx} \cdot e^{-\beta(x)} \, dx = 1 - e^{-\beta(\infty)} = 1 - P_{NC}$$

The probability density function (PDF) for a collision occurring after a particle travels a distance x through a medium can now be expressed as the sum of the two mutually exclusive events probability (probability of no interaction and probability of interaction at distance x) given by

$$PDF(x) = P_{NC} \cdot \delta(x = \infty) + \frac{d\beta}{dx} \cdot e^{-\beta(x)}$$

If we use the fact that

$$1 = \frac{(1 - P_{NC})}{(1 - P_{NC})} = (1 - P_{NC}) \cdot \frac{1}{(1 - P_{NC})} = (1 - P_{NC}) \cdot \frac{1}{G}$$

the probability density function (PDF) for a collision occurring after a particle travels a distance x through a medium is:

$$PDF(x) = P_{NC} \cdot \delta(x = \infty) + (1 - P_{NC}) \cdot \frac{1}{G} \cdot \frac{d\beta}{dx} \cdot e^{-\beta(x)}$$

Note that the PDF equation allows for the possibility of traveling an infinite distance without colliding. These are cases that occur when $\Sigma(x) \to 0$ as $x \to \infty$ (most often occurring when the solution volume is limited to a finite region and void assumed outside of this volume)

Random sampling the Monte Carlo flight path requires solving the following equation for s, the flight path distance to collision:

$$\xi = \int_0^s PDF(x) \, dx \;\; or \;\; \xi = CDF(s)$$

where ξ is a uniform random number in $[0, 1)$, $PDF(x)$ is given by the equations above, and the $CDF(x)$ is given by:

$$CDF(x) = \int_0^s CDF(x') \, dx' = P_{NC} \cdot H(x, \infty) + (1 - P_{NC}) \cdot \frac{1 - e^{-\beta(x)}}{1 - e^{-\beta(\infty)}}$$

(with $H(x, \infty)$ the Heaviside step function). Frequently we write s as:

$$s = CDF^{-1}(\xi)$$

For the infinite homogenous medium case when the cross section is a constant and independent of x the optical distance equation simplifies to:

$$\beta(x) = \Sigma x, \quad \frac{d\beta}{dx} = \Sigma, \quad P_{NC} = 0, \quad G = 1, \quad CDF(x) = \Sigma e^{-\Sigma x}$$

And the solution for

$$\xi = \int_0^s CDF(x) \, dx \quad or \quad \xi = CDF(S)$$

is

$$S = -\frac{\ln(1-\xi)}{\Sigma}$$

Since ξ and $(1-\xi)$ are both uniform distributions between 0 and 1, the above equation is commonly implemented as:

$$s = -\frac{\ln(\xi)}{\Sigma}$$

As a particle traveling the medium enters a region with a different total cross section $\Sigma(x)$, the sampled distance to the next collision s will vary. When the value of s is larger than region dimensions we need to adjust s appropriately; this can result in a lot of computation time spent trying to figure out distances to boundaries.

We can avoid this situation by utilizing the concept of factitious scattering method. When using the fictitious scattering method, the material actual total cross section is replaced with a fictitious total cross section for the purposes of finding the distance to next collision. As described in Chapter 4, using the fictitious total cross section eliminates the need to check and compute distances to current region boundaries, resulting in a computational time saving..

5.4.1.4. *New particle position*

The particle's new and old position is related by:

$$x_{new} = x_{old} + S \, \Omega_{x_{new}}$$

$$y_{new} = y_{old} + S \, \Omega_{y_{new}}$$

$$z_{new} = z_{old} + S \, \Omega_{z_{new}}$$

The computed location is tested against the geometry boundaries to determine if the particle is still inside the geometry. If the particle is still in the geometry, the transport continues; otherwise the history terminates and a new history is started. Both the forward and adjoint methods use the same formula to compute the particle new position.

5.4.1.5. *Sampling the energy and direction following scattering events*

For the current particle energy, a cumulative probability values (CDF) are pre tabulated for all possible group-to-groups scatters for both transport modes. These cumulative probability values are used to sample the new energy group after a scattering event. Once the new to group is determined, the cosine of scattering angle is picked from a tabulated cumulative probability values for all possible cosine scattering angles for the particular group-to-group transfer (which are also precalculated). The CDF is used to determine the cosine of the scattering deflection angle, θ.

The new direction Ω_{new} is computed using the relationship between the old direction, Ω_{old}, the deflection angle, θ, and a uniformly chosen azimuthal angle, φ as described by Carter and Cashwell (Carter & Cashwell, 1975):

$$\Omega_{old} = \left(\Omega_{x_{old}}, \Omega_{y_{old}}, \Omega_{z_{old}} \right)$$

$$\Omega_{x_{new}} = \Omega_{x_{old}} Cos\theta + \frac{Sin\theta}{\sqrt{1 - \Omega_{z_{old}}^2}} \left(\Omega_{x_{old}} \Omega_{z_{old}} Cos\varphi - \Omega_{y_{old}} Sin\varphi \right)$$

$$\Omega_{y_{new}} = \Omega_{y_{old}} Cos\theta + \frac{Sin\theta}{\sqrt{1 - \Omega_{z_{old}}^2}} \left(\Omega_{y_{old}} \Omega_{z_{old}} Cos\varphi + \Omega_{x_{old}} Sin\varphi \right)$$

$$\Omega_{z_{new}} = \Omega_{z_{old}} Cos\theta + \frac{Sin\theta}{\sqrt{1 - \Omega_{z_{old}}^2}} \left(-\left[1 - \Omega_{z_{old}}^2 \right] Cos\varphi \right)$$

In Cartesian coordinates, the new direction is found using simple vector rotation. The first rotation is around the positive **y-axis** then followed by a rotation around the **z- axis**.
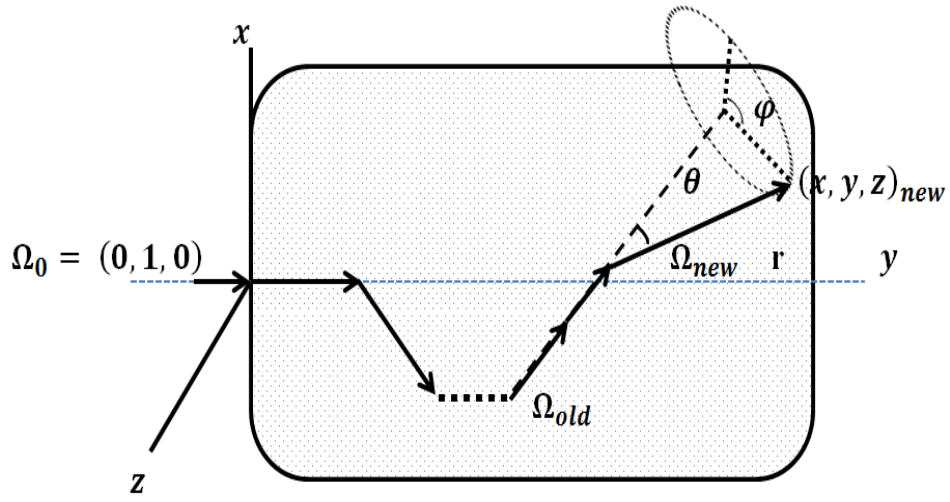
Figure 5-8 Energy and direction sampling

Chapter 6

Sample problems

To validate the computer codes developed in this project, the following testing was done:

1. A generic sample problem was defined involving an external beam source and a patient, modeled as a water cuboid with defined subregions to approximate the tumor, the brain, and the two eyes. In order to use MCNP5 multigroup option for validation, the MCNP5 12 group photon structure was employed and the Los Alamos computer code NJOY99 was used to generate the data.

2. Comparison of the 12 group data with the standard multigroup interaction cross sections was performed for hydrogen, oxygen, and water reaction rates.

3. A forward case was run with both MCNP 5 and the project code to compare the average fluxes in a vertical slice through the patient and to estimate the dose rates to the tumor and organs.

4. An adjoint case was run with both MCNP5 and the project code to compare the surface adjoint fluxes (the actual surface fluxes for MCNP5 versus the average adjoint fluxes in the top layer of voxels for the project code).

5. The surface adjoint fluxes using the project code in Step 5 were folded into the forward source used in Step 3 to implement the hybrid forward/adjoint methodology; the resulting dose rates in the tumor and the organs were compared to the doses calculated in Step 3.

The details and results of these tests are given in this chapter.

6.1. Common elements of the generic beam/patient sample problem

6.1.1. Geometry/material map

The codes require the material map be created by assigning voxel material indices to each element of a 3D (x,y,z) Cartesian grid. We can get this map either from CT data sets or built it from simple geometric shapes. For these sample problems, we defined a 50.0 cm x 50.0 cm x 50.0 cm water filled box. The box is divided into voxels of 0.5 cm x 0.5 cm x 0.5 cm, resulting in a 100x100x100 voxel grid.

The following is the used direction convention:

1. X-axis runs along the box width.
2. Y-axis runs along the box depth.
3. Z-axis runs along the box length.

The top of the box is the most negative y plane. The furthest top left corner is the minimum box point and the furthest bottom right corner is the maximum box point. Using this configuration the origin (0.0, 0.0, 0.0) is at the center of the top layer.

It is worth noting that this coordinate convention is used to describe medical images. For a set of 3-D medical images (e.g., computed tomography data) with the patient in the supine position (rested on his back) the following is the direction convention:

1. The *x-axis* runs from right to left when examining one slice of data (transverse direction) with the negative direction at patient right side and positive direction at patient left side.
2. The y-*axis* runs from top to bottom when examining one slice of data (axial direction) with the negative direction at patient bottom side (posterior position) and positive direction at patient top side (anterior position).
3. The *z-axis* follow the patient mid line with the positive direction is at the patient superior end (head) and the negative direction is at the patient inferior end (feet).

6.1.2. Radiation (forward) source

6.1.2.1. *Source energy*

The source is a photon polyenergetic source produced by a medical linear accelerator. The source distribution has a very well defined spectrum published by several authors. The source energy is designated as 6 MeV or 18 MeV. Source strength is defined at 100.00 cm away from source at a reference depth and field size (for a linear accelerator that is calibrated using source to phantom surface distance (**SSD**) method - a common calibration method - is 1.0 cGy / monitor unit at the selected energy maximum depth and 10.0 cm x 10 cm field size).

Varian 6 MeV medical linear accelerator photon spectrum as published by (Sheikh-Bagheri & Rogers, 2002). The following are a plot and listing for the spectrum distribution of the Varian 6 MeV photon beam:
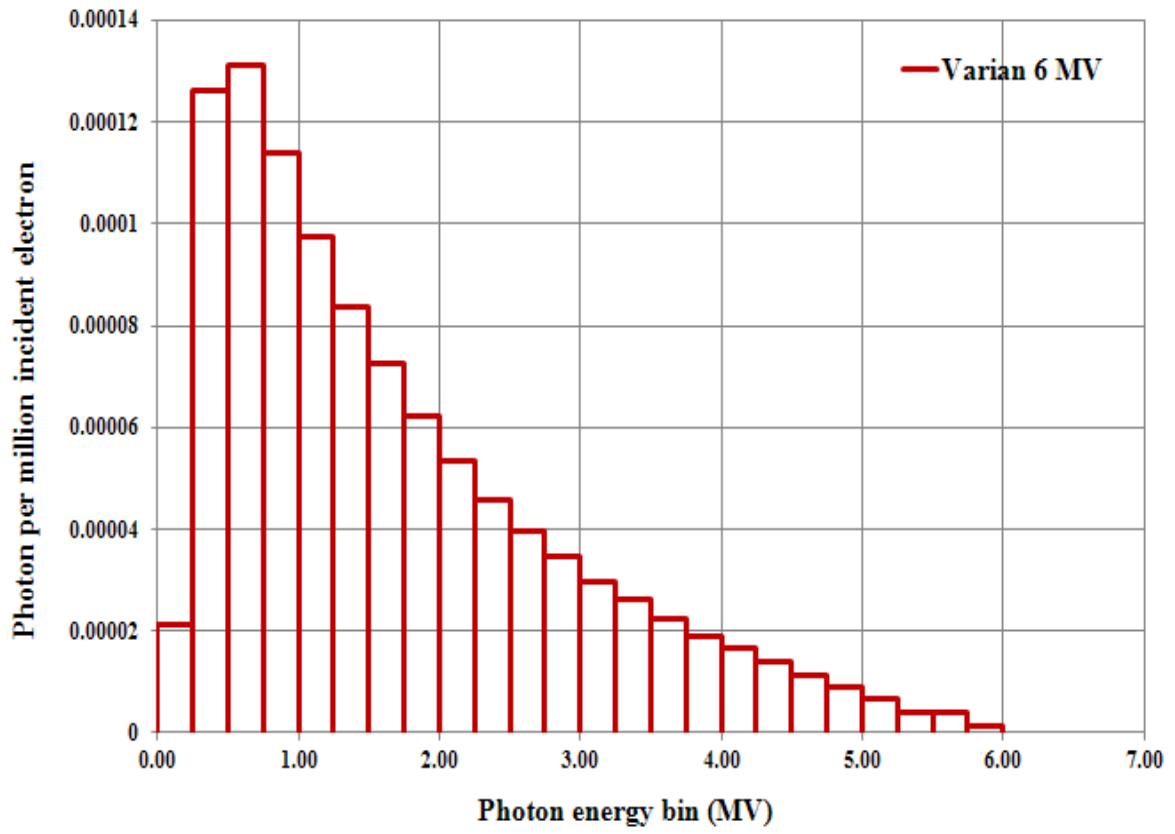
Figure 6-1 Varian 6 MeV published spectra

Table 6-1 Varian 6 MeV published spectra

Gamma Group #	Energy Bin Upper Bound (MeV)	Photons per MeV incident electrons	PDF
1	0.25	2.14E-05	0.020530
2	0.50	1.26E-04	0.120877
3	0.75	1.31E-04	0.125674
4	1.00	1.14E-04	0.109365
5	1.25	9.76E-05	0.093632
6	1.50	8.36E-05	0.080201
7	1.75	7.25E-05	0.069552
8	2.00	6.23E-05	0.059767
9	2.25	5.35E-05	0.051325
10	2.50	4.59E-05	0.044034
11	2.75	3.95E-05	0.037894
12	3.00	3.47E-05	0.033289
13	3.25	2.98E-05	0.028588
14	3.50	2.61E-05	0.025039
15	3.75	2.25E-05	0.021585
16	4.00	1.91E-05	0.018323
17	4.25	1.66E-05	0.015925
18	4.50	1.38E-05	0.013239
19	4.75	1.14E-05	0.010937
20	5.00	9.04E-06	0.008672
21	5.25	6.55E-06	0.006284
22	5.50	4.09E-06	0.003924
23	5.75	1.40E-06	0.001343
24	6.00	4.34E-08	0.000042
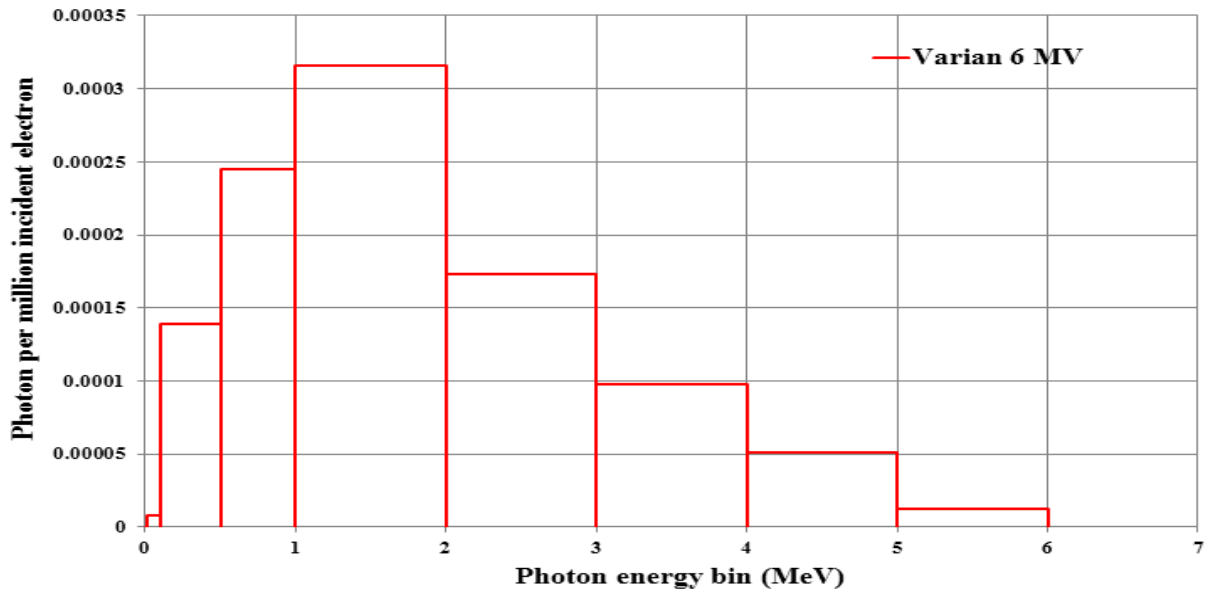
Figure 6-2 Varian 6 MeV spectra adjusted to MCNP5-MGXSNP structure

Table 6-2 Varian 6 MeV spectra adjusted to MCNP5-MGXSNP structure

Gamma Group #	Energy Bin Upper Bound (MeV)	Photons per MeV incident electrons	PDF
1	0.010	0.000000	0.000000
2	0.100	8.025E-06	0.007698
3	0.500	1.394E-04	0.133707
4	1.000	2.450E-04	0.235028
5	2.000	3.160E-04	0.303138
6	3.000	1.736E-04	0.166534
7	4.000	9.750E-05	0.093532
8	5.000	5.084E-05	0.048771
9	6.000	1.208E-05	0.011591

Note: The photons are produced as a result of slowing down electrons in a tungsten target (bremsstrahlung spectrum). The produced bremsstrahlung spectrum is forwardly peaked and is collimated to produce a maximum square field of 40.0 cm x 40.0 cm at 100.0 cm downstream from the target. The energy upper bound is in MeV and the PDF will be used to model the source distribution in MCNP5.

6.1.2.2. Source position and direction

The physical source used in actual radiation treatment can be at any position around the phantom / patient via simple source rotation. The radiation field boundary (field size) is defined at 100.0 cm away from the source by either a set of jaws and / or by multi leaf collimator. The outer radiation field shape can be squares or rectangles by adjusting the jaws from 1.0 cm x 1.0 cm up to 40.0 cm x 40.0 cm. The inner field shape can is modified using multi leaf collimator to further collimate the shape of the radiation field to conform to desired targets.

For a coplanar (same - one – plane normally designated XY) beam arrangement we will have one plane (X-Y). For each beam we will always have one central axis (CAX) and iso-center (machine physical center and treatment center). This illustrated in the Figure below:
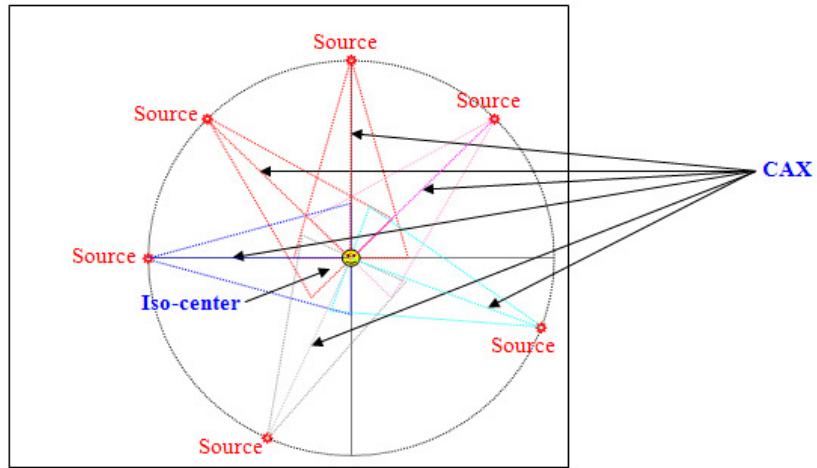
Figure 6-1 Coplanar beam arrangement

The following is an illustration of source position around the phantom:
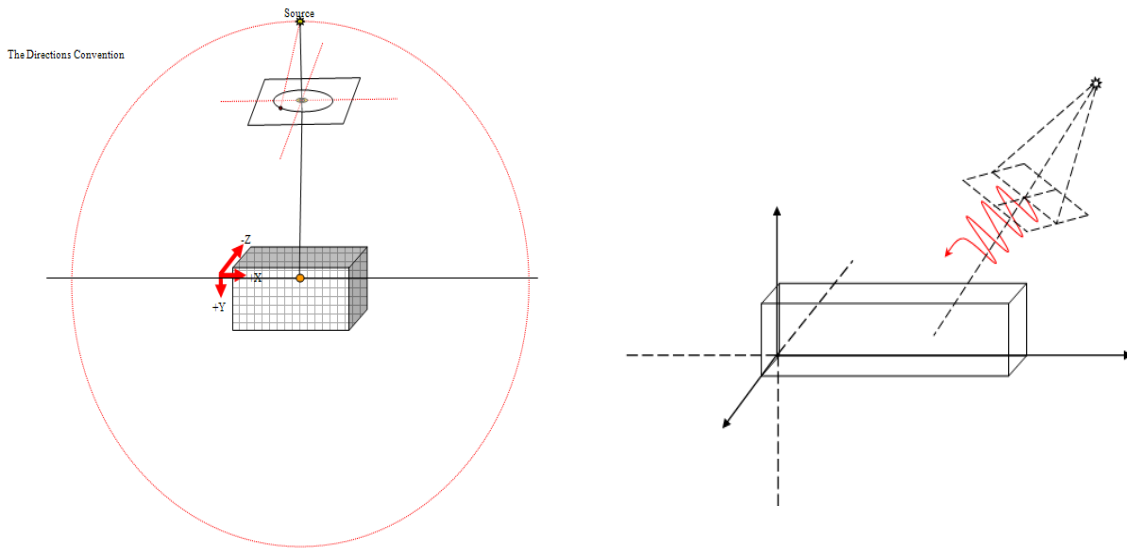
Figure 6-2 Source position around phantom

For these sample calculations, the source is positioned at 100.00 cm directly above the water box center. The particles travel straight down and limited to ~ 11.30993 cone from the source. The following is illustration of the coordinate convention used throughout the code.
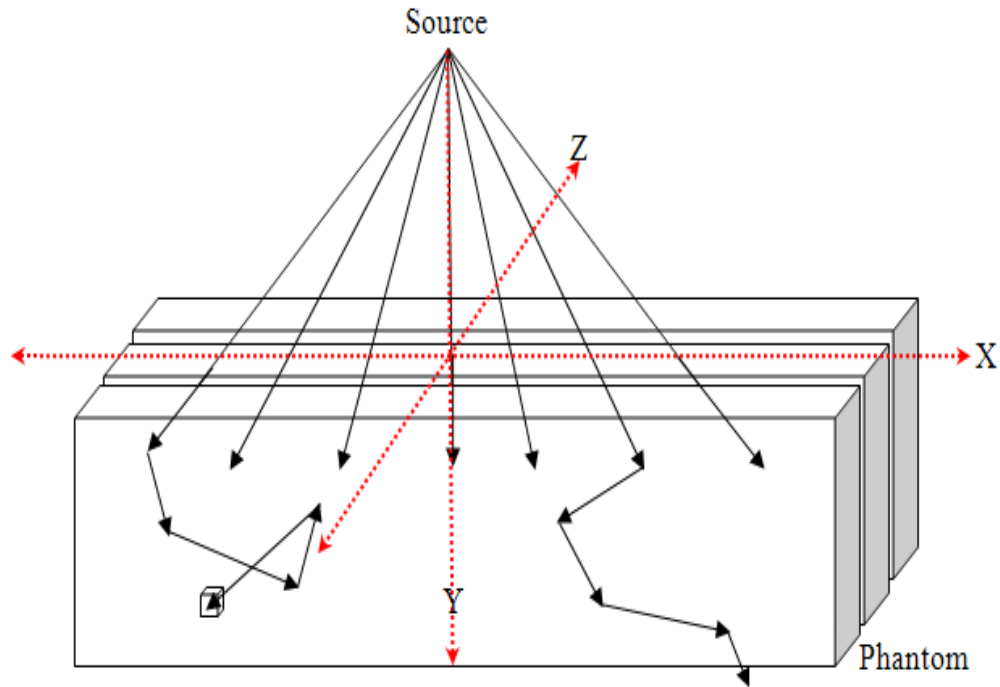
Figure 6-3 Problem coordinate convention

6.1.2.3. Source shaping

The forward source simulates the linear accelerator jaws by defining a 10.0 cm x 10.0 cm square field projected on the top of the water box. This is model in MCNP5 by creating two 0.001 cm thick void cells covering the entire water box surface. The result is a very thin 10.0 cm x 10.0 cm void window centered above the water box. The photon particle importance is set to 1 inside the window and 0 outside the window.

6.1.3. Simple geometrical region of interest (box)

This sample problem a simple region of interest in shape of a small box (for which the dose is desired) was defined inside the water box. The following is the geometric description of this region of interest:

A. **Shape:** Box.

B. **Size:** 1.5 cm x 1.5 cm x 1.5 cm.

C. **Location:** The box is centered at (0.25, 5.75, 0.25), the X-range & Z-range = [-0.50, 1.0] and the Y-range = [5.0, 6.5].

Pixel8 code will calculate surface crossings at each surface pixel. The surface crossings are separated in position, direction and energy. These separations in position (deltas in each surface direction) and direction (igloo zone division) are specified in the problem input file.

6.1.4. Patient regions of interest

In the sample problems, inside the water box, four regions of interest (for which the dose is desired) were defined: Tumor, Right eye, Left eye, and Brain. The following is the geometric description of each structure:

1. Tumor:

   D. **Shape:** Sphere.

   E. **Size:** Sphere radius = 3 pixels (1.5 cm).

   F. **Location:** The sphere starts on slice 55 and end at slice 60. The sphere center is at the end of slice 57 and at the end of 59th x-pixel and 30th y-pixel placing the structure geometric center at (4.5, 15.0, 3.0) cm.

2. Right Eye:

   A. **Shape:** Sphere.

   B. **Size:** Sphere radius = 7 pixels (3.5 cm).

   C. **Location:** The sphere starts on slice 44 and end at slice 57. The sphere center is at the end of slice 50 and at the end of the 36th x-pixel and 8th y-pixel placing the structure geometric center at (-7.0, 4.0, 0.0) cm.

3. Left Eye:

   A. **Shape:** Sphere.

   B. **Size:** Sphere radius = 7 pixels (3.5 cm).

   C. **Location:** The sphere starts on slice 44 and end at slice 57. The sphere center is at the end of slice 50 and at the end of the 64th x-pixel and 8th y-pixel placing the structure geometric center at (7.0, 4.0, 0.0) cm.

4. Brain:

   A. **Shape**: Three rectangular boxes combine to make the final structure.

   B. **Size**:

i.   Box one: width = 40 pixels (20.0 cm) and height = 25 pixels (12.5 cm) and length = 20 pixels (10.0 cm).

ii. Box two: width = 40 pixels (20.0 cm) and height = 15 pixels (7.5 cm) and length = 14 pixels (7.0 cm).

iii. Box three: width = 40 pixels (20.0 cm) and height = 55 pixels (27.5 cm) and length = 13 pixels (6.5 cm).

C.   **Location**:

i.   Box one: Starts at end of slice 32 (z = -9.0 cm) and ends at the end of slice 52 (z =1.0 cm), the box top x & y pixel 30 (x = -10.0 cm) & 34 (y = 17.0 cm) and the box lower x & y pixel 70 (x = 10.0 cm) & 59 (y = 29.5 cm).

ii. Box two: Starts at the end of slice 52 (z = 1.0 cm) and ends at slice 66 (z = 8.0 cm), the box top x & y pixel 30 (x=-10.0cm) & 42 (y = 21.0 cm) and the box lower x & y pixel 70 (x = 10.0 cm) & 57 (y = 28.5 cm).

iii. Box three: Starts at the end of slice 66 (z = 8.0 cm) and ends at slice 80 (z = 15.0 cm), the box top x & y pixel 30 (x = -10.0 cm) & 7 (y = 3.5 cm) and the box lower x & y pixel 70 (x = 10.0 cm) & 62 (y = 31.0 cm).

Table 6-3 and Table 6-4 summarize the pixel locations of these brain structures and the corresponding actual *(x,y,z)* dimensions.

Table 6-3 Summary of the brain components pixel location

	X_{min} Pixel	X_{max} Pixel	Y_{min} Pixel	Y_{max} Pixel	Z_{min} Pixel	Z_{max} Pixel
Box one	30	70	34	59	32	52
Box two	30	70	42	57	52	66
Box three	30	70	7	62	66	80

Table 6-4 Summary of the brain components actual location

	X_{min} cm	X_{max} cm	Y_{min} cm	Y_{max} cm	Z_{min} cm	Z_{max} cm
Box one	-10.0	10.0	17.0	29.5	-9.0	1.0
Box two	-10.0	10.0	21.0	28.5	1.0	8.0
Box three	-10.0	10.0	3.5	31.0	8.0	15.0

Figure 6-4 gives a pictorial representation of the location of the regions of interest in the sample problems.
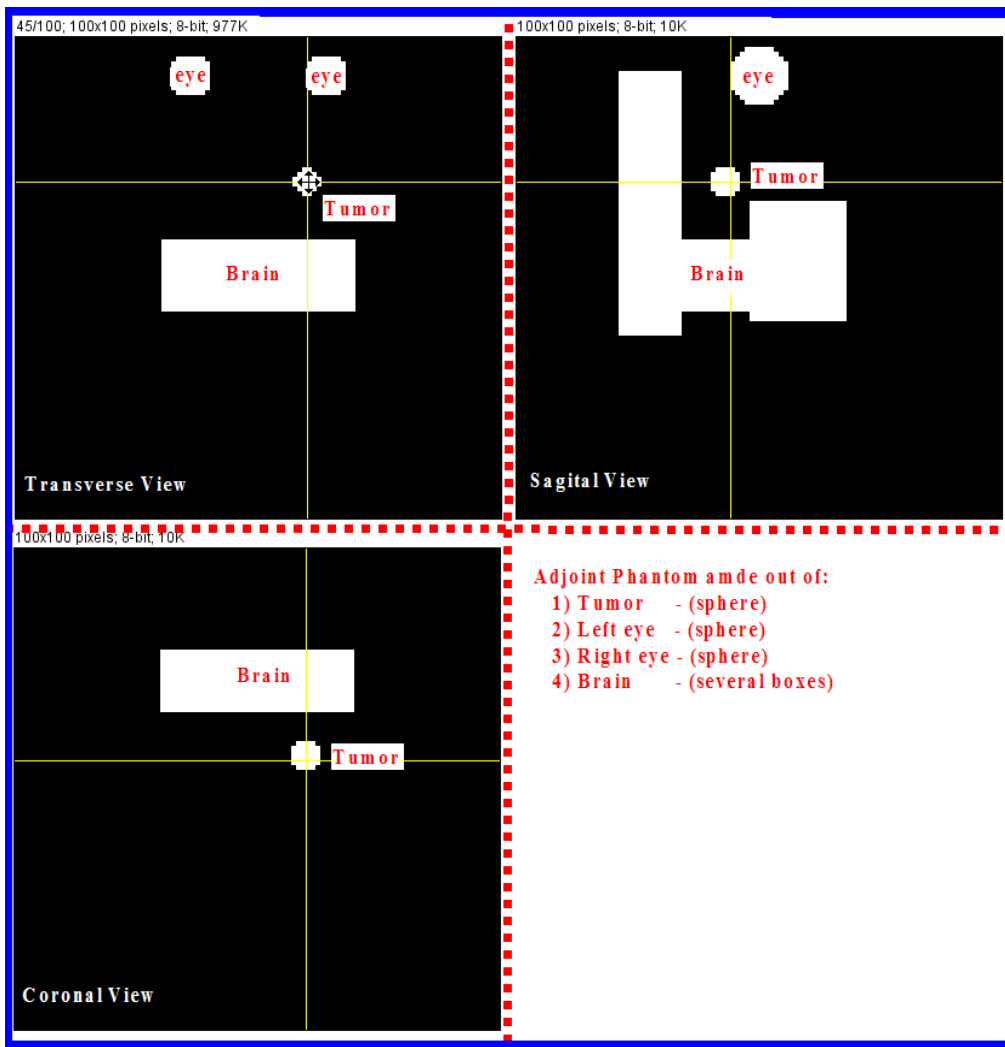
Figure 6-4 Plots of location of the regions of interest in the sample problems

6.1.5. Response function (adjoint source spectrum)

The response function used for the forward dose calculation (by multiplying by flux contributions in the regions as particles collide in them) and also for the initial adjoint source photon spectrum was created for the sample problems by numerically integrating a published Varian 6 MeV response function (shown in Table 6-5) over the 12-group structure used in the sample problems. The resulting 12-group response function is given in Table 6-6 Varian 6 MeV photon Response function (MCNP5-MGXSNP)Table 6-6,

Table 6-5 Varian 6 MeV response function (published structure)

Gamma Group #	Energy bin upper bound (MeV)	Response Function (cGy-cm^2)
1	0.25	5.23780E-10
2	0.50	1.50459E-09
3	0.75	2.60158E-09
4	1.00	3.54905E-09
5	1.25	4.37346E-09
6	1.50	5.11610E-09
7	1.75	5.79888E-09
8	2.00	6.44136E-09
9	2.25	7.01251E-09
10	2.50	7.59904E-09
11	2.75	8.09581E-09
12	3.00	8.58734E-09
13	3.25	9.10125E-09
14	3.50	9.55186E-09
15	3.75	9.99510E-09
16	4.00	1.04792E-08
17	4.25	1.09187E-08
18	4.50	1.13250E-08
19	4.75	1.18073E-08
20	5.00	1.22876E-08
21	5.25	1.27357E-08
22	5.50	1.31545E-08
23	5.75	1.35449E-08
24	6.00	1.39088E-08

Table 6-6 Varian 6 MeV photon Response function (MCNP5-MGXSNP)

Gamma Group #	Energy bin upper bound (MeV)	Response Function (cGy-cm^2)
1	0.010	3.12689E-10
2	0.100	9.90001E-10
3	0.500	3.00098E-09
4	1.000	5.29621E-09
5	2.000	7.76637E-09
6	3.000	9.74813E-09
7	4.000	1.15586E-08
8	5.000	1.33190E-08
9	6.000	1.49516E-08

6.2. Verification of 12-group data from NJOY99

The Pixel8 and Voxel8 programs use groupwise interaction and heat deposition cross sections produced by the Los Alamos NJOY99 code, which gets its basic energy-dependent cross sections from the readily available evaluated nuclear data format (ENDF) data files.

To verify the data used in the sample calculations, a comparison was made between multi-group microscopic cross sections generated by NJO99 and multigroup cross sections data extracted from the MCNP-MGXSNP cross sections files provided with the MCNP5 code for hydrogen (1000.01g) and oxygen (8000.01g).

The following reactions were extracted for each of the isotopes:

1. Total cross section (MT = 501).
2. Coherent scattering cross section (MT = 502).
3. Incoherent scattering cross section (MT = 504).
4. Pair production cross section (MT = 516).

Table 6-7 through Table 6-14 show the comparison between the given reaction rates for the two isotopes. The comparison for the first three reactions (i.e., excluding pair production) is excellent, with only a single value with an error above 1%, this being in the lowest energy group for oxygen (probably due to a difference in the physical models for treating low energy photon reactions like fluorescence and Bremsstrahlung). Larger difference are seen for the pair

production cross sections, but the absolute values of the cross section indicate that this reaction is just a few percent of the scattering cross section for the energy groups with high errors; the effect of these differences on the dose calculation should be small.

In summary, this comparison indicates that NJOY99 is being used correctly to create the cross sections.

Table 6-7 Hydrogen MCNP5 versus NJOY99 microscopic total cross section

Gamma Group #	Energy Bin Upper Bound (MeV)	MCNP	NJOY99	Compare % Difference
1	20	4.99585E-02	5.00082E-02	0.10%
2	9	6.03208E-02	6.03286E-02	0.01%
3	8	6.53167E-02	6.52400E-02	0.12%
4	7	7.16049E-02	7.15598E-02	0.06%
5	6	7.97787E-02	8.00025E-02	0.28%
6	5	9.07175E-02	9.05768E-02	0.16%
7	4	1.06286E-01	1.06199E-01	0.08%
8	3	1.30708E-01	1.31149E-01	0.34%
9	2	1.77736E-01	1.78039E-01	0.17%
10	1	2.49298E-01	2.49748E-01	0.18%
11	0.5	3.91364E-01	3.92704E-01	0.34%
12	0.1	5.25555E-01	5.26634E-01	0.21%

Table 6-8 Hydrogen MCNP5 versus NJOY99 microscopic coherent cross

Gamma Group #	Energy Bin Upper Bound (MeV)	MCNP	NJOY99	Compare % Difference
1	20	3.67705E-08	3.69064E-08	0.37%
2	9	6.45139E-08	6.47800E-08	0.41%
3	8	8.31110E-08	8.32596E-08	0.18%
4	7	1.10860E-07	1.11264E-07	0.36%
5	6	1.55268E-07	1.55795E-07	0.34%
6	5	2.33669E-07	2.34701E-07	0.44%
7	4	3.91946E-07	3.92837E-07	0.23%
8	3	7.93448E-07	7.95408E-07	0.25%
9	2	2.50979E-06	2.51490E-06	0.20%
10	1	1.00438E-05	1.00622E-05	0.18%
11	0.5	1.38648E-04	1.38525E-04	0.09%
12	0.1	1.23532E-03	1.23971E-03	0.36%

Table 6-9 Hydrogen MCNP5 versus NJOY99 microscopic incoherent cross section

Gamma Group #	Energy Bin Upper Bound (MeV)	MCNP	NJOY99	Compare % Difference
1	20	4.62183E-02	4.62297E-02	0.02%
2	9	5.76170E-02	5.75353E-02	0.14%
3	8	6.29983E-02	6.28132E-02	0.29%
4	7	6.96547E-02	6.95146E-02	0.20%
5	6	7.81807E-02	7.83742E-02	0.25%
6	5	8.95164E-02	8.93816E-02	0.15%
7	4	1.05534E-01	1.05450E-01	0.08%
8	3	1.30377E-01	1.30810E-01	0.33%
9	2	1.77687E-01	1.77988E-01	0.17%
10	1	2.49288E-01	2.49738E-01	0.18%
11	0.5	3.91225E-01	3.92565E-01	0.34%
12	0.1	5.24300E-01	5.25375E-01	0.21%

Table 6-10 Hydrogen MCNP5 versus NJOY99 microscopic pair production cross section

Gamma Group #	Energy Bin Upper Bound (MeV)	MCNP	NJOY99	Compare % Difference
1	20	3.74025E-03	3.77851E-03	1.02%
2	9	2.70373E-03	2.79315E-03	3.31%
3	8	2.31837E-03	2.42670E-03	4.67%
4	7	1.95005E-03	2.04504E-03	4.87%
5	6	1.59786E-03	1.62819E-03	1.90%
6	5	1.20084E-03	1.19499E-03	0.49%
7	4	7.52261E-04	7.48357E-04	0.52%
8	3	3.30758E-04	3.37645E-04	2.08%
9	2	4.64079E-05	4.90613E-05	5.72%
10	1			
11	0.5			
12	0.1			

Table 6-11 Oxygen MCNP5 versus NJOY99 microscopic total cross section

Gamma Group #	Energy Bin Upper Bound (MeV)	MCNP	NJOY99	Compare % Difference
1	20	5.31021E-01	5.32199E-01	0.22%
2	9	5.84892E-01	5.87139E-01	0.38%
3	8	6.13464E-01	6.15308E-01	0.30%
4	7	6.52282E-01	6.54401E-01	0.32%
5	6	7.06066E-01	7.08486E-01	0.34%
6	5	7.79676E-01	7.78503E-01	0.15%
7	4	8.87199E-01	8.86891E-01	0.03%
8	3	1.06334E+00	1.06838E+00	0.47%
9	2	1.42449E+00	1.42848E+00	0.28%
10	1	1.99643E+00	2.00133E+00	0.25%
11	0.5	3.17376E+00	3.18718E+00	0.42%
12	0.1	5.16900E+00	5.24894E+00	1.55%

Table 6-12 Oxygen MCNP5 versus NJOY99 microscopic coherent cross

Gamma Group #	Energy Bin Upper Bound (MeV)	MCNP	NJOY99	Compare % Difference
1	20	1.33662E-05	1.33169E-05	0.37%
2	9	2.34510E-05	2.33750E-05	0.32%
3	8	3.02112E-05	3.00441E-05	0.55%
4	7	4.02979E-05	4.01478E-05	0.37%
5	6	5.64608E-05	5.62157E-05	0.43%
6	5	8.49860E-05	8.46867E-05	0.35%
7	4	1.42551E-04	1.41744E-04	0.57%
8	3	2.88128E-04	2.86987E-04	0.40%
9	2	9.10674E-04	9.07008E-04	0.40%
10	1	3.63765E-03	3.62853E-03	0.25%
11	0.5	4.86921E-02	4.86863E-02	0.01%
12	0.1	3.72903E-01	3.75561E-01	0.71%

Table 6-13 Oxygen MCNP5 versus NJOY99 microscopic incoherent cross section

Gamma Group #	Energy Bin Upper Bound (MeV)	MCNP	NJOY99	Compare % Difference
1	20	3.69741E-01	3.70044E-01	0.08%
2	9	4.60928E-01	4.60544E-01	0.08%
3	8	5.03975E-01	5.02794E-01	0.23%
4	7	5.57223E-01	5.56428E-01	0.14%
5	6	6.25425E-01	6.27338E-01	0.31%
6	5	7.16099E-01	7.15436E-01	0.09%
7	4	8.44214E-01	8.44035E-01	0.02%
8	3	1.04263E+00	1.04698E+00	0.42%
9	2	1.42077E+00	1.42434E+00	0.25%
10	1	1.99253E+00	1.99743E+00	0.25%
11	0.5	3.10977E+00	3.12266E+00	0.41%
12	0.1	4.06360E+00	4.07110E+00	0.18%

Table 6-14 Oxygen MCNP5 versus NJOY99 microscopic pair production cross section

Gamma Group #	Energy Bin Upper Bound (MeV)	MCNP	NJOY99	Compare % Difference
1	20	1.61263E-01	1.62139E-01	0.54%
2	9	1.23936E-01	1.26567E-01	2.12%
3	8	1.09453E-01	1.12478E-01	2.76%
4	7	9.50131E-02	9.79258E-02	3.07%
5	6	8.05781E-02	8.10834E-02	0.63%
6	5	6.34832E-02	6.29717E-02	0.81%
7	4	4.28291E-02	4.26991E-02	0.30%
8	3	2.04069E-02	2.10853E-02	3.32%
9	2	2.75718E-03	3.17661E-03	15.21%
10	1			
11	0.5			
12	0.1			

6.3. Sample problem 1: Forward case

The first full calculation is a forward calculation that uses the beam source impinging straight down onto the top of the patient box. The problem was run with both Voxel8 and MCNP5 in multigroup mode. For comparison of the results, both of them captured a vertical "slice" 2D flux map through the center of the water box at $z = 0.5\ cm$. Figure 6-5 shows the resulting flux map for the MCNP5 calculation and Figure 6-6 shows the equivalent map for the Voxel8 calculation. The MCNP5 and Voxel8 maps were compared using three points maximum, minimum, and weighted average. Table 6-15 gives a summary of this comparison. The position for the maximum and minimum points was determined from the MCNP5 calculation. Then the corresponding Voxel8 calculation location values were looked up and compared to the MCNP5 result. The weighted average was calculated for each map using a frequency table. When the comparison point is in the useful beam area (i.e. maximum point and along beam central axis up to a depth 0f 25 cm) these results show good agreement between MCNP5 and Voxel8 calculation. Larger differences are found at the peripheries due to small quantity of scattered photons arriving at these locations. These locations are not useful clinically and can be ignored. Reduction in the large differences can be achieved by implementing more variance reduction

techniques (i.e. the population control method such as geometry splitting and Russian Roulette, or modified sampling methods such as forced collisions). Russian Roulette was implemented in the Voxel8 code but not the forced collision method. Forced collision can be implemented at end of particle history. The voxels along the ray from the end of history location to the boundary are determined. Then contribution to each voxel is made based on the probability of a particle arriving at the voxel.
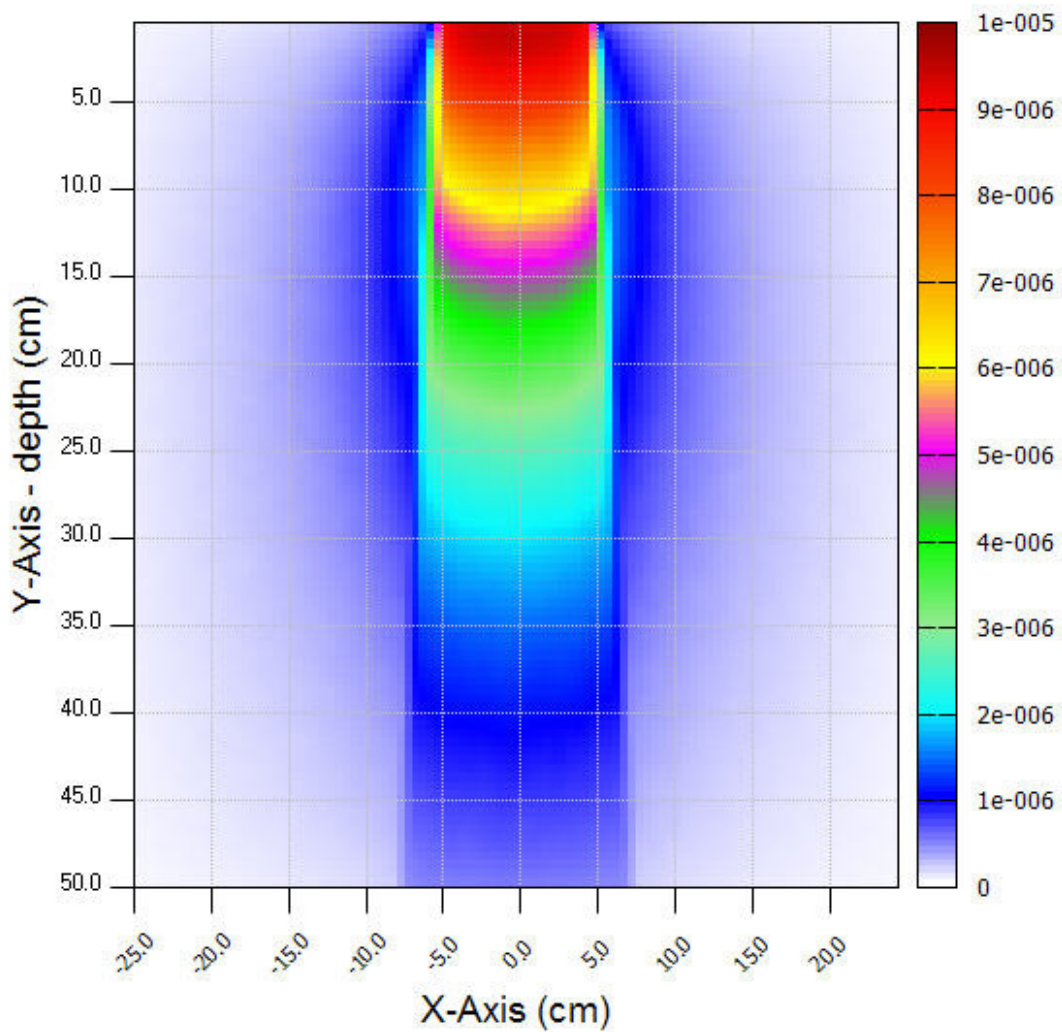
Figure 6-5 MCNP5 flux map for forward problem (per source particle)
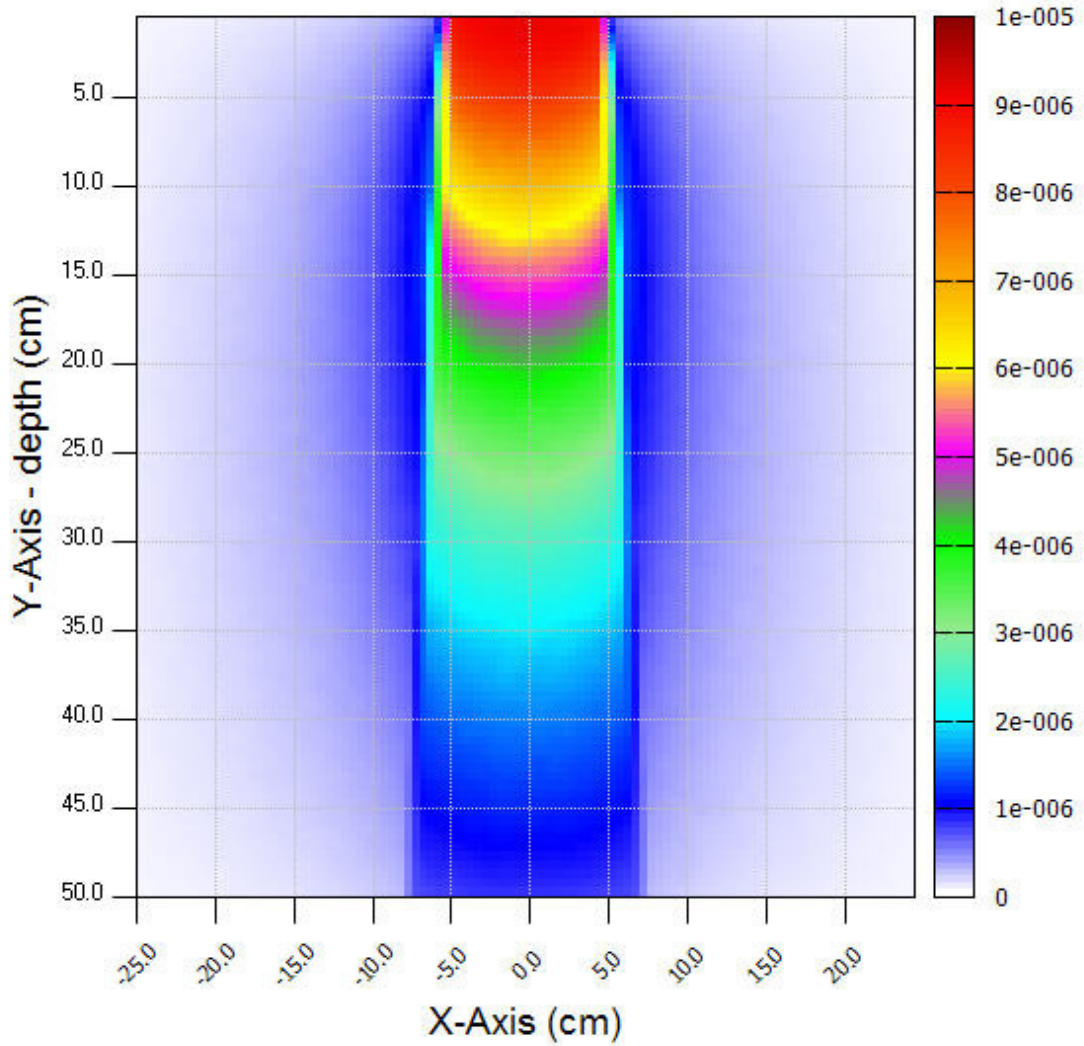
Figure 6-6 Voxel8 flux map for forward problem (per source particle)

Table 6-15 Summary of Results for forward problem

Value	Fluence (1/cm^2)		
	MCNP5	**Voxel8**	**Difference%**
Maximum (0.75, 0.75)	9.44794E-06 +/- 0.403%	9.132354E-06 +/- 0.525%	3.40%
Minimum (24.25,49.75)	2.37421E-08 +/- 7.63%	2.9403903E-08 +/- 7.57%	21.31%
Weighted Average	1.071899E-06 +/- 2.32%	1.114044E-06 +/- 2.88%	3.86%
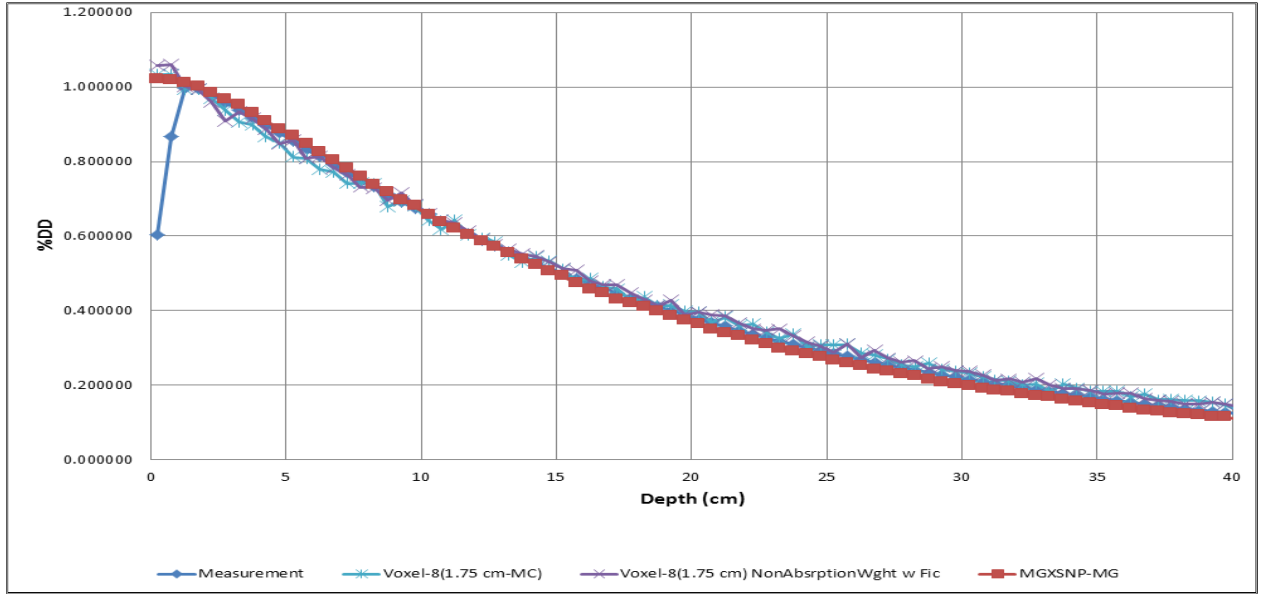
Figure 6-7 Normalized forward flux along CAX for measurement, MCNP5 & Voxel8

6.4. Sample problem 2: Adjoint case

The second set of calculations was adjoint calculations for a simple box and for the four structures of interest as defined in Section 6.1: Tumor, right eye, left eye, and brain. For each of these cases, a 2D map of the surface adjoint fluxes on the top surface were compared for both Pixel8 and MCNP5 in multigroup mode. The following figures and table document the results:

1. For the box region, Figure 6-8and Figure 6-9 give the resulting maps, with Table 6-16 showing a comparison of the maximum, minimum and weighted average values in the map.

2. For the tumor region, Figure 6-10 and Figure 6-11 give the resulting maps, with Table 6-17 showing a comparison of the maximum, minimum and weighted average in the map.

3. For the right eye region, Figure 6-12 and Figure 6-13 give the resulting maps, with Table 6-18 showing a comparison of the maximum, minimum and weighted average values in the map.

4. For the left eye region, Figure 6-14 and Figure 6-15 give the resulting maps, with Table 6-19 showing a comparison of the maximum, minimum and weighted average values in the map.

5. For the brain region, Figure 6-16 and Figure 6-17 give the resulting maps, with Table 6-20 showing a comparison of the maximum, minimum and weighted average values in the map.

These results show the following:

1. For the simple box region adjoint multigroup MCNP5 and Pixel8 calculation showed excellent agreement. The largest deviation was at the minimum value with a pixel location that is not clinically significant. This large deviation is due to the low number of particles arriving at the pixel. Reduction in the deviation can be achieved by implementing further variance reduction techniques. The visible large dose pixels that appear in the Pixel8 plot are due to the adjoint weights becoming greater than one after scattering event. The Pixel8 algorithm did not employ any population control variance reduction technique such as

weight window. Implementing such variance reduction techniques will reduce these deviations.

2. For the tumor region adjoint multigroup MCNP5 and Pixel8 calculation showed a maximum deviation of 10.39%. The largest deviation was at the minimum value. Again the minimum value location is not clinically significant. This large deviation is due to the low number of particles arriving at the pixel. The deviation at the maximum point is attributed to structure pixilation, possible geometrical positioning error and coding error that we could not find at the time of dissertation writing. Again the visible large dose pixels appear and they are attributed to the reason given above.

3. For the right eye region adjoint multigroup MCNP5 and Pixel8 calculation showed a maximum deviation of 11.00%. The largest deviation was at the minimum value which is at a location that is not clinically significant and due to the low number of particles arriving at the pixel location. The deviation at the maximum point is attributed to structure pixilation, possible geometrical positioning error and coding error that we could not find at the time of dissertation writing. Again the visible large dose pixels appear and they are attributed to the reason given above.

4. For the left eye region adjoint multigroup MCNP5 and Pixel8 calculation showed better agreement at the maximum point within 1.00%. The largest deviation was at the minimum value which is at a location that is not clinically significant and due to the low number of particles arriving at the pixel location. Again the visible large dose pixels appear and they are attributed to the reason given above.

5. For the complicated and large brain region adjoint multigroup MCNP5 and Pixel8 calculation showed large deviations. The deviations are attributed to structure pixilation, a discovered geometrical error and possible coding error that we could not find at the time of dissertation writing. Again the visible large dose pixels appear and they are attributed to the reason given above.

The weighted average value was computed from a generated frequency table of the 2D map.
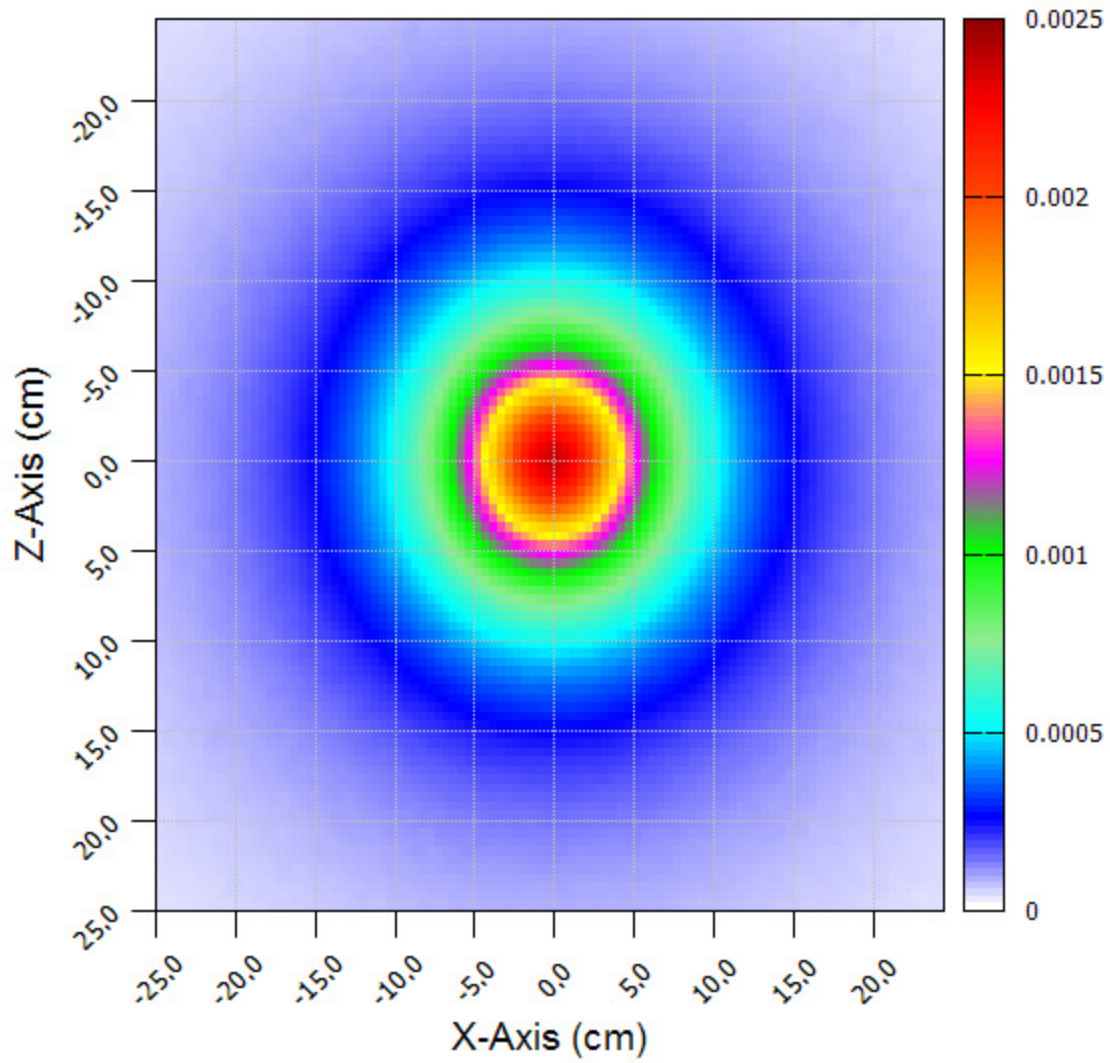
Figure 6-8 MCNP5 surface flux map for adjoint problem: Box
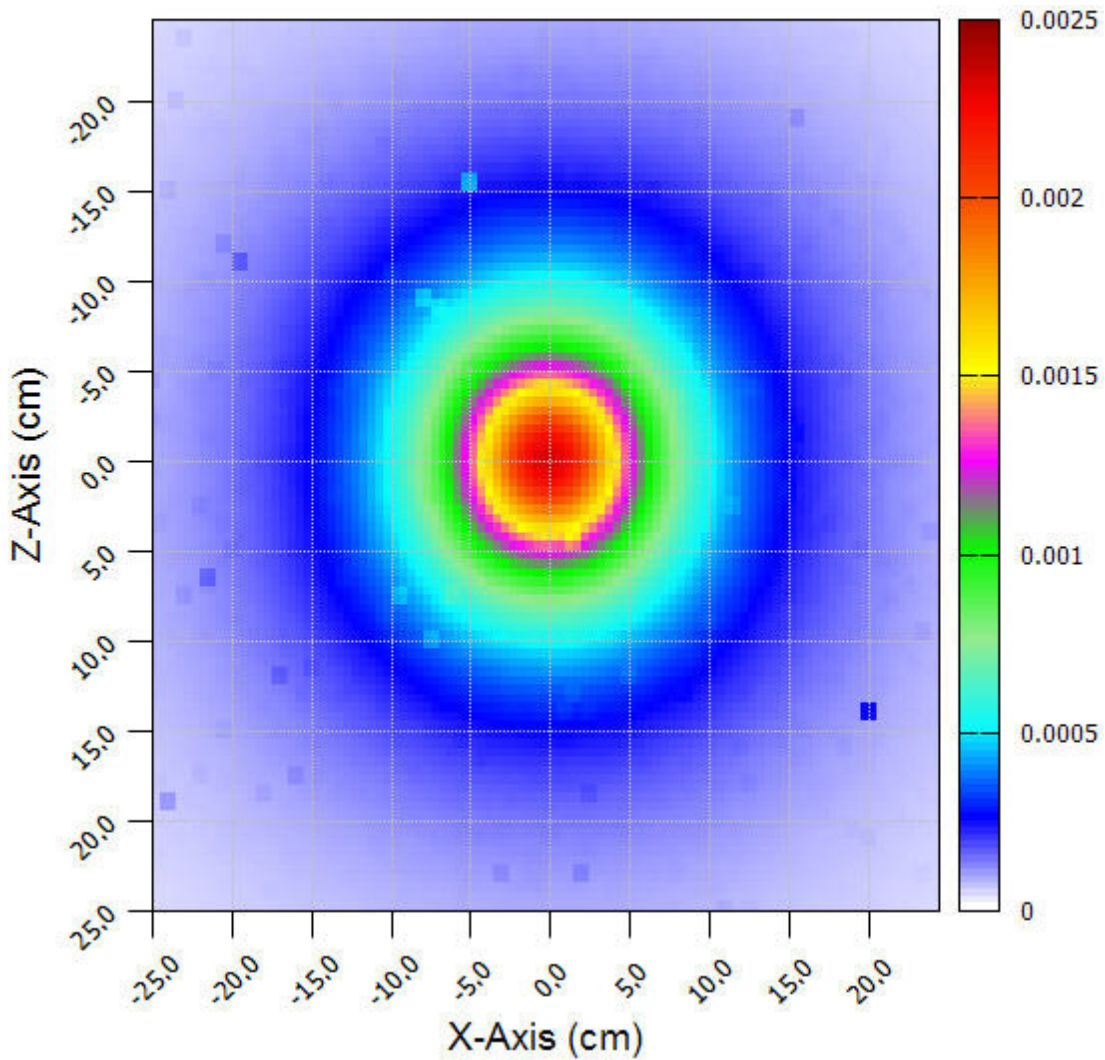
Figure 6-9 Pixel8 surface flux map for adjoint problem: Box

Table 6-16 Summary of Results for adjoint problem: Box

Value	Fluence (cGy/cm^2)		% Difference
	MCNP5	Pixel8	
Maximum (0.25,0.25)	2.36865E-03 +/- 0.297%	2.33172E-03 +/- 0.222%	1.57%
Minimum (-24.75, 24.75)	2.80921E-05 +/- 5.505%	3.46025E-05 +/- 3.078%	20.77%
Weighted Average	2.81394E0-4 +/- 2.503%	2.83882E-04 +/- 0.88%	0.88%
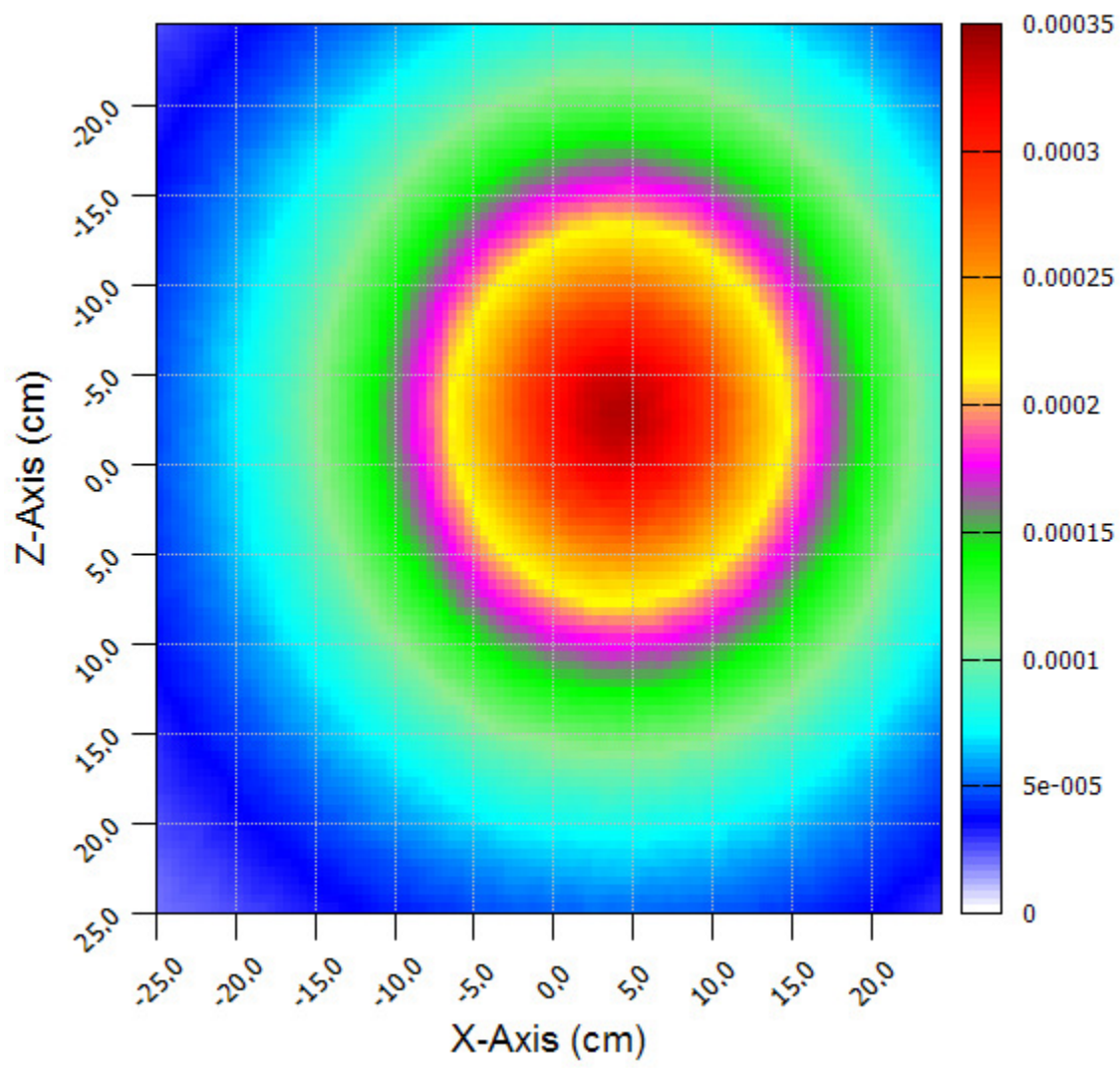
Figure 6-10 MCNP5 surface flux map for adjoint problem: Tumor
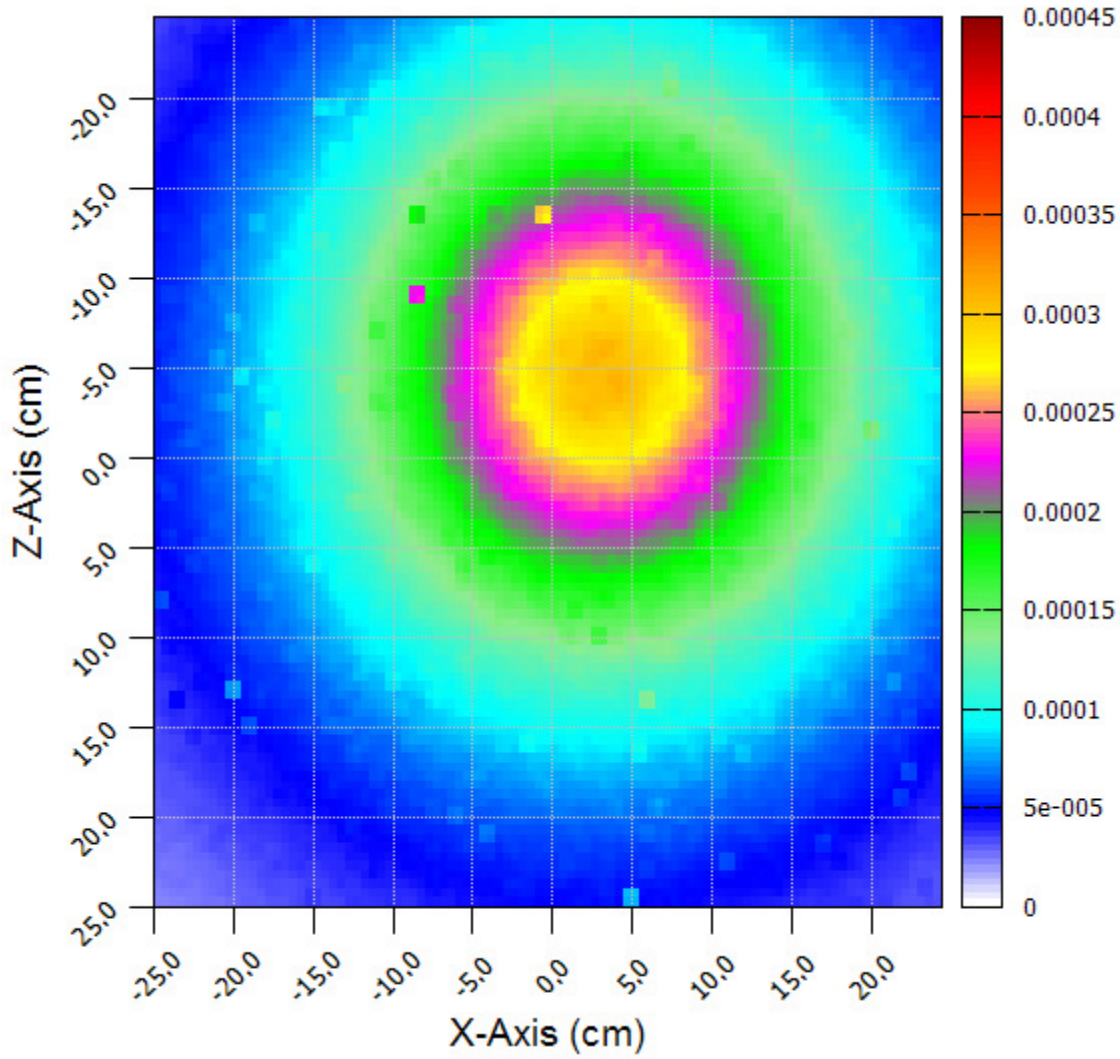
Figure 6-11 Pixel8 surface flux map for adjoint problem: Tumor

Table 6-17 Summary of Results for adjoint problem: Tumor

Value	Fluence (1/cm^2)		% Difference
	MCNP5	Pixel8	
Maximum (3.75,2.75)	3.23942E-04 +/- 0.858%	3.04541E-04 +/- 2.30%	6.17%
Minimum (-24.25,-24.75)	1.84468E-5 +/- 4.903%	2.04679E-05 +/- 5.770%	10.39%
Weighted Average	1.15757E-04 +/- 2.381%	1.12671E-04 +/- 4.219%	2.70%
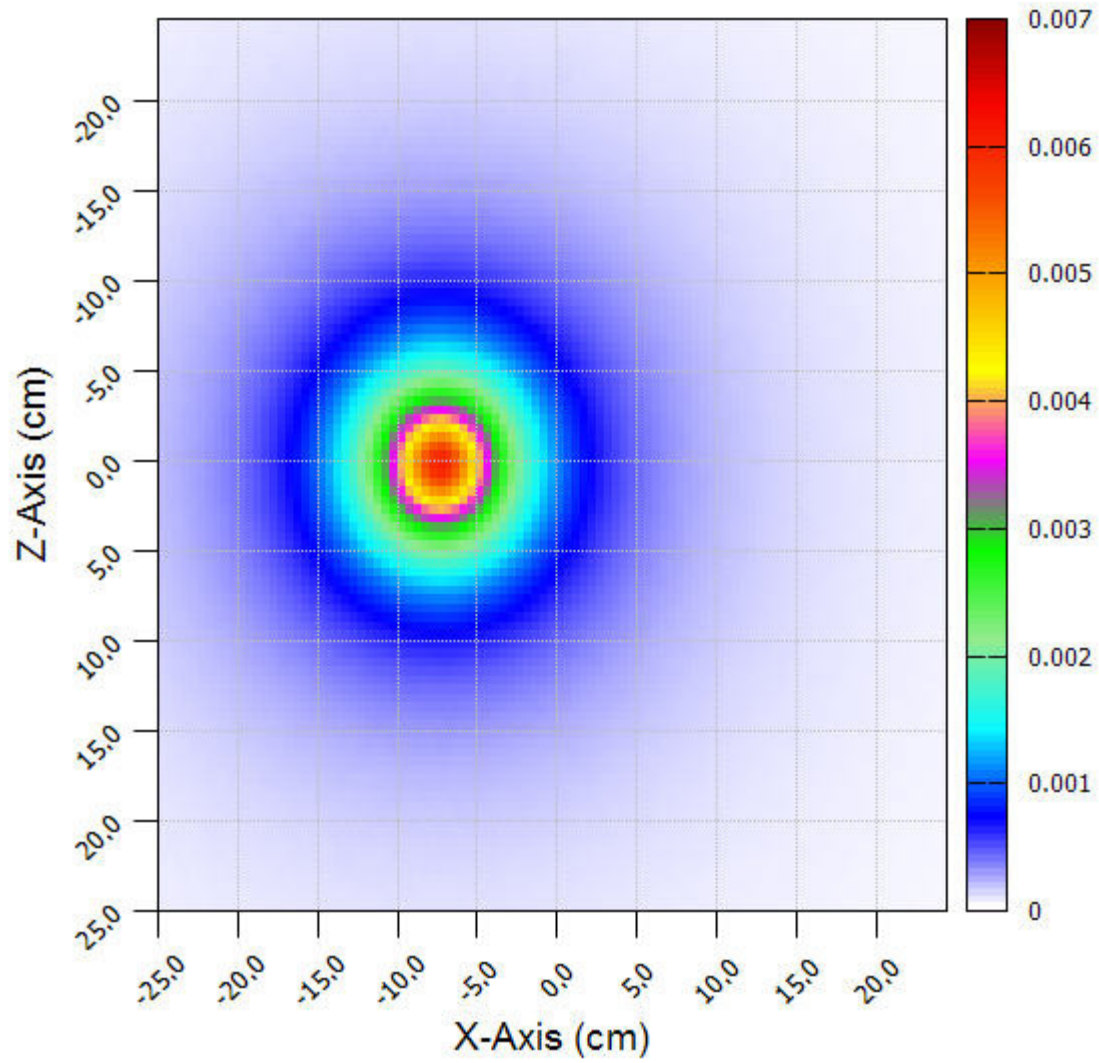
Figure 6-12 MCNP5 surface flux map for adjoint problem: Right eye
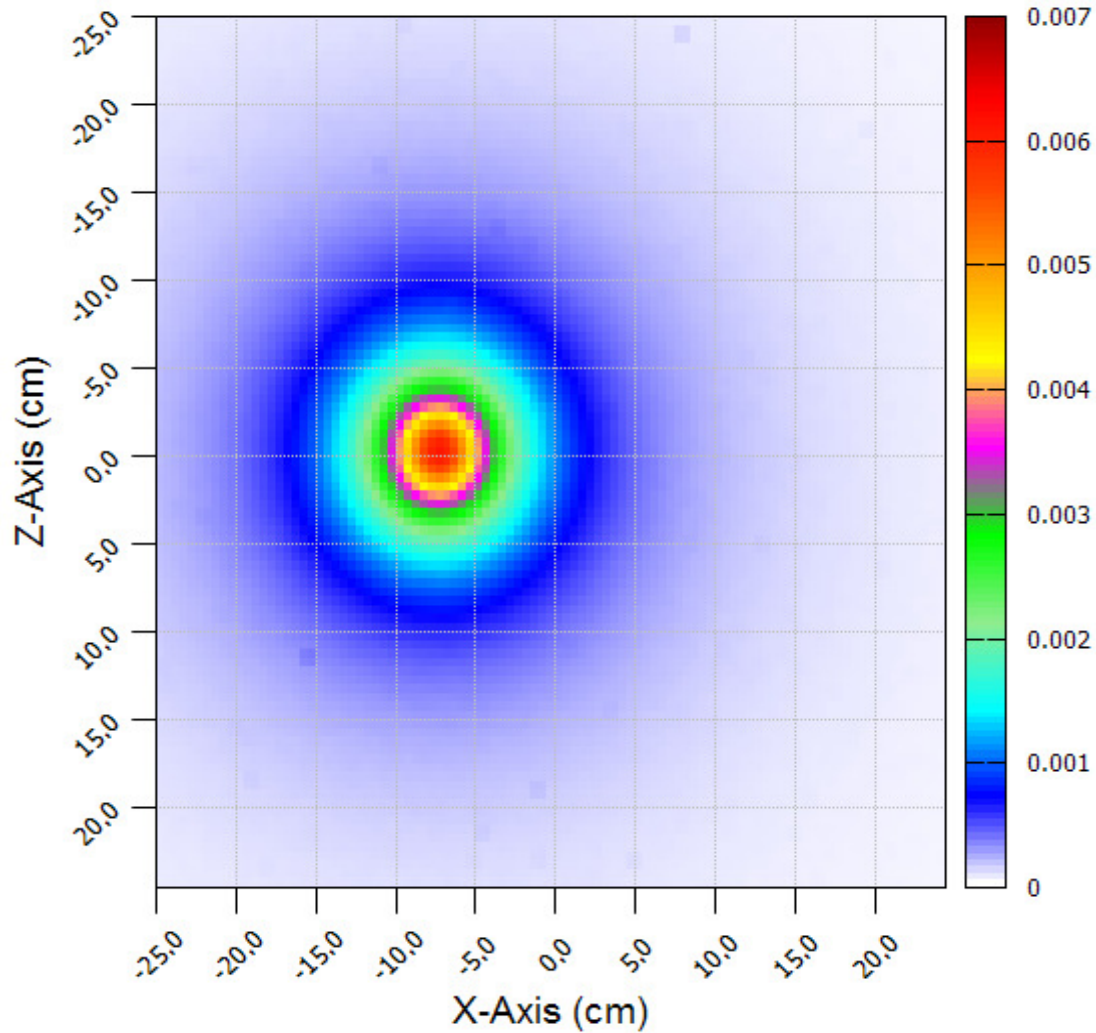
Figure 6-13 Pixel8 surface flux map for adjoint problem: Right eye

Table 6-18 Summary of Results for adjoint problem: Right eye

	Fluence (cGy/cm^2)		
Value	**MCNP5**	**Pixel8**	**% Difference**
Maximum (-7.25,0.25)	6.06000E-03 +/- 0.202%	6.17760E-03 +/- 1.617%	6.61%
Minimum (23.25,-24.75)	1.68641E-05 +/- 9.199%	1.88279E-05 +/- 7.85%	11.00%
Weighted Average	3.71487E-04 +/- 3.232%	3.4579E-04 +/- 4.322%	7.16%
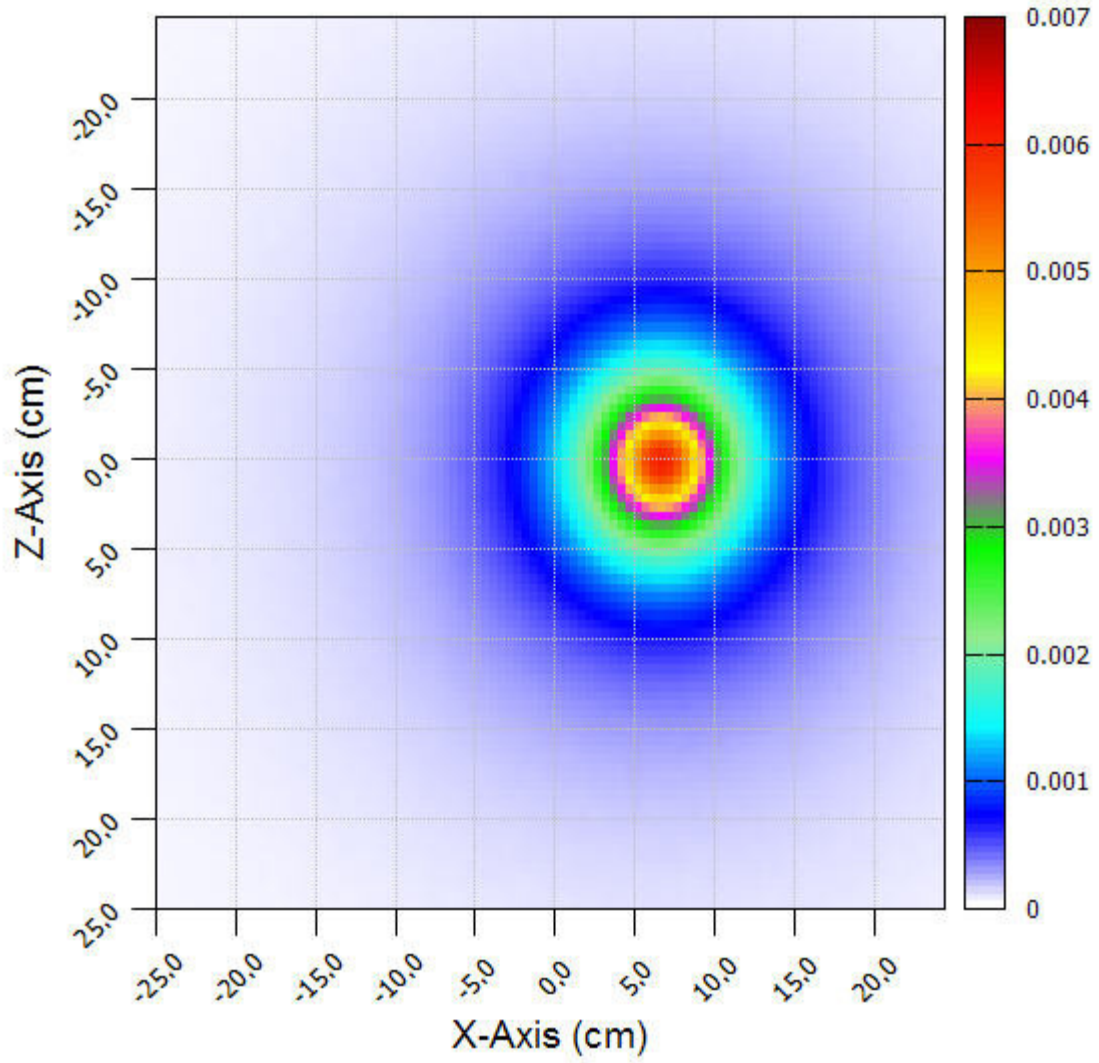
Figure 6-14 MCNP5 surface flux map for adjoint problem: Left eye
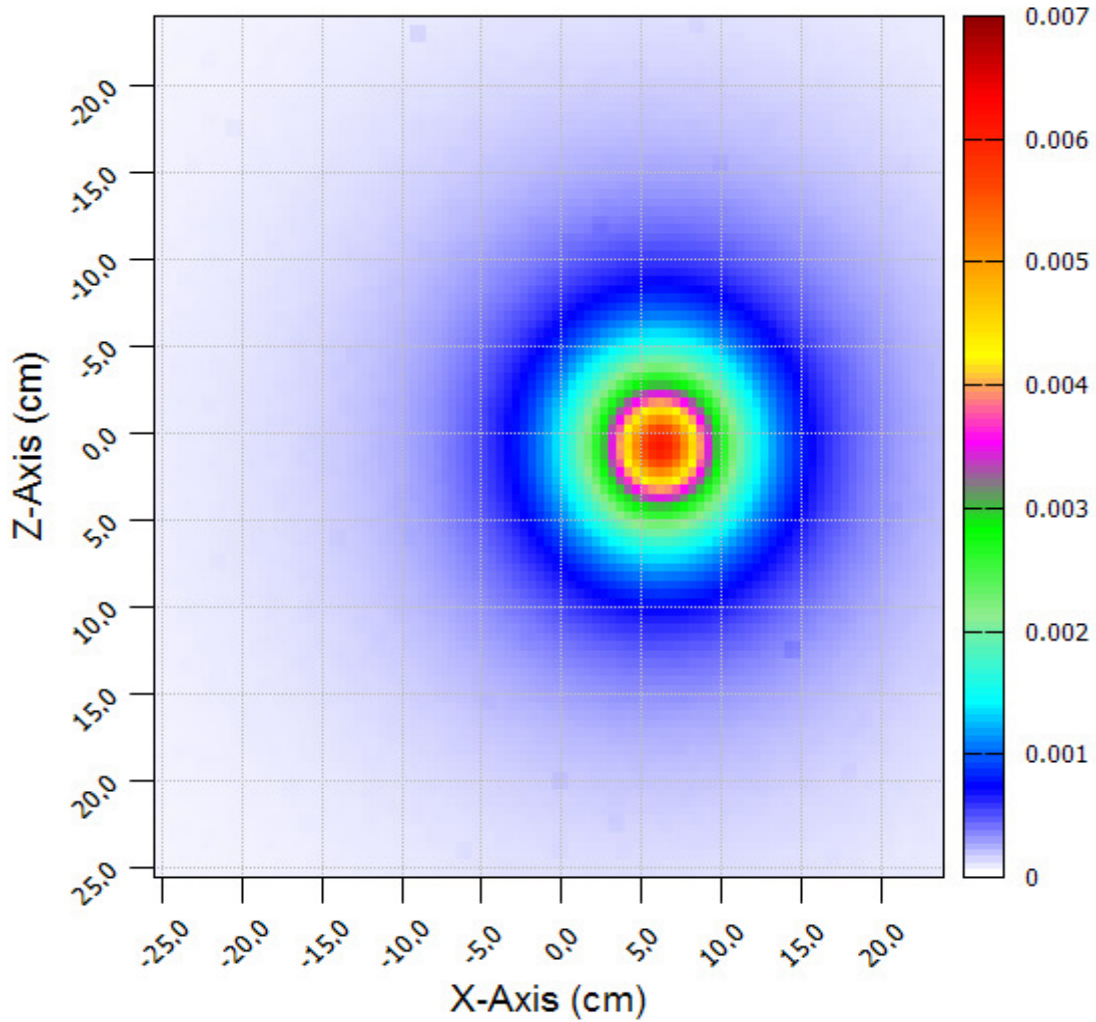
Figure 6-15 Pixel8 surface flux map for adjoint problem: Left eye

Table 6-19 Summary of Results for adjoint problem: Left eye

	Fluence (cGy/cm^2)		
Value	**MCNP5**	**Pixel8**	**% Difference**
Maximum (7.25,0.25)	6.0381E-03 +/- 0.201%	6.08275E-03 +/- 0.21%	0.74%
Minimum (-24.75,24.75)	1.70507E-05 +/- 8.797%	2.18755E-05 +/- 7.990%	24.79%
Weighted Average	3.71477E-04 3.229%	3.45934E-04 +/- 4.513%	7.12%
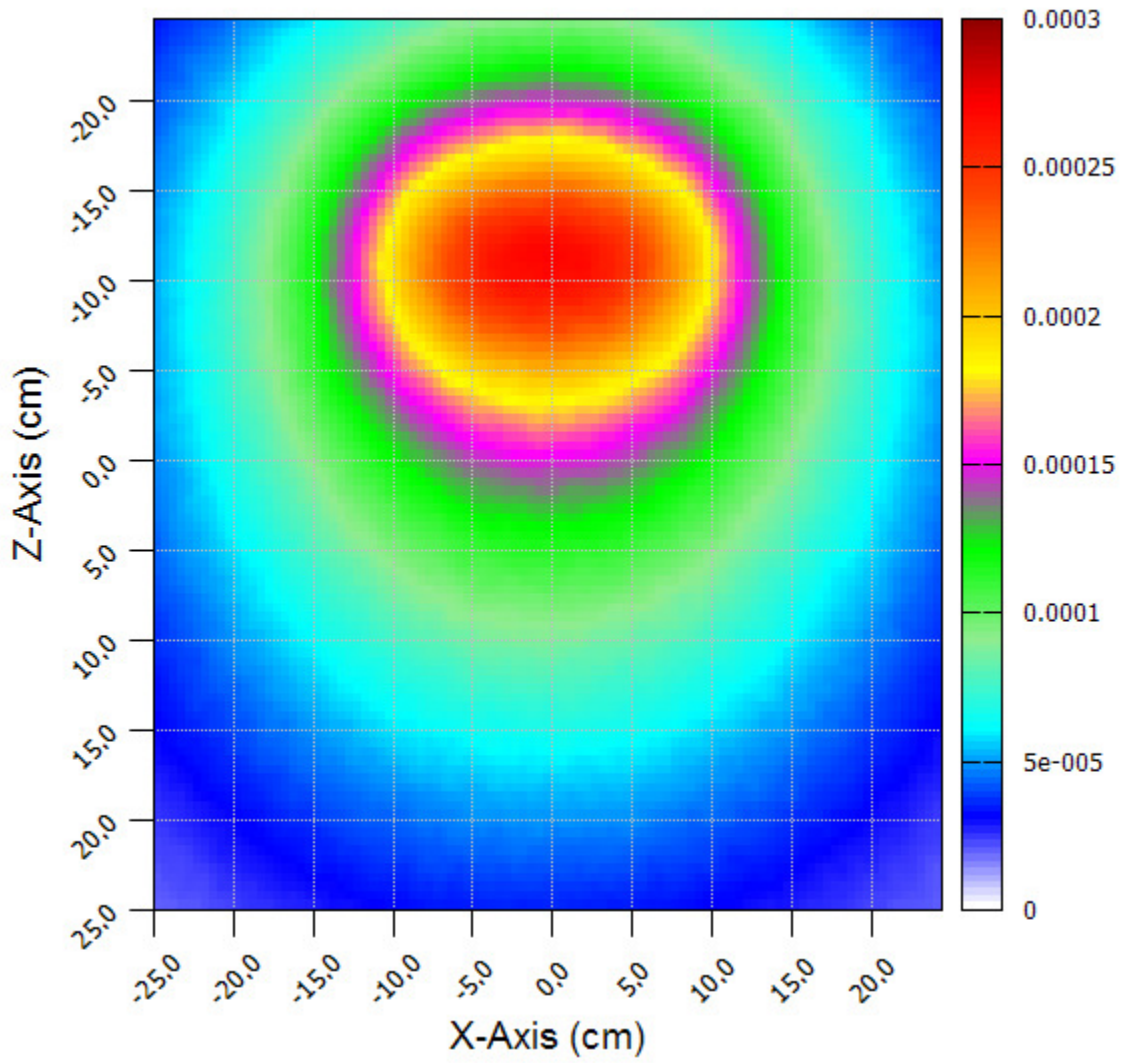
Figure 6-16 MCNP5 surface flux map for adjoint problem: Brain
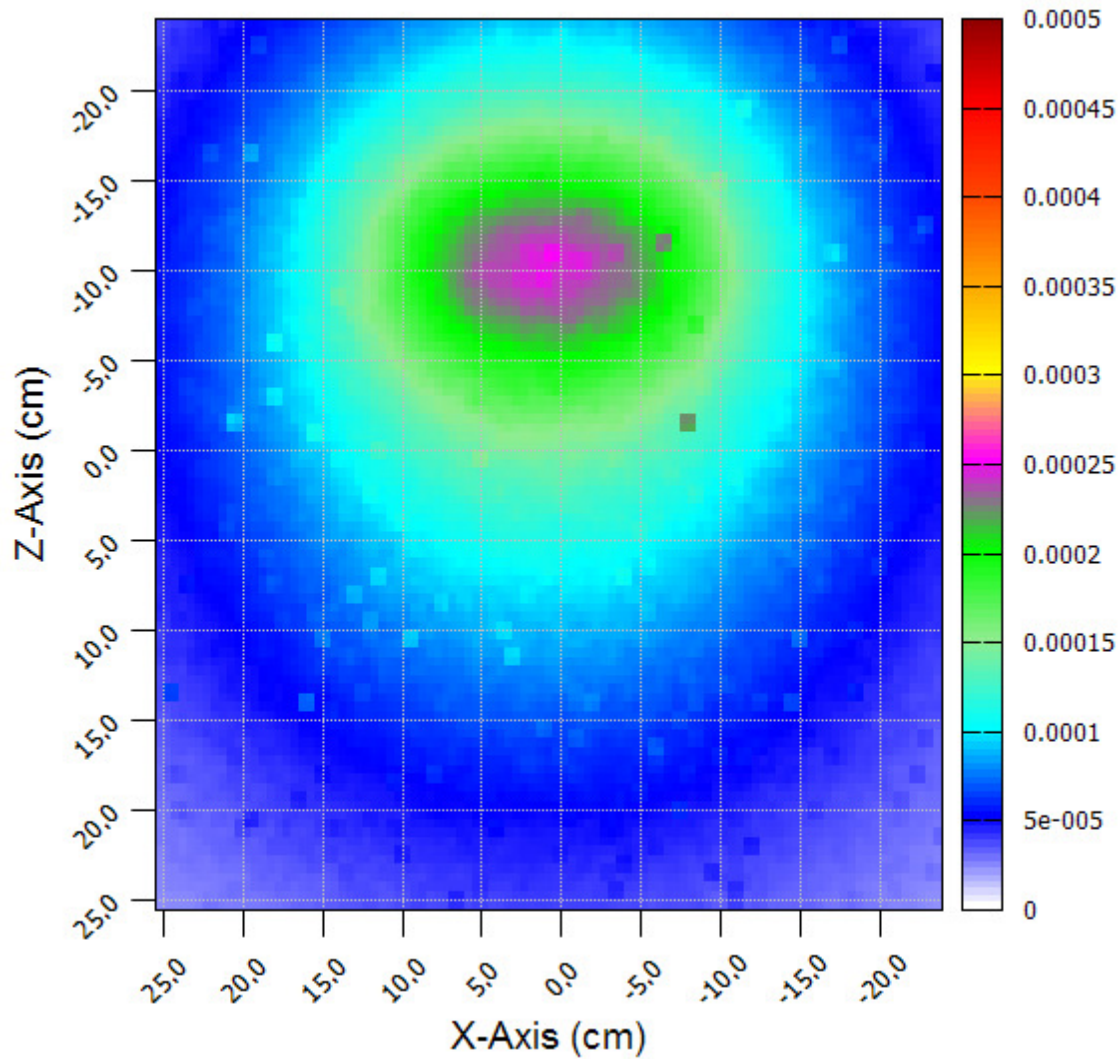
Figure 6-17 Pixel8 surface flux map for adjoint problem: Brain

Table 6-20 Summary of Results for adjoint problem: Brain

Value	Adjoint Fluence (cGy/cm^2)		
	MCNP5	Pixel8	% Difference
Maximum (0.25,4.25)	1.04056E-04 +/- 1.772%	7.45955E-05 +/-1.789	32.98%
Minimum (-24.25,-24.75)	1.77514E-05 +/- 4.193%	1.18301E-05 +/- 3.732%	40.03%
Weighted Average	5.81601E-05 2.634%	4.86977E-05 +/- 3.495%	17.71%

6.5. Sample problem 3: Hybrid forward/adjoint case

The final case tested the hybrid forward/adjoint methodology by comparing the dose in the four structures computed calculated using:

- A single forward MCNP5 calculation which—instead of creating the flux maps described in Section 6.4—used an F4 tally and the 12-group dose response functions to comp compute the dose rate in each of the four structures.

- A hybrid forward/adjoint surface integration using the surface adjoint flux maps from the four adjoint calculations described in Section 6.3. These surface dose sensitivity values were folded into the surface forward fluxes by position, direction, and energy group to also estimate the structure dose rates.

These two ways of computing the structure doses are compared in Table 6-21 through Table 6-24 for each of the four structures used in the sample problems. The MCNP5 and Pixel8 results show an agreement between 4.8955% - 8.181%. The deviation is due to region of interest pixilation and possible geometrical positioning errors introduced during the adjoint calculation.

Table 6-21 Summary of hybrid forward/adjoint results: Tumor

Gamma Group #	Energy bin upper bound (MeV)	Response (cGy)	Relative error (%)
1	0.010	0.00000E+00	0.00%
2	0.100	3.42794E-14	0.72%
3	0.500	2.96674E-13	0.41%
4	1.000	3.92613E-13	0.46%
5	2.000	7.61435E-13	0.40%
6	3.000	5.75613E-13	0.52%
7	4.000	4.03112E-13	0.67%
8	5.000	2.51975E-13	0.91%
9	6.000	6.80292E-14	1.86%
	Total	2.78373E-12	0.22%
	Pixel8 results	2.592670E-12	0.800%
	Difference	7.107%	

Table 6-22 Summary of hybrid forward/adjoint results: Right eye

Gamma Group #	Energy bin upper bound (MeV)	Response (cGy)	Relative error (%)
1	0.010	0.00000E+00	0.00%
2	0.100	2.69256E-14	0.36%
3	0.500	2.38840E-13	0.20%
4	1.000	1.67970E-13	0.27%
5	2.000	2.42108E-13	0.27%
6	3.000	1.61357E-13	0.37%
7	4.000	1.06317E-13	0.50%
8	5.000	6.47456E-14	0.69%
9	6.000	1.73201E-14	1.41%
	Total MCNP5	1.02558E-12	0.13%
	Pixel8 results	1.109128E-12	0.398%
	Difference	7.828%	

Table 6-23 Summary of hybrid forward/adjoint results: Left eye

Gamma Group #	Energy bin upper bound (MeV)	Response (cGy)	Relative error (%)
1	0.010	0.00000E+00	0.00%
2	0.100	2.69212E-14	0.36%
3	0.500	2.38445E-13	0.20%
4	1.000	1.68483E-13	0.27%
5	2.000	2.41317E-13	0.27%
6	3.000	1.60905E-13	0.37%
7	4.000	1.07009E-13	0.50%
8	5.000	6.47643E-14	0.69%
9	6.000	1.72584E-14	1.41%
	Total MCNP5	1.02510E-12	0.13%
	Pixel8 results	9.445316E-13	0.398%
	Difference	8.181%	

Table 6-24 Summary of hybrid forward/adjoint results: Brain

Gamma Group #	Energy bin upper bound (MeV)	Response (cGy)	Relative error (%)
1	0.010	0.00000E+00	0.00%
2	0.100	1.79715E-14	0.13%
3	0.500	1.07281E-13	0.08%
4	1.000	7.50288E-14	0.10%
5	2.000	1.19812E-13	0.09%
6	3.000	8.56401E-14	0.13%
7	4.000	6.00521E-14	0.16%
8	5.000	3.73172E-14	0.22%
9	6.000	1.04133E-14	0.45%
	Total MCNP5	5.13516E-13	0.05%
	Pixel8 results	4.889777E-13	0.079%
	% Difference	4.895%	

Chapter 7

Conclusions and future work

7.1. Conclusions

This project has successfully developed a new Monte Carlo code for use in radiation therapy treatment planning with the following characteristics:

1. Capability of performing either forward or adjoint photon transport calculations;
2. Implementation of fictitious scattering as a more efficient utilization of computer time when used with a voxelized geometry description;
3. Implementation of a hybrid forward/adjoint calculation scheme to allow precalculated adjoint calculations of patient organ surface dose response functions to be coupled with fast-running forward transport of source surface fluxes from photon sources.

The code has been successfully tested versus MCNP5 in the calculation of a simulated water-based patient/source configuration. The results show that the method is working properly.

7.2. Future work

This project represents a proof-of-principle implementation to demonstrate the viability of the innovations included in the code. In order for this work to reach clinical treatment planning application, more work will be needed in the areas of:

1. Debug the code to minimize structure pixelating errors and eliminate structure positioning errors.
2. Optimization of the code to minimize analysis time.
3. Testing of the code against multi-region problems.
4. Testing of the optimized code against a wider range of clinical problems to validate the accuracy, efficacy, and efficiency of the approach versus current methods in clinical use.

REFERENCES

1. ANSI/ANS-6.1.1. (1977). *"Neutrons and gamma-ray flux-to-dose-rate factors".* (ANS-6.1.1).

2. Armstrong, J. G., Burman, C., Leibel, S., Fontenla, D., Kutcher, G., Zelefsky, M., & Fuks, Z. (1993). Three-dimensional conformal radiation therapy may improve the therapeutic ratio of high dose radiation therapy for lung cancer. *Int J Radiat Oncol Biol Phys, 26*(4), 685-689.

3. Bell, G. I., & Glasstone, S. (1970). *Nuclear Reactor Theory.* New York: Van Nostrand Reinhold.

4. Bentel, G. C., Nelson, C. E., & Noell, K. T. (1982). *Treatment planning and dose calculation in radiation oncology* (3rd ed.). New York: Pergamon.

5. Brown, F. B., & Martin, W. R. (2003, April 6-11). *"Direct Sampling of Monte Carlo Flight Paths in Media with Continuously Varying Cross-sections".* Paper presented at the ANS Mathematics and Computation Topical Meeting, Gatlinburg, TN.

6. Carol, M. (1994, March 20–24). *"Integrated 3-D Conformal Multivane Intensity Modulation Delivery System for Radiotherapy".* Paper presented at the XIth International Conference on the Use of Computers in Radiation Therapy, Manchester, UK.

7. Carter, L., & Cashwell, E. (1975). Particle Tranport Simulation with the Monte Carlo method.

8. Carter, L., Cashwell, E., & Taylor, W. (1972). Monte Carlo sampling with continuously varying cross sections along flight paths. *Nucl. Sci. Eng, 48*, 403-411.

9. Cashwell, E., Neergaard, J., Taylor, W., & Turner, G. (1972). MCN: A Neutron Monte Carlo Code: Los Alamos Scientific Lab., N. Mex.(USA).

10. Cashwell, E. D., & Everett, C. J. (1959). *A practical manual on the Monte Carlo method for random walk problems* (Vol. 37): Pergamon Press New York.

11. Chetty, I. J., Curran, B., Cygler, J. E., DeMarco, J. J., Ezzell, G., Faddegon, B. A., . . . Ma, C.-M. C. (2007). Report of the AAPM Task Group No. 105: Issues associated with clinical implementation of Monte Carlo-based photon and electron external beam treatment planning. *Med Phys, 34*(12), 4818-4853.

12. Chui, C.-S., Chan, M. F., Yorke, E., Spirou, S., & Ling, C. C. (2001). Delivery of intensity-modulated radiation therapy with a conventional multileaf collimator: comparison of dynamic and segmental methods. *Med Phys, 28*(12), 2441-2449.

13. Colvett, K. (2006). The history of radiation oncology. *South Med J, 99*(10), 1155-1156.

14. Cramer, S. N. (1977). Application of the Fictitious Scattering Radiation Transport Model for Deep-Penetration Monte Carlo Calculations. Oak Ridge National Laboratory: Oak Ridge National Laboratory.

15. Difilippo, F. C. (1998). Forward and adjoint methods for radiotherapy planning. *Med Phys, 25*(9), 1702-1710.

16. Dowsett, D. J., Kenny, P. A., & Johnston, R. E. (1998). *The physics of diagnostic imaging* (1st ed.). London ; New York: Chapman & Hall Medical.

17. Duderstadt, J. J. (1976). Nuclear reactor analysis.

18. Dupree, S. A., & Fraley, S. K. (2004). *A Monte Carlo Primer*: Springer.

19. Goldstein, M., & Regev, D. (1999). Igo - A Monte Carlo Code For Radiotherapy Planning [219-223].

20. Hall, E. J. (1988). *Radiobiology for the radiologist* (3rd ed.). Philadelphia: Lippincott.

21. Irving, D. (1971). The adjoint Boltzmann equation and its simulation by Monte Carlo. *Nuclear Engineering and Design, 15*, 273-293.

22. Jeraj, R., & Keall, P. (1999). Monte Carlo-based inverse treatment planning. *Phys Med Biol, 44*(8), 1885.

23. Johnson, J., Emmett, M., Rhoades, W., & Childs, R. (1992). A User's Manual for MASH 1.0-A Monte Carlo Adjoint Shielding Code System: DTIC Document.

24. Kalos, M. H., & Whitlock, P. A. (2008). *Monte carlo methods*: John Wiley & Sons.

25. Kawrakow, I., & Fippel, M. (2000). Investigation of variance reduction techniques for Monte Carlo photon dose calculation using XVMC. *Phys Med Biol, 45*(8), 2163.

26. Langer, M., & Leong, J. (1987). Optimization of beam weights under dose-volume restrictions. *International Journal of Radiation Oncology* Biology* Physics, 13*(8), 1255-1260.

27. Lewis, E. E., & Miller, W. F. (1984). Computational methods of neutron transport.

28. Ljungberg, M., Larsson, A., & Johansson, L. (2005). A new collimator simulation in SIMIND based on the delta-scattering technique. *Nuclear Science, IEEE Transactions on, 52*(5), 1370-1375.

29. Lux, I., & Koblinger, L. (1991). Monte Carlo particle transport methods: neutron and photon calculations (Vol. 102): CRC press Boca Raton.

30. Mageras, G., & Mohan, R. (1993). Application of fast simulated annealing to optimization of conformal radiation treatments. *Med Phys, 20*(3), 639-647.

31. Metcalfe, P., Kron, T., & Hoban, P. (1997). *The physics of radiotherapy X-rays from linear accelerators*. Madison, Wis.: Medical Physics Pub.

32. Mohan, R., Chui, C., & Lidofsky, L. (1985). Energy and angular distributions of photons from medical linear accelerators. *Med Phys, 12*(5), 592-597.

33. Morgan-Fletcher, S. (2001). Prescribing, Recording and Reporting Photon Beam Therapy (Supplement to ICRU Report 50), ICRU Report 62. ICRU, pp. ix+ 52, 1999 (ICRU Bethesda, MD) $65.00 ISBN 0-913394-61-0. *The British Journal of Radiology, 74*(879), 294-294.

34. Nath, R., Biggs, P. J., Bova, F. J., Ling, C. C., Purdy, J. A., van de Geijn, J., & Weinhous, M. S. (1994). AAPM code of practice for radiotherapy accelerators: report of AAPM Radiation Therapy Task Group No. 45. *Med Phys, 21*(7), 1093-1121.

35. Papanikolaou, N., Battista, J. J., Boyer, A. L., Kappas, C., Klein, E., Mackie, R. T., . . . Van Dyk, J. (2004). TISSUE INHOMOGENEITY CORRECTIONS FOR MEGAVOLTAGE PHOTON BEAMS.

36. Papanikolaou, N., & Klein, E. E. (2008). 1.7. Heterogeneity corrections should be used in treatment planning for lung cancer. *Colin G. Orton and William R. Hendee*, 32.

37. Purdy, J. A. (1997). "The Development of Intensity Modulated Radiation Therapy" in 1st NOMOS IMRT Workshop. In W. Advanced Medical Publishing (Madison (Ed.). Durango, Colorado.

38. Roesch, W. C., & Attix, F. H. (1968). Basic concepts of dosimetry. *Radiation dosimetry, 1*, 1-41.

39. Rogers, D. (2006). Fifty years of Monte Carlo simulations for medical physics. *Phys Med Biol, 51*(13), R287.

40. Sheikh-Bagheri, D., & Rogers, D. (2002). Monte Carlo calculation of nine megavoltage photon beam spectra using the BEAM code. *Med Phys, 29*(3), 391-402.

41. Soderstrom, S., & Brahme, A. (1992). Selection of suitable beam orientations in radiation therapy using entropy and Fourier transform measures. *Phys Med Biol, 37*(4), 911.

42. Sontag, M. R., & Cunningham, J. (1978). Clinical application of a CT based treatment planning system. *Computerized tomography, 2*(2), 117-130.

43. Spanier, J., & Gelbard, E. M. (1969). Monte Carlo principles and neutron transport problems. *Reading, Mass., USA*.

44. Spirou, S. V., & Chui, C. S. (1994). Generation of arbitrary intensity profiles by dynamic jaws or multileaf collimators. *Med Phys, 21*(7), 1031-1041.

45. Tenney, C., Bowsher, J., & Jaszczak, R. (2004). *A delta-scatter Monte Carlo model of a rotating parallel-hole collimator for/sup 131/I brain tumor imaging.* Paper presented at the Nuclear Science Symposium Conference Record, 2004 IEEE.

46. Thwaites, D. I., & Tuohy, J. B. (2006). Back to the future: the history and development of the clinical linear accelerator. *Phys Med Biol, 51*(13), R343-362. doi: 10.1088/0031-9155/51/13/R20

47. Units, I. C. o. R., & Measurements. (1978). *Dose Specification for Reporting External Beam Therapy with Photons and Electrons*: International Commission on Radiation Units and Measurements.

48. Vijayakumar, S., Myrianthopoulos, L. C., Rosenberg, I., Halpern, H. J., Low, N., & Chen, G. T. (1991). Optimization of radical radiotherapy with beam's eye view techniques for non-small cell lung cancer. *Int J Radiat Oncol Biol Phys, 21*(3), 779-788.

49. Williams, J. R., & Thwaites, D. I. (2000). *Radiotherapy physics--in practice* (2nd ed.). Oxford New York: Oxford University Press.

50. Woodcock, E. R., Murphy, T., Hemmings, P. J., & Longworth, T. C. (1965). *Techniques Used in the GEM Code for Monte Carlo Neutronics Calculations in Reactors and Other Systems of Complex Geometry.* Paper presented at the Proc. Conf. Applications of Computing Methods to Reactor Problems, Argonne National Laboratory.

APPENDIXES

Appendix A

Cross section and Transport data generation

A.1. Data needed for Monte Carlo transport

When transporting a particle in a medium several important basic parameters about the particle state are needed to chart the particle random walk through the medium correctly. Examples of such particle state parameters are:

1. Particle initial position, direction and energy,
2. Type of interactions occurring during the random walk to determine the scattered particle energy and new direction.

As a result accurate knowledge of the particle physics and ability to model it probabilistically is essential to make accurate decision during the particle random walk. It is common to use an input data file to provide all necessary particle data to chart the random walk accurately.

On the first hand, our research interested is beams of photon particles used in radiotherapy, hence particles that are in the mega electron volt energy range, we will concentrate only on the most dominant photon interactions in that energy range. The photon interactions in this energy are mainly scattering events (such as Compton, Rayleigh scattering and pair production). Secondly, our research interested is focused on finding the adjoint solution for the Boltzmann transport equation. Solving such equation requires the use of multi-group cross section data. "**NJOY99**" code system is a software package that can generate multi-group cross sections from an ENDF file. "**NJOY99**" is a system of codes that was developed at "***Los Alamos national lab"*** and is provided by "*Radiation Information Safety Center*" (RISC) group at Oakridge, Tennessee. "**NJOY99**" code system can produce multi-group cross section data needed to transport particles in the forward and adjoint mode for each energy group in the problem materials. The photon interaction cross sections generated by "**NJOY99**" is:

1. Scattering cross sections (e.g., Coherent, Incoherent and Pair production).
2. Scattering heat cross sections (used to predict Kerma / Absorbed dose for all the scattering interaction mentioned above).
3. Total cross section.
4. Total heat cross section (used to predict Kerma / Absorbed dose).

5. Group to group scattering cross sections for all interactions mention above.

6. Distribution of Group to group cosine of scattering angle for all interactions above.

The cross sections produced by "**NJOY99**" code system for any element in question (provided that initial input parameters are given) are microscopic and need to be post processed. I a code was developed that will process the "**NJOY99**" output data file and produce data in a format useful for particle transport.

A.2. General flow of problem parameter specification

To prepare a problem specific input deck with cross sections and transport data useful for transport problems three basic parameters needs to be specified. These parameters are the problem elemental components, involved particle energy group structure and the particles energy distribution (photon source energy spectrum). Once these parameters are specified cross sections and transport data can be generated. The final component of this data is dependent on the problem mode. In the forward mode we need to specify several forward source (beam) parameters while in the adjoint mode we need to specify adjoint source parameters.

This general process flow is illustrated in Figure A-1. We start the process by creating problem material map. The result of this step is a list of elemental components present in the problem. We then need to specify the energy group structure of the problem particles. This energy group structure can be either a user defined structure or selected from "**NJOY99**" built-in group structure. Then we specify the problem particles energy distribution (photon source energy spectrum).
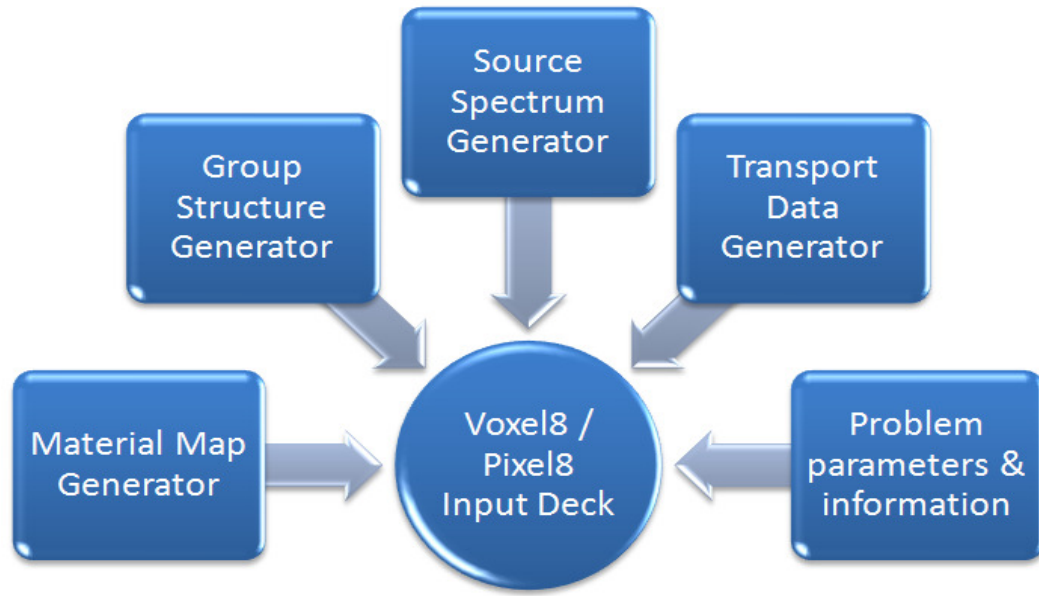
Figure A-1 General data generation flow

These parameters are feed into the cross section and transport data generator. The result is an "ASII" file that contains the problem specific cross sections and transport data for both modes (i.e., forward and adjoint). The following is a brief description of each component.

A.3. Material Map Generator

The main interface allows the user to either go to a patient database or physics data mode. Selecting the patient database invokes the "***Material map generator***" module. The "***Material map generator***" module enables the user to either import CT axial images or create a phantom data set as illustrated in Figure A-2. The result of the "***Material map generator***" is a set of data files in matrix (table) format. Each file represents a *Z* coordinate level. The file data points are integers that represent material that resides in that voxel. The matrix row represents *X* coordinate level and matrix column represents *Y* coordinate level. A summary of the data files CT numbers tally is also produced to be used when generating cross section data.
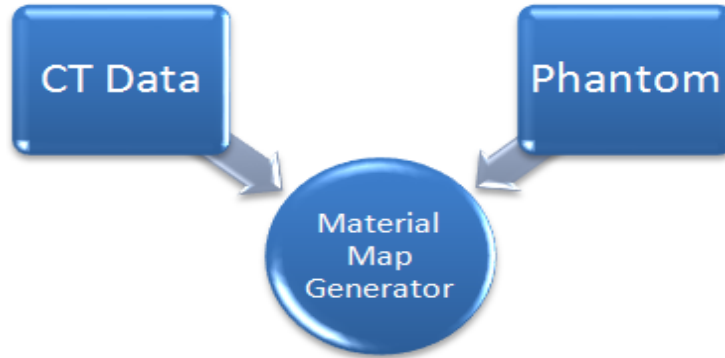
Figure A-2 Material map generator

A.4. Energy group structure generator

Specification of source particles energy structure is needed and used in the following modules:

    a. Cross section and transport data generation.

    b. Source photon spectrum generation.

    c. Forward and adjoint Monte Carlo transport.

Energy structure can be either designed or read from an existing list of files. The existing structure files are NJOY99 internal energy structures. The result of this module is an "ASCII" file that lists the energy structure boundaries. This file is used in the NJOY99 interface to produce a batch file that run "**NJOY99**". Figure A-3 is illustrates this process.
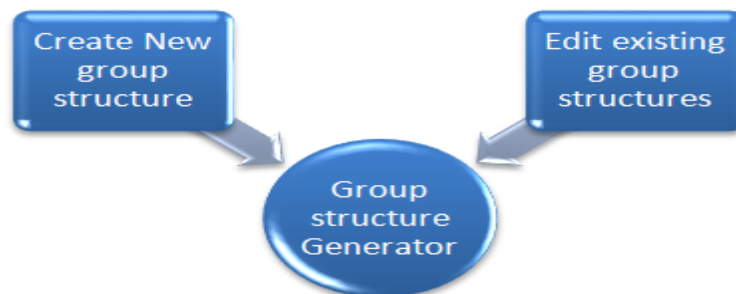
Figure A-3 Energy group structure generator

A.5. Source spectrum energy structure adjuster

Once the group structure is defined the photon source energy spectrum can be selected. The user selects a photon spectrum from published data. This is illustrated in Figure A-4. Then the code adjusts the spectrum energy bins to match the selected group structure energy bins. As a result an "ASCII" file that will contain information about our:

    a) Choice of photon spectrum,

    b) Number of photon spectrum energy bins after adjustment

    c) CDF for each energy bin after adjustment.
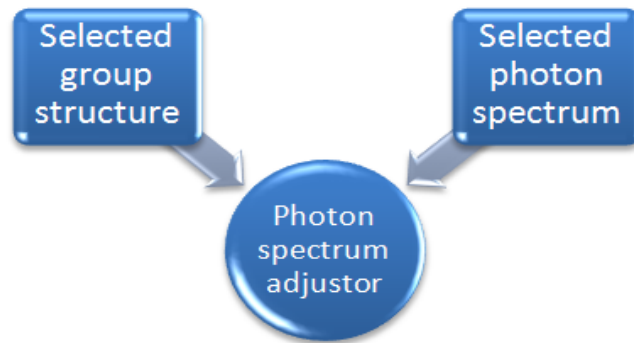
Figure A-4 Source spectrum energy structure adjuster

Once all these initial problem parameters are specified the cross section and transport data generation steps starts by initiating the "**NJOY99**" interface.

A.6. Microscopic Cross section data generation using "NJOY99" code system

To generate the microscopic group cross sections for problem materials we need to run "**NJOY99**" code system. To run "**NJOY99**" we need to specify an energy group structure and provide the code system an evaluated nuclear data file "**ENDF**". The energy group structure can be either a user-specified energy structure or a built-in energy structure. A user interface was developed to aid in viewing built-in, and design new energy group structure. The "**ENDF**" file used is the "*ENDF/B-VI*" for *photo-atomic interactions*. This file is available in public domain

from the "*International Atomic Energy Agency*" nuclear data services branch. A user interface was designed to assist in running the "**NJOY99**" code system. Figure A-5 describes the rest of the parameters needed to generate the microscopic group cross section by the "**NJOY99**" code system. The result of running this interface is an "ASCII" file that contains all available microscopic photon cross sections for the specified elements.

Figure A-5 "NJOY99" interface that generate elemental group microscopic cross section

A.7. Generation of transport data

Once "**NJOY99**" output file is generated we can generation of transport data. A special interface was built to facilitate this task. In this interface the user makes the following choices:

a) "**NJOY99**" output file to use.
b) Select problem material as:

    I.   Element

    II.   Tissue

The result of is the needed data to perform forward and adjoint Monte Carlo transport. The process is illustrated in Figure A-6.
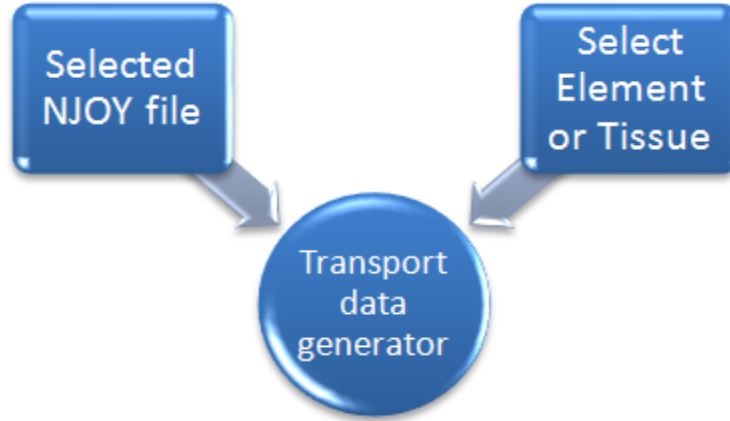
Figure A-6 Transport data generation

A.7.1 Total macroscopic cross section

"NJOY99" generates different interaction reactions cross section data in units of $\left(\frac{barn}{atom}\right)$. The following is a procedure to convert the generated data to appropriate units of $\left(\frac{1}{cm}\right)$:

1. A single isotope atomic density $\rho_{N_{A_{isotope}}}$ is the number of atoms in a unit volume of the isotope and is computed from:

$$\rho_{N_{A_{isotope}}} = \frac{\rho_{isotope}\left(\frac{g}{cm^3}\right)}{A_{isotope}\left(\frac{g}{mole}\right)} \times N_A\left(\frac{atoms}{mole}\right) = \frac{\rho_{isotope} \times N_A}{A_{isotope}}\left(\frac{atoms}{cm^3}\right)$$

2. For a material made of several isotopes ($i = 1, \cdots, N$) the ith isotope atomic density $\left(\rho_{N_{A_{isotope}}}\right)_i$ with density contribution $\left(\rho_{isotope}\right)_i \left(\frac{g}{cm^3}\right)$ to the material density $\rho_{material}\left(\frac{g}{cm^3}\right)$ is:

$$\left(\rho_{N_{isotope}}\right)_i = \frac{\left(\rho_{isotope}\right)_i \left(\frac{g}{cm^3}\right)}{\left(A_{isotope}\right)_i \left(\frac{g}{mole}\right)} \times N_A\left(\frac{atoms}{mole}\right)$$

$$\left(\rho_{N_{isotope}}\right)_i = \left(\frac{\rho_{isotope}}{A_{isotope}}\right)_i \times N_A\left(\frac{atoms}{cm^3}\right)$$

For a material with known isotope weight fraction contribution $\left(f_{isotope}\right)_i$ the isotope i density $\left(\rho_{isotope}\right)_i$ in the material is computed from $\left(\rho_{isotope} = f_{isotope} \times \rho_{material}\right)_i$ isotope i atomic density is computed by substituting $\left(f_{isotope} \times \rho_{material}\right)_i$ for isotope i density $\rho_{isotope}$ in the above equation:

$$\left(\rho_{N_{A_{isotope}}}\right)_i = \left(\frac{f_{isotope}}{A_{isotope}}\right)_i \times \rho_{material} \times N_A \left(\frac{atoms}{cm^3}\right)$$

3. For a certain reaction type a single isotope macroscopic cross section $\Sigma_{Rxn\,Type}^{isotope}$ in units of $\left(\frac{1}{cm}\right)$ from the same microscopic cross section $\sigma_{Rxn\,Type}^{isotope}$ in units of $\left(\frac{barn}{atom}\right)$ is computed as follow:

$$\Sigma_{Rxn\,Type}^{isotope} = \rho_{N_{A_{isotope}}} \left(\frac{atoms}{cm^3}\right) \times \sigma_{Rxn\,Type}^{isotope} \left(\frac{barn}{atom}\right) \times 10^{-24} \left(\frac{cm^2}{barn}\right)$$

$$\Sigma_{Rxn\,Type}^{isotope} = \frac{\rho_{isotope} \times N_A}{A_{isotope}} \left(\frac{atoms}{cm^3}\right) \times \sigma_{Rxn\,Type}^{isotope} \left(\frac{barn}{atom}\right) \times 10^{-24} \left(\frac{cm^2}{barn}\right)$$

$$\Sigma_{Rxn\,Type}^{isotope} = \left(\frac{\sigma_{Rxn\,Type}^{isotope} \times N_A \times \rho_{isotope} \times 10^{-24}}{A_{isotope}}\right)$$

$$\Sigma_{Rxn\,Type}^{isotope} = \sigma_{Rxn\,Type}^{isotope} \times \left(\frac{\rho_{isotope}}{A_{isotope}}\right) \times (N_A \times 10^{-24}) \left(\frac{1}{cm}\right)$$

It is customary to compute the macroscopic cross section in a unit of $\left(\frac{cm^2}{g}\right)$ to eliminate the density effect (mass cross section). The above equation becomes:

$$\frac{\Sigma_{Rxn\,Type}^{isotope}}{\rho_{isotope}} = \left(\frac{\sigma_{Rxn\,Type}^{isotope}}{A_{isotope}}\right) \times (N_A \times 10^{-24}) \left(\frac{cm^2}{g}\right)$$

4. For a material composed of several isotopes $(i = 1, \cdots, N)$ and $\left(f_{isotope}\right)_i$ is the weight fraction contribution of isotope i to the material density, the density independent macroscopic cross section is:

$$\frac{\Sigma_{Rxn\,Type}^{material}}{\rho_{material}} = \sum_{i=1}^{N} \left(f_{isotope}\right)_i \times \left(\frac{\Sigma_{Rxn\,Type}^{isotope}}{\rho_{isotope}}\right)_i \left(\frac{cm^2}{g}\right)$$

$$\frac{\Sigma_{Rxn\,Type}^{material}}{\rho_{material}} = \sum_{i=1}^{N} (f_{isotope})_i \times \left(\frac{\sigma_{Rxn\,Type}^{isotope}}{A_{isotope}}\right)_i \times (N_A \times 10^{-24}) \left(\frac{cm^2}{g}\right)$$

Multiply by $\rho_{material}$:

$$\Sigma_{Rxn\,Type}^{material} = (N_A \times 10^{-24}) \times \sum_{i=1}^{N} \left((f_{isotope})_i \times \rho_{material}\right) \times \left(\frac{\sigma_{Rxn\,Type}^{isotope}}{A_{isotope}}\right)_i \left(\frac{1}{cm}\right)$$

Since $(\rho_{isotope})_i = (f_{isotope})_i \times \rho_{material}$ in the material then:

$$\Sigma_{Rxn\,Type}^{material} = (N_A \times 10^{-24}) \times \sum_{i=1}^{N} \left(\frac{\rho_{isotope} \times \sigma_{Rxn\,Type}^{isotope}}{A_{isotope}}\right)_i \left(\frac{1}{cm}\right)$$

In summary:

1. The mass macroscopic cross section (per unit density):

    a. Isotope i:

    $$\left(\frac{\Sigma_{Rxn\,Type}^{isotope}}{\rho_{isotope}}\right)_i = \left(\frac{\sigma_{Rxn\,Type}^{isotope}}{A_{isotope}}\right)_i \times (N_A \times 10^{-24}) \left(\frac{cm^2}{g}\right) \qquad \text{(ANSI/A NS-6.1.1)}$$

    b. Material with $(f_{isotope})_i$ weight fraction for isotope i :

    $$\frac{\Sigma_{Rxn\,Type}^{material}}{\rho_{material}} = \sum_{i=1}^{N} (f_{isotope})_i \times \left(\frac{\Sigma_{Rxn\,Type}^{isotope}}{\rho_{isotope}}\right)_i \left(\frac{cm^2}{g}\right) \qquad (2)$$

2. The macroscopic cross section (per cm):

    a. Isotope i :

    $$(\Sigma_{Rxn\,Type}^{isotope})_i = \left(\sigma_{Rxn\,Type}^{isotope} \times \frac{\rho_{isotope}}{A_{isotope}}\right)_i \times (N_A \times 10^{-24}) \left(\frac{1}{cm}\right)$$

    b. Material with f_i weight fraction of isotope i :

    $$\Sigma_{Rxn\,Type}^{material} = \sum_{i=1}^{N} (f_{isotope})_i \times \rho_{material} \times \left(\frac{\Sigma_{Rxn\,Type}^{isotope}}{\rho_{isotope}}\right)_i \left(\frac{1}{cm}\right)$$
    $$\Sigma_{Rxn\,Type}^{material} = (\rho_{material} \times N_A \times 10^{-24})$$
    $$\times \sum_{i=1}^{N} \left(\sigma_{Rxn\,Type}^{isotope} \times \frac{f_{isotope}}{A_{isotope}}\right)_i \left(\frac{1}{cm}\right) \qquad (3)$$

A.7.2 Total heat macroscopic cross section

NJOY99 generates different heat reactions cross section data in units of $(eV - barn)$. According to the NJOY99 manual the heat cross section is the product of the particular microscopic cross section and the average energy released as a result of the interaction. Therefore the above unit is thought of as $\left(\frac{eV - barn}{Collision - atom}\right)$ The following is a procedure to convert this generated data to appropriate units of $\left(\frac{MeV - cm^2}{g}\right)$ and $(cGy - cm^2)$:

1. For a certain reaction type we can compute a heat macroscopic cross section for a single isotope $\Sigma_{x-Heat}^{isotope}$ in units of $\left(\frac{eV}{cm}\right)$ from the same microscopic cross section $\sigma_{x-Heat}^{isotope}$ in units of $(eV - barn)$ is computed as follow:

$$\Sigma_{x-Heat}^{isotope} = \rho_{N_{A_{isotope}}} \left(\frac{atoms}{cm^3}\right) \times \sigma_{x-Heat}^{isotope} \left(\frac{eV - barn}{atom}\right) \times 10^{-24} \left(\frac{cm^2}{barn}\right)$$

$$\Sigma_{x-Heat}^{isotope} = \frac{\rho_{isotope} \times N_A}{A_{isotope}} \left(\frac{atoms}{cm^3}\right) \times \sigma_{x-Heat}^{isotope} \left(\frac{eV - barn}{atom}\right) \times 10^{-24} \left(\frac{cm^2}{barn}\right)$$

$$\Sigma_{x-Heat}^{isotope} = \left(\frac{\sigma_{x-Heat}^{isotope} \times N_A \times \rho_{isotope} \times 10^{-24}}{A_{isotope}}\right)$$

$$\Sigma_{x-Heat}^{isotope} = \left(\frac{\rho_{isotope} \times N_A \times 10^{-24}}{A_{isotope}}\right) \times \sigma_{x-Heat}^{isotope} \left(\frac{eV}{cm}\right)$$

Converting the units to $\left(\frac{MeV}{cm}\right)$ by multiplying by $\left(\frac{1 \times 10^{-6} MeV}{eV}\right)$ we get:

$$\Sigma_{x-Heat}^{isotope} = \left(\frac{\rho_{isotope} \times N_A \times 10^{-30}}{A_{isotope}}\right) \times \sigma_{x-Heat}^{isotope} \left(\frac{MeV}{cm}\right)$$

it is customary to report the heat macroscopic cross section in a unit of $\left(\frac{MeV - cm^2}{g}\right)$ to eliminate the density effect (mass cross section). This is done by dividing above equation by the density:

$$\frac{\Sigma_{x-Heat}^{isotope}}{\rho_{isotope}} = \left(\frac{N_A \times 10^{-30}}{A_{isotope}}\right) \times \sigma_{x-Heat}^{isotope} \left(\frac{MeV - cm^2}{g}\right)$$

2. For a material composed of several isotopes $(i = 1, \cdots, N)$ and $(f_{isotope})_i$ is isotope i weight fraction contribution to the material density, therefore; the density independent macroscopic cross section is:

$$\frac{\Sigma_{x-Heat}^{material}}{\rho_{material}} = \sum_{i=1}^{N}(f_{isotope})_i \times \left(\frac{\Sigma_{x-Heat}^{isotope}}{\rho_{isotope}}\right)_i \left(\frac{MeV - cm^2}{g}\right)$$

Substitute the isotope mass heat cross section in this equation we get:

$$\frac{\Sigma_{x-Heat}^{material}}{\rho_{material}} = \sum_{i=1}^{N}(f_{isotope})_i \times \left(\frac{\sigma_{x-Heat}^{isotope}}{A_{isotope}}\right)_i \times (N_A \times 10^{-30})\left(\frac{MeV - cm^2}{g}\right)$$

$$\frac{\Sigma_{x-Heat}^{material}}{\rho_{material}} = (N_A \times 10^{-30})\sum_{i=1}^{N}\left(\frac{f_{isotope} \times \sigma_{x-Heat}^{isotope}}{A_{isotope}}\right)_i \left(\frac{MeV - cm^2}{g}\right)$$

3. To convert $\left(\frac{MeV-cm^2}{g}\right)$ to $\left(\frac{MeV}{cm}\right)$ we multiply the equation by $\rho_{material}$ to get:

$$\Sigma_{x-Heat}^{material} = (N_A \times 10^{-30}) \times \sum_{i=1}^{N}(f_{isotope})_i \times \rho_{material} \times \left(\frac{\sigma_{x-Heat}^{isotope}}{A_{isotope}}\right)_i \left(\frac{MeV}{cm}\right)$$

Since $(\rho_{isotope})_i = (f_{isotope})_i \times \rho_{material}$ then:

$$\Sigma_{x-Heat}^{material} = (N_A \times 10^{-30}) \times \sum_{i=1}^{N}\left(\frac{\rho_{isotope} \times \sigma_{x-Heat}^{isotope}}{A_{isotope}}\right)_i \left(\frac{MeV}{cm}\right)$$

4. Assuming that the energy released in an interaction is deposited in a voxel with weight $Wght_{voxel}$ .The energy released in a voxel is:

$$Energy\ Released_{voxel} = \frac{\Sigma_{x-Heat}^{material}}{Wght_{voxel}}\left(\frac{MeV}{g-cm}\right)$$

for a voxel with volume V_{voxel} and density ρ_{voxel} the voxel weight is:

$$Wght_{voxel} = \rho_{voxel} \times V_{voxel}$$

the energy released in a voxel per interaction become:

$$Energy\ Released_{voxel} = \frac{\Sigma_{x-Heat}^{material}}{\rho_{voxel} \times V_{voxel}}\left(\frac{MeV}{g-cm}\right)$$

substitute the last equation in the step above in we get:

$$Energy\ Released_{voxel} = \frac{N_A \times 10^{-30}}{\rho_{voxel} \times V_{voxel}} \times \sum_{i=1}^{N}\left(\frac{\rho_{isotope} \times \sigma_{x-Heat}^{isotope}}{A_{isotope}}\right)_i \left(\frac{MeV}{g-cm}\right)$$

5. To convert $\left(\frac{MeV}{g-cm}\right)$ to $\left(\frac{cGy}{cm}\right)$ we compute the $\left(\frac{cGy}{MeV/g}\right)$ factor:

$$\frac{1000\ g}{kg} \times \frac{1.602 \times 10^{-13} joule}{MeV} \times \frac{Gy}{joule/kg} \times \frac{100\ cGy}{Gy} = 1.602 \times 10^{-8}\ \frac{cGy}{MeV/g}$$

The absorbed dose in a voxel D_{voxel} for each interaction:

$$\frac{D_{voxel}}{interaction} = \frac{N_A \times 1.602 \times 10^{-38}}{\rho_{voxel} \times V_{voxel}} \times \sum_{i=1}^{N} \left(\frac{f_{isotope} \times \sigma_{x-Heat}^{isotope}}{A_{isotope}} \right)_i \left(\frac{cGy}{cm} \right)$$

6. For photon fluence of a $\phi \left(\frac{particles}{cm^2} \right)$ the reaction rate $\dot{R}$ for any type of interaction in a volume (number of interaction) is:

$$\dot{R} = \Sigma \phi$$

therefore, absorbed dose in a voxel from all particle interaction:

$$D_{voxel} = \frac{D_{voxel}}{interaction} \left(\frac{cGy}{cm} \right) \times \phi \left(\frac{particles}{cm^2} \right)$$

$$D_{voxel} = \frac{N_A \times \phi \times 1.602 \times 10^{-38}}{\rho_{voxel} \times V_{voxel}} \times \sum_{i=1}^{N} \left(\frac{f_{isotope} \times \sigma_{x-Heat}^{isotope}}{A_{isotope}} \right)_i (cGy)$$

The absorbed dose per photon fluence is:

$$\frac{D_{voxel}}{\phi} = \frac{N_A \times 1.602 \times 10^{-38}}{\rho_{voxel} \times V_{voxel}} \times \sum_{i=1}^{N} \left(\frac{f_{isotope} \times \sigma_{x-Heat}^{isotope}}{A_{isotope}} \right)_i (cGy - cm^2)$$

In summary:

1. The mass macroscopic heat cross section (per unit density):

   a. Isotope i:

$$\left(\frac{\Sigma_{x-Heat}^{isotope}}{\rho_{isotope}} \right)_i \left(\frac{MeV - cm^2}{g} \right) = \left(\frac{\sigma_{x-Heat}^{isotope}}{A_{isotope}} \right)_i \times (N_A \times 10^{-30}) \left(\frac{MeV - cm^2}{g} \right)$$

   b. Material with $(f_{isotope})_i$ weight fraction for isotope i :

$$\frac{\Sigma_{x-Heat}^{material}}{\rho_{material}} \left(\frac{MeV - cm^2}{g} \right) = \sum_{i=1}^{N} (f_{isotope})_i \times \left(\frac{\Sigma_{x-Heat}^{isotope}}{\rho_{isotope}} \right)_i \left(\frac{MeV - cm^2}{g} \right)$$

2. The macroscopic heat cross section $\left(\frac{MeV}{cm} \right)$:

107

a. Isotope i :

$$\left(\Sigma^{isotope}_{x-Heat}\left(\frac{MeV}{cm}\right)\right)_i = \left(\sigma^{isotope}_{x-Heat} \times \frac{\rho_{isotope}}{A_{isotope}}\right)_i \times (N_A \times 10^{-30})\left(\frac{MeV}{cm}\right)$$

b. Material with f_i weight fraction of isotope i :

$$\Sigma^{material}_{x-Heat}\left(\frac{MeV}{cm}\right) = \sum_{i=1}^{N}(f_{isotope})_i \times \rho_{material} \times \left(\frac{\Sigma^{isotope}_{x-Heat}}{\rho_{isotope}}\right)_i\left(\frac{MeV}{cm}\right)$$

$$\Sigma^{material}_{x-Heat}\left(\frac{MeV}{cm}\right) = (\rho_{material} \times N_A \times 10^{-30}) \times \sum_{i=1}^{N}\left(\frac{\sigma^{isotope}_{x-Heat} \times f_{isotope}}{A_{isotope}}\right)_i\left(\frac{MeV}{cm}\right)$$

c. Absorbed dose in a voxel from photon fluence of a $\phi\left(\frac{particles}{cm^2}\right)$:

$$\frac{D_{voxel}}{\phi} = \frac{N_A \times 1.602 \times 10^{-38}}{\rho_{voxel} \times V_{voxel}} \times \sum_{i=1}^{N}\left(\frac{f_{isotope} \times \sigma^{isotope}_{x-Heat}}{A_{isotope}}\right)_i (cGy - cm^2)$$

A.8. Scattering cross sections and its probability

The scattering cross sections are defined using the following two independent variables (hence double differential):

a) ENERGY – The Energy group of the Incident photon to the scattered photon.
b) ANGULAR - The scattering angle for the scattered photon (the result is angular distribution).

"**NJOY99**" generates three microscopic scattering cross sections:

a) Coherent Scattering – Raleigh Scattering:

There is no energy loss occur during this interaction. The incident photon emerges with the same energy but traveling in a different direction. The differential scattering cross section at location $\vec{r}$ is denoted by $\sigma_{Coherent}\left(\vec{r}, \Omega' \cdot \Omega, E \to E\right)$

b) Incoherent Scattering – Compton Scattering:

The incident photon emerges from the reaction in a different direction. The photon loses some energy in the interaction. The differential cross section at location r is denoted by $\sigma_{Incoherent}\left(\vec{r}, \Omega' \cdot \Omega, E \rightarrow E\right)$

c) Pair Production is considered a scattering interaction:

Therefore, in general (for all energy and scattering angles) the overall scattering cross section is defined to be:

$$\sigma_{Scattering} = \sigma_{Coherent} + \sigma_{Incoherent} + \sigma_{Pair\ Production}$$

Therefore, the individual contribution from each reaction to the overall scattering cross section:

$$Coherent = \frac{\sigma_{Coherent}}{\sigma_{Scattering}}$$

$$Incoherent = \frac{\sigma_{Incoherent}}{\sigma_{Scattering}}$$

$$Pair\ Production = \frac{\sigma_{Pair\ Production}}{\sigma_{Scattering}}$$

We can convert this cross section to macroscopic cross section using the same method used describe to generate macroscopic total cross section from microscopic cross section. This scattering cross section:

$\Sigma_{Scattering}(r, E) = $ describe the probability of scattering per unit path length $\left[\frac{1}{cm}\right]$

In a scattering event, the incident photon will change both direction of motion and energy. The quantity that will describe the state of the scattered photon is called the differential cross section. The energy distribution of photon emerging from a scattering reaction is given by a macroscopic differential scattering cross section $\Sigma_{Scattering}(E' \rightarrow E)$, where

$\Sigma_{Scattering}(E' \rightarrow E)dE$ characterizes the probability that a photon with an

initial energy $\grave{E}$ will scatter into dE around E.

109

The macroscopic scattering cross section is related to the probability that a photon with initial energy E will suffer a collision regardless of final energy $\grave{E}$, then the integral of the macroscopic differential scattering cross section, $\sigma_{Scattering}(E' \rightarrow E)$ over all final energies $\grave{E}$ is the total scattering cross section:

$$\Sigma_{Scattering}(E') = \int_0^\infty \Sigma_{Scattering}(E' \rightarrow E)dE$$

the dimension of this differential cross section is $\left[\frac{cm^2}{nucleus} \, MeV\right]$. We define the probability that a photon with initial energy $\grave{E}$ will scatter into dE around E is given by:

$$p(E' \rightarrow E)dE = \frac{\Sigma_{Scattering}(E' \rightarrow E)}{\Sigma_{Scattering}(E')}dE$$

this is the probability density function in $\left[\frac{1}{MeV}\right]$. The microscopic differential scattering cross section is defined as:

$$\Sigma_{Scattering}(E' \rightarrow E) = \Sigma_{Scattering}(E') \times p(E' \rightarrow E)$$

The angular distribution for photon emerging from a scattering reaction is given by a microscopic differential cross section, $\Sigma_{Scattering}(\widehat{\Omega}' \rightarrow \widehat{\Omega})$, where

$\Sigma_{Scattering}(\widehat{\Omega}' \rightarrow \widehat{\Omega})$ Characterizes the probability that a photon with an initial angle $\widehat{\Omega}\grave{}$ will scatter into $d\widehat{\Omega}$ around $\widehat{\Omega}$.

The integral of the microscopic differential scattering cross section, $\Sigma_{Scattering}(\widehat{\Omega}' \rightarrow \widehat{\Omega})$, over all final directions $\grave{\Omega}$ is the scattering cross section:

$$\Sigma_{Scattering}(E) = \int_0^\infty \Sigma_{Scattering}(E, \widehat{\Omega}' \rightarrow \widehat{\Omega})d\widehat{\Omega}$$

the dimension of this differential cross section is $\left[\frac{cm^2}{nucleus} \, Seteradian\right]$. We define the probability that a photon with initial directions Ω will scatter into $d\grave{\Omega}$ around $\grave{\Omega}$ is given by:

$$p(\widehat{\Omega}' \rightarrow \widehat{\Omega})d\widehat{\Omega} = \frac{\Sigma_{Scattering}(\widehat{\Omega}' \rightarrow \widehat{\Omega})}{\Sigma_{Scattering}(E)}d\widehat{\Omega}$$

this is the probability density function in [steradian -1]. The macroscopic differential scattering cross section is defined as:

$$\Sigma_{Scattering}\left(E, \widehat{\Omega}' \to \widehat{\Omega}\right) = \Sigma_{Scattering}(E)\, p\left(\widehat{\Omega}' \to \widehat{\Omega}\right)$$

Since the macroscopic differential cross section can depend on:

1. Photon Energy
2. Target nuclide
3. The initial direction Ω
4. The final direction Ω'

Note that the dependence on the initial and final direction is rare, but the dependence is stronger on the angle θ between the initial and final direction, hence the $\widehat{\Omega} \cdot \widehat{\Omega}$. Since that the direction vector is a unit vector therefore if we define:

$$\mu_0 = \widehat{\Omega}' \cdot \widehat{\Omega} = cos\theta$$

Hence

$$\Sigma_{Scattering}\left(E, \widehat{\Omega}' \to \widehat{\Omega}\right) = \Sigma_{Scattering}\left(E, \widehat{\Omega}' \cdot \widehat{\Omega}\right) = \Sigma_{Scattering}(E, \mu_0)$$

We can define

$$d\Omega = sin\theta\, d\theta\, d\phi = -d(cos\theta)d\phi = -d\mu_0 d\phi$$

therefore

$$\Sigma_{Scattering}(E) = \int_0^{2\pi} d\phi \int_0^{\pi} \Sigma_{Scattering}\left(E, \widehat{\Omega}' \to \widehat{\Omega}\right) d\widehat{\Omega}$$

$$\Sigma_{Scattering}(E) = \int_0^{2\pi} d\phi \int_0^{\pi} \Sigma_{Scattering}\left(E, \widehat{\Omega}' \cdot \widehat{\Omega}\right) sin\theta d\theta$$

$$\Sigma_{Scattering}(E) = \int_0^{2\pi} d\phi \int_{-1.0}^{+1.0} \Sigma_{Scattering}(E, \mu_0) d\mu_0$$

$$\Sigma_{Scattering}(E) = 2\pi \int_{-1.0}^{+1.0} \Sigma_{Scattering}(E, \mu_0) d\mu_0$$

For the purpose of our code we need to generate the total group scattering cross section. This value is generated using the following equation:

$$\Sigma_{Scattering}(E) = \Sigma_{Coherent}(E) + \Sigma_{Incoherent}(E) + \Sigma_{Pair\ Production}(E)$$

Further, the group to group macroscopic scattering cross section is computed from the microscopic cross section data generated by "NJOY99" using the same method describe to generate total macroscopic cross section. For the purpose of our problem we used the zero order of the Legendre polynomial to be our cross section.

A.9. Forward scattering probability

The forward scattering probability is derived from the total cross and forward scattering cross section. Total cross section is the sum of absorption and scattering cross section. The forward probability of scattering for a group is the result of dividing the forward scattering cross section by the total cross section as shown:

$$Scattering\ Probability_{forward,g} = \frac{\Sigma_{Scatt-forward,g}}{\Sigma_{Total,g}}$$

The result is a number between 0 and 1. When a random number is drawn and the value is between 0 and the scattering probability the type of interaction occurring is ***downward scattering interaction***. If the random number drawn is above the scattering probability the occurring interaction is absorption

A.10. Adjoint scattering probability

For the adjoint formalism, the group to group scattering cross section data need to be arranged. The data for the same final group is collected and arranged then a new adjoint group to group cross is computed. This cross section is simply for the same final group is the sum of all individual group to group scattering cross section as shown:

$$\Sigma_{Scatt-adjoint,g'} = \sum_{g'=1}^{G} \sum_{g=1}^{G} \Sigma_{Scatt,\ g \rightarrow g'}$$

The adjoint scattering probability is derived from the total cross and adjoint scattering cross section. Total cross section is the sum of absorption and scattering cross section. The adjoint probability of scattering for a group is the result of dividing the adjoint scattering cross section by the total cross section as shown:

$$Scattering\ Probability_{adjoint,g'} = \frac{\Sigma_{Scatt-adjoint,g'}}{\Sigma_{Total,g'}}$$

For this ratio the result might not be a number between 0 and 1. When a random number is drawn and the value is between 0 and the adjoint scattering probability the type of interaction occurring is ***upward scattering interaction***. If the random number drawn is above the scattering probability the occurring interaction is absorption.

A.11. Group to group scattering probability

The group to group scattering probability is generated from the:

1. The group total scattering cross section;
2. The group to group scattering cross section.

1. Forward group to group scattering probability

The forward group to group scattering probability is computed by dividing the group to group scattering cross section by the group total scattering cross section as shown below:

$$Group\ to\ group\ scattering\ Probability_{Forward,g'} = \frac{\Sigma_{Scatt,g \to g'}}{\Sigma_{Scatt-forward,g}}$$

The ratios produce is then used to create a CDF. For the forward input file the first entry of the CDF data point is for the ***lowest down to energy group*** and the last data point is for the ***current energy group***.

A.12. Adjoint group to group scattering probability

Then adjoint group to group scattering probability is computed by dividing the group to group scattering cross section by the newly computed above adjoint group to group scattering cross section as shown:

$$Group\ to\ group\ scattering\ Probability_{Adjoint,g} = \frac{\Sigma_{Scatt,g \to g'}}{\Sigma_{Scatt-adjoint,g'}}$$

The ratios produce is then used to create a CDF. For the adjoint input file the first entry of the CDF data point is for the ***current energy group*** and the last data point is for the energy ***highest up scatter group***.

A.13. Group to group cosine of scattering angle

"**NJOY99**" produce group to group cosine scattering angle cross sections. This data is presented by "**NJOY99**" as a Legendre polynomial coefficient. The maximum order of the polynomial coefficient is specified by the user as part of "**NJOY99**" code system needed input parameters. The resultant data need to be processed to be used in particle transport. It is well known in the literature that presentation of cross section as Legendre polynomial coefficient can cause the cross section to be negative for polynomials with coefficient order higher than 1. The negative cross section does not make any physical sense and can cause the computed probabilities to be negative.

For cross sections presented by Legendre polynomial with polynomial order one or higher codes such as "MORSE" and "KENO" eliminates the negative cross section problem by computing the average cosine of the scattering angle using the zero and first Legendre polynomial coefficient as follow:

$$\bar{\mu}(g \rightarrow g') = \frac{\Sigma_{Scatt-P1}^{g \rightarrow g'}}{\Sigma_{Scatt-P0}^{g \rightarrow g'}}$$

This value gets tabulated for each $g \rightarrow g'$ interaction.

"**Morse-SGC NUREG-CR-200**" document describe the method we used to generate scattering cosine scattering angles and their corresponding probability. Using this method for all the possible group to group scattering five possible cosine of scattering angles and their corresponding probability was generated and tabulated.

For our problem I used both methods. The final code version uses the "**Morse-SGC NUREG-CR-200**" tabulated values.

Appendix B

Pixel8/Voxel8 input deck description

B.1. Type of cross sections generated and used

In this thesis the interaction types are reduced to absorption and scattering cross sections only. The absorption cross section is the physical absorption interaction while the scattering cross section is the sum of the physical coherent, incoherent and pair production interactions. The generated transport cross section data is arranged by groups. For each group we generate a probability of absorption and of scatter, heat cross section for each interaction as well as total cross section and heat cross section.

The designed code has two main programs that represent two problem mode:

1. Forward Monte Carlo method transport
2. Adjoint Monte Carlo transport.

The "transport data" file used is dependent on the problem mode. The input data deck name for each mode is:

1. Forward mode: "**ForwardFicMC.in**"
2. Adjoint mode: "**AdjointFicMC.in**"
3. Folder mode: "**Folder.in**". this file built from a the files specified in bullet 1 and 2.

B.2. General description of input files

The "transport data" file follows a general format. In general the file consists of eight major sections. These sections have the following general description:

1. Section 1: Problem information and needed Monte Carlo parameters.
2. Section 2: Source spectrum description.
3. Section 3: Phantom-Patient Information.
4. Section 4: Source location and emission methods.
5. Section 5: Problem material information.
6. Section 6: Cross sections and transport data for each energy group & material.
7. Section 7: Group to group scattering probabilities for each problem material.
8. Section 8: Group to group scattering angles for each problem material.

B.3. Forward Monte Carlo with / without Fictitious scattering input deck

The forward Monte Carlo input deck contains the following problem specific information:

1. **Section 1**: This section has general problem information and needed Monte Carlo parameters. Image of this data is shown in Figure B-1. The data read from this section is used to setup proper problem directories and turn proper program flags. The following is description of each item:

    a. Problem Type. The available are:

        i. Forward where it can be:

            1. Spectrum Percent Depth Dose.

            2. Group Percent Depth Dose.

            3. Beam Simulation / Computation.

    b. Number particles to run – number of histories.

    c. Particle tracks:

        i. Flag.

        ii. Number of tracks per track file.

        iii. Number of tracks used to plot.

    d. Particle history:

        i. Flag.

        ii. At what run to start writing particle history.

        iii. At what run to stop writing particle history.

    e. CAX percent depth dose compare flag.

    f. Source phantom entrance plot:

        i. Flag.

        ii. Number of points to plot.

    g. When to annunciate on the screen the random walk being process. This serves as a Monte Carlo progress indicator.

    h. Write trouble shooting file flag.

    i. Russian Roulette parameters:

        i. Particle weight cut-off.

        ii. Particle Survival Probability

```
[Problem Information]
Problem Type =GroupPDD
Problem Name = Beam Sim
Number Particles to Use = 5000000
##xxxxxxxxxxxxxxxxxxxxxxxxxxxxxxxxxxxxxxxxxxxxxxxxxxxxxxxxxxxxxxxx
Plot particle tracks = .True.
Write Particle Track Every =10000000
Particle Track Save Dir  =Particle_Track
Particle tracks file number = 4
Number of particle tracks plotted = 150
##xxxxxxxxxxxxxxxxxxxxxxxxxxxxxxxxxxxxxxxxxxxxxxxxxxxxxxxxxxxxxxxx
Write particle history = .True.
Particle history file number = 5
Particle history write start = 50
Particle history write end = 150
##xxxxxxxxxxxxxxxxxxxxxxxxxxxxxxxxxxxxxxxxxxxxxxxxxxxxxxxxxxxxxxxx
CAX PDD Compare flag = .True.
##xxxxxxxxxxxxxxxxxxxxxxxxxxxxxxxxxxxxxxxxxxxxxxxxxxxxxxxxxxxxxxxx
Source phantom entrance plot flag = .True.
Source phantom entrance plot file number = 6
Source phantom entrance plot number of points = 1000
##xxxxxxxxxxxxxxxxxxxxxxxxxxxxxxxxxxxxxxxxxxxxxxxxxxxxxxxxxxxxxxxx
When To Stamp = 50000
##xxxxxxxxxxxxxxxxxxxxxxxxxxxxxxxxxxxxxxxxxxxxxxxxxxxxxxxxxxxxxxxx
Trouble shoot write flag = .True.
Trouble shoot file number = 3
##xxxxxxxxxxxxxxxxxxxxxxxxxxxxxxxxxxxxxxxxxxxxxxxxxxxxxxxxxxxxxxxx
Particle Weight Cut-Off = 0.001
Particle Survival Probability = 0.1
################################################################
```

Figure B-1 Input file view of section 1 data

2. **Section 2**: Source information as shown in Figure B-2.

```
[Problem Source Information]

[Energy Group Structure]
GRP STRUCTURE NAME = 01_pixilated_94.VB
NUMGRP = 93
ENERGY GROUP STRUCTURE - GROUP UPPER BOUND =
Number of Data Entry PerLine =5
2.00000E+04|3.00000E+04|4.50000E+04|6.00000E+04|7.00000E+04
          ⋮
1.95000E+07|1.97500E+07|2.00000E+07

##xxxxxxxxxxxxxxxxxxxxxxxxxxxxxxxxxxxxxxxxxxxxxxxxxxxxxxxxxxxxxxxx
[Photon spectrum]

[Energy Group Photon Spectrum]
VALUES ARE AT - GROUP UPPER BOUND
SOURCE SPECTRUM FILE NAME = 2100_6xMeV.dat
NUMBER OF GROUP SPECTRUM POINTS = 39
COMPUTED PROBLEM GROUP ENERGY SPECTRUM=
SPECTURM Number of Data Entry PerLine =5
 9.44850E-06| 9.44850E-06| 9.44850E-06| 9.44850E-06| 9.44850E-06
          ⋮
2.87410E-07| 1.26290E-07| 7.60600E-09| 7.60600E-19

##xxxxxxxxxxxxxxxxxxxxxxxxxxxxxxxxxxxxxxxxxxxxxxxxxxxxxxxxxxxxxxxx
COMPUTED PROBLEM CDF GROUP ENERGY SPECTRUM=
CDF Number of Data Entry PerLine =5
 0.046977| 0.093954| 0.140931| 0.187908| 0.234885
          ⋮
0.999333| 0.999961| 0.999999| 1.000000

##xxxxxxxxxxxxxxxxxxxxxxxxxxxxxxxxxxxxxxxxxxxxxxxxxxxxxxxxxxxxxxxx
Selection Array Number of Entries = 1000
Selection Array Data =
SA Number of Data Entry PerLine =15
 001| 001| 001| 001| 001| 001| 001| 001| 001| 002| 002| 002| 002
          ⋮
031| 032| 032| 032| 032| 032| 032| 032| 033| 033| 033| 033| 033| 033| 034
 034| 034| 034| 034| 035| 035| 035| 036| 036| 037
##xxxxxxxxxxxxxxxxxxxxxxxxxxxxxxxxxxxxxxxxxxxxxxxxxxxxxxxxxxxxxxxx
6 MV standard CAX PDD
Number of point in PDD curve = 95
0.25    0.603598
          ⋮
47.25   0.008733
```

Figure B-2 Input file view of section 2 data

The information is:

a. Energy group structure:
    i. Name
    ii. Number of groups
    iii. Energy bins upper limit (tabulated in rows with a given number of entries per row).

b. Source photon spectrum:
    i. File name.
    ii. Number of source spectrum points.
    iii. Source spectrums bin frequencies (tabulated in rows with a given number of entries per row).
    iv. Source spectrums bin CDF (tabulated in rows with a given number of entries per row).
    v. Source spectrums selection array information and it values as shown in Figure B-3:
        1. Number of entries.
        2. Number of entries per each line of search array data.
        3. Search array data in rows.

```
Varian_6MV_MCNP5_MGXSNP.dat
Selection Array Number of Entries = 1000
Selection Array Data =
SA Number of Data Entry PerLine =15
 002| 002| 002| 002| 002| 002| 002| 002| 003| 003| 003| 003| 003| 003| 003
 003| 003| 003| 003| 003| 003| 003| 003| 003| 003| 003| 003| 003| 003| 003
 003| 003| 003| 003| 003| 003| 003| 003| 003| 003| 003| 003| 003| 003| 003
 003| 003| 003| 003| 003| 003| 003| 003| 003| 003| 003| 003| 003| 003| 003
 003| 003| 003| 003| 003| 003| 003| 003| 003| 003| 003| 003| 003| 003| 003
 003| 003| 003| 003| 003| 003| 003| 003| 003| 003| 003| 003| 003| 003| 003
 003| 003| 003| 003| 003| 003| 003| 003| 003| 003| 003| 003| 003| 003| 003
 003| 003| 003| 003| 003| 003| 003| 003| 003| 003| 003| 003| 003| 003| 003

                                   ●
                                   ●
                                   ●
                                   ●
 007| 007| 007| 007| 007| 007| 007| 007| 007| 007| 007| 007| 007| 007| 007
 007| 007| 007| 007| 007| 007| 007| 007| 007| 007| 007| 007| 007| 007| 007
 007| 007| 007| 007| 007| 007| 007| 007| 007| 008| 008| 008| 008| 008
 008| 008| 008| 008| 008| 008| 008| 008| 008| 008| 008| 008| 008| 008| 008
 008| 008| 008| 008| 008| 008| 008| 008| 008| 008| 008| 008| 008| 008| 008
 008| 008| 008| 008| 008| 008| 008| 008| 008| 008| 008| 008| 008| 009| 009
 009| 009| 009| 009| 009| 009| 009| 009| 009| 009

######################################################################
```

Figure B-3 Input file view of photon spectrum search array

    c. The standard reference beam data information:

        i. Name of standard beam.

        ii. Number of points in the standard reference beam data.

        iii. Standard reference beam data in rows.

As a result of processing this section the following data is read to assist in the particle random walk decisions:

    i. Then number of spectrum groups.

    ii. The number of search array points (normally multiple of 1000).

    iii. The photon spectrum CDF as one dimensional array.

    iv. The photon spectrum search array values as one dimensional array.

The search array is used to speed up the search for the particle initial group. In doing this we eliminate the need to look through the entire array every time we start a new history. The following is description of how the search array is used during particle random walk:

    i. A random number is drawn.

    ii. The random number is converted to an integer by multiplying it with search array number of points to produce a search array index (e.g., between 1and 1000 for array of 1000 dimension).

    iii. The computed index is converted to spectrum group number (saved array value).

    iv. The selected spectrum group is tested against its actual CDF and adjusted accordingly if it fails the test.

3. **Section 3**: Phantom-Patient Information as shown in Figure B-4:

    a. Material map box dimension (e.g., X-Length, Y-Length and Z-Length.)

    b. Length ranges (e.g., Low and high value for each dimension.)

    c. Voxel dimension.

    d. First voxel corner coordinate.

    e. Material Map type:

        i. Homogenous.

        ii. Nonhomogeneous.

```
[Phantom-Patient Information]
X-Length      = 50.0
Y-Length      = 50.0
Z-Length      = 50.0
Low-X-RANGE   = -25.0
High-X-RANGE  = +25.0
Low-Y-RANGE   = 0.0
High-Y-RANGE  = +50.0
Low-Z-RANGE   = -25.0
High-Z-RANGE  = +25.0
Voxel-DX      = 0.5
Voxel-DY      = 0.5
Voxel-DZ      = 0.5
FirstVoxelXValue = -25.0
FirstVoxelYValue = 0.0
FirstVoxelZValue = -25.0

[Material Map Details]
Material Map Type = Homogeneous
##Material Map Type = NonHomogeneous
MaterialMap=
```

Figure B-4 Input file view of section 3 data

4. **Section 4**: Source position and beam blocking (Linac-Specifications and Field Parameters) parameters as illustrated in Figure B-5.

```
!================================================
#xxxx   Linac-Specification   xxxxxxxxxxxxxxxx
!================================================
[Linac-Specification]

[Field Parameters]
Source-X = 0.0
Source-Y = -100.0
Source-Z = 0.0
Iso-X = 0.0
Iso-Y = 0.0
Iso-Z = 0.0
Source Axial Distance = 100.00
Source Mid MLC Distance = 51.00
Enclosed Limits is at Distance = 100.00
Maximum Field Size at SAD = 40.00
Magnification Factor = 0.510000
Field Type = Open
Number of Leaf Pairs = 60
Number of Plan Beams = 1
Beam Angle = 0.0
Jaws Type = Symmetric
MinX = -5.000
MaxX = 5.000
MinY = -5.000
MaxY = 5.000
```

Figure B-5 Input file view of section4

This information is:

  a. Source coordinates.

  b. Isocenter coordinates.

  c. Source Axial Distance.

  d. Source Middle MLC Distance.

  e. Enclosed Limits is at Distance.

  f. Maximum field size at source axial distance (used to compute maximum angle of the primary collimator opening. This will affect particle initial weight.

  g. Magnification Factor

  h. Field Type as shown in Figure B-6:

```
##If FieldType is MLC or blocked you well have more things to follow:

#For MLC - Fields
###Field Type = MLC
###Beam Angle = 0.0
###Number Limits Sets = 25

##FirstLeafPair = 18
##LastLeafPair = 42


#MinX = -5.264
#MaxX = 4.800
#MinY = -6.500
#MaxY = 6.000

Limits [Ymin,Ymax], [Xmin,XMax], {Leaf Thickness} =
18|  -6.50|  -6.00|  -4.706|   0.040|   0.50
19|  -6.00|  -5.50|  -2.759|   1.670|   0.50
                    •
                    •
41|   5.00|   5.50|  -1.913|   2.630|   0.50
42|   5.50|   6.00|  -4.457|   2.040|   0.50
```

Figure B-6 Input file view of section 4 MLC leaf data

The field can be either:

  i. Open.

  ii. Blocked (MLC or Block). If the field blocked we can read the following:

    1. If MLC's you will have MLC data information (e.g., number of limit points, first and last leaf pair followed by listing of the leaf

number, minimum, maximum of X and Y jaws and leaf thickness given in rows of data.

2. If block you will have Block data information (e.g., number of polygon data points followed by listing of (x, y) coordiantes)

i. Number of Leaf Pairs.

j. Number of Plan Beams.

k. Beam Angle

l. Jaws Type:

    i. Symmetric.

    ii. Asymmetric.

m. Jaw limits (list the maximum and minimum for the X and Y jaws.)

This is illustrated in Figure B-7 below:

```
#OR For MLC/blocked fields (these points are from the MLC leafs)
#PolygonNumberPoints =   100
FieldAsPolygonVertices-(Anticlockwise)-(x,y) =
   0.040| -6.50
   0.040| -6.00
   1.670| -6.00
        ●
        ●
        ●
  -2.759| -6.00
  -4.706| -6.00
  -4.706| -6.50
```

Figure B-7 Input file view of section 4 MLC/blocked field data

5. **<u>Section 5</u>**: This section contains needed information regarding the materials present in the problem. Figure B-8 illustrate the organization of this section. This information is:

a. Number of materials in the problem.

b. Listing of materials in problem.

c. Problem material information including:

    i. Elemental composition of each material followed by:

        1. Density.

        2. Z number.

        3. Atomic weight.

        4. Weight fraction

```
[Material]

XSFactor = 6.0221412927E-01|HeatFactor = 5.8104830095E+09

Total Number Selected Material = 2

XS in units of (1/cm) | Heat in Units of (cGy-cm^2)

#Chem Symb.|Density|NJOY Material Number = Mass Number (A)-{(Znumber / ZoverA)}


nSelElem=0



#Tissue Name|Density|NJOY Material Number = Mass Number (A)-{(Znumber / ZoverA)}:Mass Fraction

nSelTissue=2

Water|1.00000|100=1.00794:0.11190|800=15.99936:0.88810

Dry_Air|0.00121|600=12.01105:0.00012|700=14.00672:0.75527|800=15.99936:0.23178|1800=39.94762:0.01283


Number of Materials in the File = 2

Materials in the File = Water|Dry_Air
```

Figure B-8 Input file view of section 5 data

6. **Section 6**: For each problem present material the cross sections are listed in rows with several columns. The rows represent groups as shown in Figure B-9 and each column is:

   a. Column 1: Group number.

   b. Column 2: Middle group structure energy bin.

   c. Column 3: Absorption probability,

   d. Column 4: Absorption heat cross section.

   e. Column 5: Down scattering probability.

   f. Column 6: Scattering heat cross section

   g. Column 7: Total cross section.

   h. Column 8: Total heat cross section.

```
Material = Water

Material-Water|Probability [fraction (0-1)],Heat XS units (cGy - cm^2), GXS data units (1/cm)

GRP#|EBinMidPoint|AbsorptionProb|AbsorptionHeat|ScatteringProb|ScatteringHeat|TotalXs|TotalHeat

001|  1.500E+04|  0.821551|  3.17625E-10|  0.178449|  1.44732E-12|  1.68577E+00|  3.19073E-10

002|  2.500E+04|  0.521716|  1.04721E-10|  0.478284|  3.60411E-12|  5.09757E-01|  1.08325E-10

                              ⋮

092|  1.963E+07|  0.000004|  2.11689E-14|  0.999996|  4.69357E-09|  1.81720E-02|  4.69360E-09

093|  1.988E+07|  0.000004|  2.11455E-14|  0.999996|  4.74906E-09|  1.81210E-02|  4.74908E-09
```

Figure B-9 Input file view of section 6 data

The following is how read data read from this section is used:

i. The first two columns indicate current group number and the mid bin value and primarily used for plotting purposes.

ii. The absorption or scattering probability is used to decide whether the interaction is absorption or scattering. The absorption probability is not being used currently.

iii. The absorption heat is being used for the simulation. The dose contributed to that problem is the value of the absorption heat cross section, if the type of interaction is an absorption reaction. If it was a scattering section, the scattering heat cross section would be contributed to dose.

iv. The total cross section is used to determine the distance to the interaction site.

v. The total heat cross section not used in the current program.

7. **Section 7**: Tabulation of group to group scattering probabilities for each material in the problem as shown in Figure B-10. Each group data is in one row. The number of data rows in this table is given. The following is the sequence of data in the each group row:

   a. Initial group.
   b. Final group (down scatter group).
   c. Number of probability points following in this data line.
   d. The current group CDF table entries. The first value represents the maximum probability for scattering to the lowest energy group while the last two entries is the range of probabilities for scattering to the current group.


```
Material-Water|Probability of Scattering from Initial Group to Final Group
Number Scattering Probability Data Points = 3683
InitialGRP|FinalGRP|# Points|Group probabilities from final group (Elow) to initial group (Ehigh)
001|001|001|  1.000000
002|001|002|  0.238026|  1.000000
003|002|002|  0.195221|  1.000000
                          ●
                          ●
                          ●
015|008|008|  0.069308|  0.320842|  0.499638|  0.590323|  0.705273|  0.710737|  0.895670|  1.000000
016|008|009|  0.036768|  0.277800|  0.435613|  0.509717|  0.599736|  0.603980|  0.742901|  0.914789|  1.000000
```

Figure B-10 Input file view of section 7 data

125

The data in this section is arranged as initial group and the lowest final group. After that the probability is given from the lowest final group to the initial group. The number of probability values varies from 1 all the way to the maximum number based on the lowest final group. When this data is read into the program four two dimensional arrays are created indicating the material number and group number. The following is what data arrays are created:

1. The first array stores the lowest down group.
2. The second array stores the index of the group probability starting point.
3. The third array stores the index of the group probability ending point.
4. The fourth array has a second dimension that is equal to the maximum scatter data records. This array stores the down scatter group to group probability.

8. **Section 8**: Tabulation of the group to group scattering angles for each material in the problem. Each group data is in one row. The input deck contains two types of cosine scattering data. The following is a description of both types:

   a. **Type I**: Average of cosine scattering angle as described in the Mores code shown in Figure B-11. The number of data rows in this table is given. The following is the sequence of data in the each group row. :

      i. Initial group.
      ii. Final group (scatter down to group.)
      iii. Zero Order Legendre coefficient.
      iv. First order Legendre coefficient.
      v. The computed average cosine scattering angle.

```
##########################################################################
#############   Mores & Keno scattering angle angular treatment   #######
##########################################################################

Material-Water|Average Cosine scattering angle as defined by Morse code
Number Average Cosine scattering angle Data Lines = 68
InitialGRP|FinalGRP|L.O.Zero|L.O.first|Average MU
001|001|   1.60304E-01|   1.23741E-02|   0.0771914
002|001|   1.81645E-02| -6.04299E-03| -0.3326821
002|002|   1.10479E-01|   3.15195E-02|   0.2852995
003|002|   5.51261E-02|   2.92316E-03|   0.0530268
003|003|   2.76270E-02|   2.38010E-02|   0.8615130

                        ●

                        ●

                        ●

                        ●

012|010|   2.39451E-03|   5.96653E-04|   0.2491753
012|011|   2.68862E-03|   5.62893E-04|   0.2093614
012|012|   4.07036E-03|   1.01783E-03|   0.2500599



##################################################################
```

Figure B-11 Input file view of section 8 data of type I

b. **Type II**: Tabulates the angular probability distribution function of cosine scattering angle shown in Figure B-12. Further; the number of group to group data lines in the table, the number of cosine of scattering angle values and its corresponding probability per data line is also listed. The following is the sequence of data in the each group row:

c. Initial group.

d. Final group (scatter down to group.)

e. A sequence of cosine of scattering angle values followed by the same number of the probability distribution value of these cosines scattering angle.

```
##############################################################################
#############   Dr. Pevey scattering angle angular treatment  (NUREG200)  ######
##############################################################################


Material-Water|AngularPDF-Cosine Scattering Angle @ given Probability
Number GTG Scattering XS Data Lines = 68
Number of GTG cosine scattering angle (MU) points = 5
Number of Probability points for listed MU values = 5
InitialGRP|FinalGRP|xx Cosine Scattering Angle - xx probabilities for those MUs
   1    1 -0.91057 -0.54530  0.03275  0.59400  0.93520 0.120504 0.200907 0.222312 0.260010 0.196266
   2    1 -0.92421 -0.61411 -0.11305  0.42963  0.82429 0.225061 0.331402 0.252033 0.148646 0.042858
   2    2 -0.90257 -0.51448  0.07038  0.61312  0.93117 0.073415 0.150205 0.215651 0.310234 0.250495
   3    2 -0.91104 -0.55070 -0.00558  0.50628  0.84894 0.097120 0.202317 0.274693 0.312579 0.113290
   3    3 -0.55633  0.34230  0.64166  0.84925  0.97356 0.000001 0.000339 0.152598 0.487389 0.359673
   4    2 -0.93145 -0.66184 -0.26817  0.11462  0.36598 0.103910 0.220714 0.290371 0.285140 0.099864
   4    3 -0.87941 -0.38679  0.41775  0.69300  0.90218 0.001483 0.003308 0.236438 0.525466 0.233304

                                        ●

                                        ●

                                        ●

                                        ●

  12    9 -0.69391 -0.12266  0.55915  0.96449  0.98643 0.000000 0.000000 0.000005 0.838774 0.161221
  12   10 -0.69385 -0.12240  0.55957  0.97307  0.98927 0.000000 0.000000 0.000004 0.649490 0.350506
  12   11 -0.69368 -0.12159  0.56086  0.97933  0.99429 0.000000 0.000000 0.000002 0.490565 0.509433
  12   12 -0.99539 -0.14269  0.26378  0.98355  0.99660 0.000000 0.000001 0.000000 0.284857 0.715142
##############################################################################
```

Figure B-12 Input file view of section 8 data of type II

The (μ) value and its corresponding probability are tabulated in each line. To store this data in a compact way it is read for each problem material into the program using the following arrays:

1. Two dimensional array that stores the starting group for the specified group to group scattering. Index one represents the material number and second index represents the particular group to group scattering (data line).

2. Two dimensional array that stores the final down group for the specified group to group scattering. Index one represents the material number and second index represents the particular group to group scattering (data line).

3. Three dimensional array that store the specified (μ) values. Index one represents the material number and second index represents the particular

128

group to group scattering (data line) and index three represent the listed (μ) value.

4. Three dimensional array that store the specified probability for the given (μ) values. Index one represents the material number and second index represents the particular group to group scattering (data line) and index three represent the listed probability value for the listed (μ) value.

B.4. Adjoint Monte Carlo with Fictitious scattering input deck

The adjoint input deck sections 1, 2, 3 and 5 are identical to the forward input deck. The rest of the sections are similar to the forward input deck with modifications that is suitable for adjoint transport. Method of data generation was described in the previous appendix. Here we will describe data organization only.

1. **Section 4**: Adjoint source location. As illustrated in Figure B-13 the user specifies:
   a. Region of interest name (ROI).
   b. Number of region of interest indices.
   c. List of all voxel indices for the region of interest (i, j, k). These indices will be converted to (x, y, z) values using voxel dimension.

```
[ROI Indices]
Name of ROI = Box
Number of ROI Indices = 27
Indices List XXXX|YYYY|ZZZZ
0050|0011|0050
0050|0012|0050
0050|0013|0050
0051|0011|0050
0051|0012|0050
0051|0013|0050
0052|0011|0050
0052|0012|0050
        ●
        ●
        ●
0051|0011|0052
0051|0012|0052
0051|0013|0052
0052|0011|0052
```

Figure B-13 Adjoint Input file view of section 4 (ROI) indices

2. **Section 6**: For each problem material cross sections and transport data for each energy group are listed as shown in Figure B-14. The rows represent groups (Figure B - 9) and each column is:

   a. Column 1: Group number.

   b. Column 2: Middle group structure energy bin.

   c. Column 3: Absorption probability,

   d. Column 4: Absorption heat cross section.

   e. Column 5: Up scattering probability.

   f. Column 6: up scattering heat cross section

   g. Column 7: Total cross section.

   h. Column 8: Total heat cross section.

```
[Adjoint-GTG-XSData]
################################################################################
Material = Water
Heat Factor =   1.282E-07
Material-Water|Probability [fraction (0-1)],Heat XS units (cGy-cm^2), GXS data units (1/cm)
GRP#|EBinMidPoint|AbsorptionProb|AbsorptionHeat|ScatteringProb|ScatteringHeat|TotalXs|TotalHeat
001|  5.500E+04|  0.127307|  1.20511E-10|  0.847143|  3.03535E-10|  2.10671E-01|  3.12689E-10
002|  3.000E+05|  0.003986|  9.63996E-12|  1.763553|  1.75291E-09|  1.32796E-01|  9.90001E-10
003|  7.500E+05|  0.000108|  7.60154E-13|  1.108199|  3.32604E-09|  8.35978E-02|  3.00098E-09
004|  1.500E+06|  0.000034|  3.47468E-13|  1.072950|  5.68275E-09|  5.96543E-02|  5.29621E-09
005|  2.500E+06|  0.000018|  2.50657E-13|  0.681254|  5.29097E-09|  4.44820E-02|  7.76637E-09
006|  3.500E+06|  0.000014|  2.19556E-13|  0.504274|  4.91579E-09|  3.67471E-02|  9.74813E-09
007|  4.500E+06|  0.000011|  2.04600E-13|  0.410587|  4.74587E-09|  3.20795E-02|  1.15586E-08
008|  5.500E+06|  0.000010|  1.95209E-13|  0.352720|  4.69792E-09|  2.90320E-02|  1.33190E-08
009|  6.500E+06|  0.000009|  1.89476E-13|  0.312154|  4.66725E-09|  2.66596E-02|  1.49516E-08
010|  7.500E+06|  0.000008|  1.84993E-13|  0.265355|  4.40284E-09|  2.49302E-02|  1.65922E-08
011|  8.500E+06|  0.000007|  1.82326E-13|  0.202332|  3.69937E-09|  2.36603E-02|  1.82835E-08
012|  1.450E+07|  0.000006|  1.76087E-13|  0.192600|  4.62489E-09|  2.11337E-02|  2.40128E-08
```

Figure B-14 Adjoint Input file view of section 6 material cross sections and transport data

In this section the total & absorption cross section is identical to the forward cross sections. The scattering cross section and scattering probability is different than the forward input file data. These values are generated using the method described in the previous section.

3. **Section 7**: Tabulation of group to group scattering probabilities for each problem material as shown in Figure B-15. Each group data is in one row. The number of data rows in this table is given. The following is the sequence of data in the each group row:

   a. Initial group.

   b. Final group (up scatter group).

   c. Number of probability points following in this data line.

   d. The current group CDF table entries. The first value represents the maximum probability for scattering to the current energy group while the last two entries is the range of probabilities for scattering to the highest energy group.

```
###First probability entry  is for Initial group & last entry is for Final up group###
Material-Water|Probability of Scattering from Initial Group to Final Group
Number Scattering Probability Data Points = 68
InitialGRP|FinalUpGRP|Group probabilities from final group (Elow) to initial group (Ehigh)
001|002|002|  0.898220|  1.000000
002|012|011|  0.471743|  0.707130|  0.801633|  0.853400|  0.889367|  0.917013|  0.939583|  0.958516|  0.974866|  0.989287|  1.000000
003|012|010|  0.298210|  0.539348|  0.654902|  0.736357|  0.800337|  0.853514|  0.898757|  0.938269|  0.973433|  1.000000
004|012|009|  0.229395|  0.463297|  0.601493|  0.702380|  0.783354|  0.850983|  0.909432|  0.961136|  1.000000
005|012|008|  0.186652|  0.424099|  0.579554|  0.697207|  0.792521|  0.873702|  0.945196|  1.000000
006|012|007|  0.163624|  0.396789|  0.565980|  0.700712|  0.815276|  0.917110|  1.000000
007|012|006|  0.156005|  0.388932|  0.573643|  0.732006|  0.875171|  1.000000
008|012|005|  0.166843|  0.411648|  0.624063|  0.819495|  1.000000
009|012|004|  0.202199|  0.482985|  0.745732|  1.000000
010|012|003|  0.276316|  0.638037|  1.000000
011|012|002|  0.438376|  1.000000
012|012|001|  1.000000
```

Figure B-15 Input file view of section 7 data

The data in this section is arranged as initial group and the highest final group. After that the probability is given from the current group to the highest final group. The number of probability values varies from 1 all the way to the maximum number based on the highest final group. When this data is read into the program four two dimensional arrays are created indicating the material number and group number. The following is what data arrays are created:

   i.   The first array stores the current group.

   ii.   The second array stores the index of the group probability starting point.

   iii. The third array stores the index of the group probability ending point.

   iv.   The fourth array has a second dimension that is equal to the maximum scatter data records. This array stores the up scatter group to group probability.

131

4. **Section 8**: Tabulation of group to group scattering angles for each material. Each group data is in one row. The input deck contains two types of cosine scattering data. The following is a description of both types:

   a. **Type I**: Average of cosine scattering angle as described in the Mores code shown in Figure B-16. The number of data rows in this table is given. The following is the sequence of data in the each group row. :
      i. Initial group.
      ii. Final group (up scatter group.)
      iii. Zero Order Legendre coefficient.
      iv. First order Legendre coefficient.
      v. The computed average cosine scattering angle.

```
###################################################################
#############   Mores & Keno scattering angle angular treatment   #######
###################################################################

Material-Water|Average Cosine scattering angle as defined by Morse code
Number Average Cosine scattering angle Data Lines = 68
InitialGRP|FinalGRP|L.O.Zero|L.O.first|Average MU
001|001|   1.60304E-01|   1.23741E-02|   0.0771914
001|002|   1.81645E-02| -6.04299E-03| -0.3326821
002|002|   1.10479E-01|   3.15195E-02|   0.2852995
002|003|   5.51261E-02|   2.92316E-03|   0.0530268
002|004|   2.21318E-02| -5.56573E-03| -0.2514806
002|005|   1.21235E-02| -4.20658E-03| -0.3469767
                         ●
                         ●
                         ●
010|011|   2.39291E-03|   9.95028E-04|   0.4158225
010|012|   2.39451E-03|   5.96653E-04|   0.2491753
011|011|   2.09861E-03|   4.47919E-04|   0.2134364
011|012|   2.68862E-03|   5.62893E-04|   0.2093614
012|012|   4.07036E-03|   1.01783E-03|   0.2500599
###############################################################
```

Figure B-16 Input file view of section 8 data of type I

   b. **Type II**: Tabulates the angular probability distribution function of cosine scattering angle shown in Figure B-17. Further; the number of group to group data

132

lines in the table, the number of cosine of scattering angle values and its corresponding probability per data line is also listed. The following is the sequence of data in the each group row:

    i. Initial group.

   ii. Final group (up scatter group.)

  iii. A sequence of cosine of scattering angle values followed by the same number of the probability distribution value of these cosines scattering angle.

```
################################################################################
#############   Dr. Pevey scattering angle angular treatment  (NUREG200)  ######
################################################################################


Material-Water|AngularPDF-Cosine Scattering Angle @ given Probability
Number GTG Scattering XS Data Lines = 68
Number of GTG cosine scattering angle (MU) points = 5
Number of Probability points for listed MU values = 5
AdjIntGRP|AdjUpGRP|xx Cosine Scattering Angle - xx CDF probabilities for those MUs
001|001| -0.91057| -0.54530|  0.03275|  0.59400|  0.93520|  0.12050|  0.32141|  0.54372|  0.80373|  1.00000
001|002| -0.92421| -0.61411| -0.11305|  0.42963|  0.82429|  0.22506|  0.55646|  0.80850|  0.95714|  1.00000
002|002| -0.90257| -0.51448|  0.07038|  0.61312|  0.93117|  0.07341|  0.22362|  0.43927|  0.74950|  1.00000
002|003| -0.91104| -0.55070| -0.00558|  0.50628|  0.84894|  0.09712|  0.29944|  0.57413|  0.88671|  1.00000
002|004| -0.93145| -0.66184| -0.26817|  0.11462|  0.36598|  0.10391|  0.32462|  0.61499|  0.90013|  1.00000
002|005| -0.94247| -0.71731| -0.38979| -0.06734|  0.14566|  0.09658|  0.30509|  0.58385|  0.85783|  1.00000
002|006| -0.94541| -0.73235| -0.42399| -0.12188|  0.07878|  0.09517|  0.30168|  0.57900|  0.85077|  1.00000
002|007| -0.94664| -0.73876| -0.43906| -0.14715|  0.04564|  0.09500|  0.30164|  0.57957|  0.85062|  1.00000
002|008| -0.94883| -0.74898| -0.45874| -0.17177|  0.02252|  0.09234|  0.29434|  0.56928|  0.84333|  1.00000
                                      •
                                      •
                                      •
                                      •
                                      •
009|012| -0.69391| -0.12266|  0.55915|  0.96449|  0.98643|  0.00000|  0.00000|  0.00001|  0.83878|  1.00000
010|010| -0.72762| -0.54370|  0.33277|  0.99291|  0.99807|  0.00000|  0.00000|  0.00000|  0.20112|  1.00000
010|011| -0.99612| -0.06916|  0.04087|  0.99073|  0.99984|  0.00000|  0.00000|  0.00000|  0.84341|  1.00000
010|012| -0.69385| -0.12240|  0.55957|  0.97307|  0.98927|  0.00000|  0.00000|  0.00000|  0.64949|  1.00000
011|011| -0.77577| -0.40457|  0.20953|  0.71205|  0.99769|  0.00000|  0.00000|  0.00000|  0.00001|  1.00000
011|012| -0.69368| -0.12159|  0.56086|  0.97933|  0.99429|  0.00000|  0.00000|  0.00000|  0.49057|  1.00000
012|012| -0.99539| -0.14269|  0.26378|  0.98355|  0.99660|  0.00000|  0.00000|  0.00000|  0.28486|  1.00000
```

Figure B-17 Input file view of section 8 data of type II

The (μ) value and its corresponding probability are tabulated in each line. To store this data in a compact way it is read for each problem material into the program using the following arrays:

i. Two dimensional array that stores the starting group for the specified group to group scattering. Index one represents the material number and second index represents the particular group to group scattering (data line).

ii. Two dimensional array that stores the final up group for the specified group to group scattering. Index one represents the material number and second index represents the particular group to group scattering (data line).

iii. Three dimensional array that store the specified (μ) values. Index one represents the material number and second index represents the particular group to group scattering (data line) and index three represent the listed (μ) value.

iv. Three dimensional array that store the specified probability for the given (μ) values. Index one represents the material number and second index represents the particular group to group scattering (data line) and index three represent the listed probability value for the listed (μ) value.

Appendix C

Forward continuous and multigroup MCNP5 input deck

The following are the MCNP5 input decks used to estimate (Voxel) fluxes using MCNP5 FMESH4 tally and the deck that estimates the average dose rates in the problem regions of interest: the tumor, the brain, and both eyes. The calculations use the built-in 12 group photon cross sections, which are also used in the Pixel8 and Voxel8 calculations.

C.1. MCNP5 multigroup input deck to get flux map

```
Forward MC CAX PDD Sim - Varian 6 MV Spectrum-MCNP-MGXSNP Grp Strctre
c ********************************************************************
c      Cells  - 50.0 x 50.0 x 50.0 Water Box
c ********************************************************************
  1   1 -1 -1           imp:p=1   $ 50.0x50.0x50.0 Water box
  2   0 -2 3            imp:p=0   $ thin layer surrounding window
  3   0 -3              imp:p=1   $ 10 x 10 window
  4   0 #1 #2 #3 -100   imp:p=1   $ outside water box inside universe
  5   0 +100            imp:p=0   $ Outside universe -void

c ********************************************************************
c      Surfaces
c ********************************************************************
  100 so   200.0                              $ Universe bound
  1   RPP -25.0 25.0 0.0 50.0 -25.0 25.0   $ Water box 50.0x50.0x50.0
  2   RPP -25.0 25.0 -0.001 0.0 -25.0 25.0 $ thin Field Plate
  3   RPP -5.0 5.0 -0.001 0.0 -5.0 5.0     $ Field size 10.0 x 10.0

c ********************************************************************
c      Data Cards
c ********************************************************************
c
c Photon point source positioned at (0.0,-100.0,0.0) all particles
c travelling in direction <0.0,-1.0,0.0>. Source energy distribution
c is according to the published 2100-6MV spectrum. Direction is
c limited to a 40.0 cm diameter circle at 100.0 cm from the source.
c max angle is Acos(100/101.98=0.980581) = 11.30993-
c mu from 1.0 --> 0.980581. to normalize to the particles in the cone
c use WGT=1/fsa2 (fsa2= fraction solid angle of the cone)
c This is a 40.0 cm circle run
SDEF POS 0.0 -100.0 0.0 VEC 0.0 1.0 0.0
     ERG d1 DIR d2 PAR 2
c
c ********************************************************************
c ************    Energy Distribution 2100-6MV   ********************
c ************    Group structure MCNP-MGXSNP     ********************
c ********************************************************************
c
SI1 H 0.010  0.100  0.500  1.000  2.000  3.000  4.000  5.000  6.000
SP1 D 0.000000  0.007698  0.133707  0.235028  0.303138  0.166534
      0.093532  0.048771  0.011591
c
c ********************************************************************
c         Picking in a 11.30993 cone (Bias = 1/ 0.0097097)
c ********************************************************************
```

135

```
c
SI2 −1.0 0.9805807 1.0          $ Histogram for cosine bin limits
SP2 0.0  0.9902903 0.0097097    $ frac. solid angle for each bin
SB2 0.  0.  1.                  $ source bias for each bin
c
c *************** Materials ****************************************
c ****************************************************************
c WATER for gamma-ray transport (by mass fraction)
c ****************************************************************
c
 M1   1000 −0.11190                  $ elemental H mass fraction
      8000 −0.88810                  $ elemental O mass fraction
c
c ****************************************************************
c ******************** Problem FMESH4 Tally ***********************
c ****************************************************************
c
FC4 Multi-group Varian 6 MV Spectrum-MCNP-MGXSNP Grp Strctre
FMESH4:P GEOM=xyz
         ORIGIN=−25 0 0
         IMESH=25.   IINTS=100
         JMESH=50.    JINTS=100
         KMESH=.5   KINTS=1
         OUT=ij
         EMESH = 6.000
c
c ****************************************************************
c ***************  NJOY Dose Conversion factors    ***************
c ***************  For MCNP-MGXSNP group structure  **************
c ****************************************************************
c
 E0  0.010  0.100  0.500  1.000  2.000  3.000  4.000  5.000  6.000
 EM0 3.12689E−10  9.90001E−10  3.00098E−09  5.29621E−09  7.76637E−09
     9.74813E−09  1.15586E−08  1.33190E−08  1.49516E−08
c
c ****************************************************************
c PHYS:P EMCPF IDES NOCOH ISPN NODOP
c EMCPF = Upper energy limit for detailed photon physics treatment,
c         in MeV.
c To turn off electron production and the bremsstrahlung photons
c use IDES=1 default =0 --> thick target bremsstrahlung. To turn
c off coherent scattering NOCOH=1; photo nuclear collision ISPN=0
c Doppler energy broadening NODOP=1
c ****************************************************************
c
CUT:P J 0.01
MODE P
PHYS:P 6.000 1
MGOPT F 12
c PRINT 100 40 110 150 160 161 162
NPS 250000000
PRINT
```

C.2. Forward model for structure doses

```
Forward Eyes Tumor Brain – Varian 6MV Spectrum–MCNP–MGXSNP Grp Strctr
c ********************************************************************
c  Cells  – 50.0 x 50.0 x 50.0 Water Box with 3 structures
c ********************************************************************
 1     1 -1.0 -1              imp:p=1 $ Tumor
 2     1 -1.0 -2              imp:p=1 $ Right eye
 3     1 -1.0 -3              imp:p=1 $ Left eye
 4     1 -1.0 -4:-5:-6        imp:p=1 $ Brain
 5     1 -1.0 -7 #1 #2 #3 #4  imp:p=1 $ 50.0x50.0x50.0 Water box
 6     0 -8 9                 imp:p=0 $ thin layer above box
 7     0 -9                   imp:p=1 $ 20 x 20 window
 8     0 #1 #5 #6 #7 -100     imp:p=1 $ outside water box in universe
 9     0 +100                 imp:p=0 $ Outside universe – void
c ********************************************************************
c     Surfaces
c ********************************************************************
 1     S   4.5 15.0 3.0 1.5                     $ Tumor
 2     S  -7.0 4.0 0.0 3.5                      $ Right Eye
 3     S   7.0 4.0 0.0 3.5                      $ Left Eye
 4     RPP -10.0 10.0 17.0 29.5 -9.0   1.0 $ Brain – Box 1
 5     RPP -10.0 10.0 21.0 28.5   1.0  8.0 $ Brain – Box 2
 6     RPP -10.0 10.0  3.5 31.0   8.0 15.0 $ Brain – Box 3
 7     RPP -25.0 25.0 0.0 50.0 -25.0 25.0  $ Water box 50.0x50.0x50.
 8     RPP -25.0 25.0 -0.001 0.0 -25.0 25.0 $ thin Field Plate
 9     RPP -5.0 5.0 -0.001 0.0 -5.0 5.0    $ Field size 10.0 x 10.0
 100   so  200.0                            $ Universe bound

c ********************************************************************
c     Data Cards
c ********************************************************************
c
c Photon point source positioned at (0.0,-100.0,0.0) all particles
c travelling in direction <0.0,-1.0,0.0>. Source energy distribution
c is according to the published 2100-6MV spectrum. Direction is
c limited to a 40.0 cm diameter circle at 100.0 cm from the source.
c max angle is Acos(100/101.98=0.980581) = 11.30993-
c mu from 1.0 --> 0.980581. to normalize to the particles in the cone
c use WGT=1/fsa2 (fsa2= fraction solid angle of the cone)
c This is a 40.0 cm circle run
SDEF  POS 0.0 -100.0 0.0 VEC 0.0 1.0 0.0
      ERG d1 DIR d2 PAR 2 WGT 1.03018e2
c
c ********************************************************************
c ************  Energy Distribution 2100-6MV  ***********************
c ************  Group structure MCNP-MGXSNP   ***********************
c ********************************************************************
c
SI1 H 0.010  0.100  0.500  1.000  2.000  3.000  4.000  5.000  6.000
SP1 D 0.000000  0.007698  0.133707  0.235028  0.303138  0.166534
      0.093532  0.048771  0.011591
c
c ********************************************************************
c               Picking in a 11.30993 cone (Bias = 1/ 0.009707)
c ********************************************************************
c
SI2 -1 0.980581 1.            $ Histogram for cosine bin limits
SP2 0.0 0.99029 0.009707      $ frac. solid angle for each bin
SB2 0.  0.  1.                $ source bias for each bin
c
c ************** Materials *******************************************
```

```
c *********************************************************************
c WATER for gamma-ray transport (by mass fraction)
c *********************************************************************
c
M1    1000 -0.11190              $ elemental H mass fraction
      8000 -0.88810              $ elemental O mass fraction
c
c *********************************************************************
c ******************** Problem FMESH4 Tally ************************
c *********************************************************************
c
FC4 Tumor Absorbed dose (cGy)
F4:P 1
FC14 Right Eye Absorbed dose (cGy)
F14:P 2
FC24 Left Eye Absorbed dose (cGy)
F24:P 3
FC34 Brain Absorbed dose (cGy)
F34:P 4
c
c *********************************************************************
c ****************  NJOY99 Dose Conversion factors   ***************
c ****************  For MCNP-MGXSNP group structure   **************
c *********************************************************************
c
E0    0.010  0.100  0.500  1.000  2.000  3.000  4.000  5.000  6.000
EM0   3.12689E-10  9.90001E-10  3.00098E-09  5.29621E-09  7.76637E-09
      9.74813E-09  1.15586E-08  1.33190E-08  1.49516E-08
c
c *********************************************************************
c PHYS:P EMCPF IDES NOCOH ISPN NODOP
c EMCPF = Upper energy limit for detailed photon physics treatment,
c         in MeV.
c To turn off electron production and the bremsstrahlung photons
c use IDES=1 default =0 --> thick target bremsstrahlung. To turn
c off coherent scattering NOCOH=1; photo nuclear collision ISPN=0
c Doppler energy broadening NODOP=1
c *********************************************************************
c
CUT:P J 0.001
MODE P
PHYS:P 6.000 1
MGOPT F 12
c PRINT 100 40 110 150 160 161 162
NPS 100000000
PRINT
```

Appendix D

Adjoint MCNP5 surface cell fluxes input decks

The following are the MCNP5 input decks used to run MCNP5 in adjoint mode to compute cell fluxes using FMESH4 tally. The calculation was repeated for multiple region of interest (adjoint sources). The adjoint source distribution was derived from the region of interest response function.

D.1. Adjoint model simple Box

```
Adjoint with MCNP-MGXSNP - Adjoint Source as a box (1.50x1.50x1.50)
c **********************************************************************
c      Cells  - 50.0 x 50.0 x 50.0 Water Box
c **********************************************************************
  1   1 -1.0  -1         imp:p=1  $ Adjoint source box
  2   1 -1.0  -2 #1      imp:p=1  $ 50.0x50.0x50.0 Water box
  3   0 #2  -100         imp:p=0  $ outside water box inside universe
  4   0 +100             imp:p=0  $ Outside universe -void

c **********************************************************************
c      Surfaces
c **********************************************************************
c
  1   RPP -0.5 1.0 5.0 6.5 -0.5 1.0        $ Adjoint Source
  2   RPP -25.0 25.0 0.0 50.0 -25.0 25.0   $ Water box 50.0x50.0x50.0
  3   PY   0                               $ Crossing plane
  100 so  200.0                            $ Universe bound

c **********************************************************************
c      Data Cards
c **********************************************************************
c Adjoint source is in cell number 1. The cell is made out of
c parallelepiped with given dimensions. Points are chosen uniformly
c  within the parallelepiped.
c
SDEF  PAR=2  ERG=d1  X=d2  Y=d3  Z=d4  CEL=1
c
c **********************************************************************
c ************  Energy Distribution 2100-6MV  **********************
c ************  Group structure MCNP-MGXSNP   **********************
c **********************************************************************
c
SI1 H 0.000 0.010  0.100  0.500  1.000  2.000  3.000  4.000  5.000
      6.000
SP1 D 0.000000000  3.12689E-10  9.90001E-10  3.00098E-09  5.29621E-09
      7.76637E-09  9.74813E-09  1.15586E-08  1.33190E-08  1.49516E-08
c
c **********************************************************************
c *************** Where to pick starting points ********************
c **********************************************************************
SI2 -0.5 1.0                $ X-range for Adjoint source
SP2  0.0 1.0                $ uniform probability over the X-range
```

```
SI3  5.0 6.5                    $ Y-range for Adjoint source
SP3  0.0 1.0                    $ uniform probability over the Y-range
SI4 -0.5 1.0                    $ Z-range for Adjoint source
SP4  0.0 1.0                    $ uniform probability over the Z-range
c
c ********************************************************************
c *************** Materials ******************************************
c ********************************************************************
c WATER for gamma-ray transport (by mass fraction)
c ********************************************************************
c
 M1   1000 -0.11190                   $ elemental H mass fraction
      8000 -0.88810                   $ elemental O mass fraction
c
c ********************************************************************
c ********************  Problem FMESH4 Tally  ***********************
c ********************   Need to have EMESH   ***********************
c ******************** to run Adjoint problem **********************
c ********************************************************************
c
FC4 Adjoint with MCNP-MGXSNP - Adjoint Source a box (1.50x1.50x1.50)
FMESH4:P GEOM=xyz
         ORIGIN=-25 0 -25
         IMESH=25.   IINTS=100
         JMESH=.5    JINTS=1
         KMESH=25.   KINTS=100
         OUT=ik
         EMESH = 6.000
c
c ********************************************************************
c ***************  NJOY Dose Conversion factors    ***************
c ***************  For MCNP-MGXSNP group structure  ***************
c ********************************************************************
c
 E0  0.010  0.100  0.500  1.000  2.000  3.000  4.000  5.000  6.000
 EM0 0.000000  0.007698  0.133707  0.235028  0.303138  0.166534
     0.093532  0.048771  0.011591
c
c ********************************************************************
c PHYS:P EMCPF IDES NOCOH ISPN NODOP
c To turn off electron production and the bremsstrahlung photons
c use IDES=1 default =0 --> thick target bremsstrahlung. To turn
c off coherent scattering NOCOH=1; photo nuclear collision ISPN=0
c Doppler energy broadening NODOP=1
c ********************************************************************
c
CUT:P J 6.000
MODE P
c SSW -3
MGOPT A 12
c PRINT 100 40 110 150 160 161 162
NPS 250000000
PRINT
```

D.2. Adjoint model of tumor (Sphere)

```
Adjoint-MCNP-MGXSNP - Adjoint Source Tumor(4.5,15.0,3.0) R=1.5 cm
c ***********************************************************************
c     Cells  - 50.0 x 50.0 x 50.0 Water Box
c ***********************************************************************
  1   1 -1.0  -1 -2      imp:p=1   $ Adjoint source Tumor
  2   1 -1.0  -2 #1      imp:p=1   $ 50.0x50.0x50.0 Water box
  3   0 #2  -100         imp:p=0   $ outside water box inside universe
  4   0 +100             imp:p=0   $ Outside universe -void

c ***********************************************************************
c     Surfaces
c ***********************************************************************
c
  1   S   4.5 15.0 3.0 1.5                     $ Adjoint Source Tumor
  2   RPP -25.0 25.0 0.0 50.0 -25.0 25.0   $ Water box 50.0x50.0x50.0
  3   PY   0                                $ Crossing plane
  100 so  200.0                             $ Universe bound

c ***********************************************************************
c     Data Cards
c ***********************************************************************
c Adjoint source is in cell number 1. The cell is made out of
c parallelepiped with given dimensions. Points are chosen uniformly
c  within the parallelepiped.
c
SDEF  PAR=2  ERG=d1  X=d2  Y=d3  Z=d4  CEL=1
c
c ***********************************************************************
c ************   Energy Distribution 2100-6MV   ***********************
c ************   Group structure MCNP-MGXSNP    ***********************
c ***********************************************************************
c
SI1 H 0.000 0.010  0.100  0.500  1.000  2.000  3.000  4.000  5.000
      6.000
SP1 D 0.000000000  3.12689E-10  9.90001E-10  3.00098E-09  5.29621E-09
      7.76637E-09  9.74813E-09  1.15586E-08  1.33190E-08  1.49516E-08
c
c ***********************************************************************
c *************** Where to pick starting points *********************
c ***********************************************************************
SI2   2.5  6.5              $ X-range for Adjoint source
SP2   0.0  1.0              $ uniform probability over the X-range
SI3  13.0 17.0              $ Y-range for Adjoint source
SP3   0.0  1.0              $ uniform probability over the Y-range
SI4   1.0  5.0              $ Z-range for Adjoint source
SP4   0.0  1.0              $ uniform probability over the Z-range
c
c ***********************************************************************
c *************** Materials *******************************************
c ***********************************************************************
c WATER for gamma-ray transport (by mass fraction)
c ***********************************************************************
c
 M1   1000 -0.11190                  $ elemental H mass fraction
      8000 -0.88810                  $ elemental O mass fraction
c
c ***********************************************************************
c ******************* Problem FMESH4 Tally  ***********************
c ******************* Need to have EMESH  ***********************
```

```
c ******************* to run Adjoint problem **********************
c ********************************************************************
c
FMESH4:P GEOM=xyz
          ORIGIN=-25 0 -25
          IMESH=25.   IINTS=100
          JMESH=.5    JINTS=1
          KMESH=25.   KINTS=100
          OUT=ik
          EMESH = 6.000
c
c ********************************************************************
c ****************  NJOY99 Dose Conversion factors   ***************
c ****************  For MCNP-MGXSNP group structure   ***************
c ********************************************************************
c
 E0  0.010  0.100  0.500  1.000  2.000  3.000  4.000  5.000  6.000
 EM0 0.000000  0.007698  0.133707  0.235028  0.303138  0.166534
     0.093532  0.048771  0.011591
c
c ********************************************************************
c PHYS:P EMCPF IDES NOCOH ISPN NODOP
c To turn off electron production and the bremsstrahlung photons
c use IDES=1 default =0 --> thick target bremsstrahlung. To turn
c off coherent scattering NOCOH=1; photo nuclear collision ISPN=0
c Doppler energy broadening NODOP=1
c ********************************************************************
c
CUT:P J 6.000
MODE P
c SSW -3
MGOPT A 12
c PRINT 100 40 110 150 160 161 162
NPS 1000000
PRINT
```

D.3. Adjoint model of right eye (Sphere)

```
Adjoint-MCNP-MGXSNP - Adjoint Source RtEye(-7.0,4.0,0.0) R=3.5 cm
c ************************************************************************
c      Cells  - 50.0 x 50.0 x 50.0 Water Box
c ************************************************************************
  1   1 -1.0  -1 -2     imp:p=1  $ Adjoint source  Rt Eye
  2   1 -1.0  -2 #1     imp:p=1  $ 50.0x50.0x50.0 Water box
  3   0 #2  -100        imp:p=0  $ outside water box inside universe
  4   0 +100            imp:p=0  $ Outside universe -void

c ************************************************************************
c      Surfaces
c ************************************************************************
c
  1   S  -7.0 4.0 0.0 3.5                   $ Adjoint Source Rt Eye
  2   RPP -25.0 25.0 0.0 50.0 -25.0 25.0    $ Water box 50.0x50.0x50.0
  3   PY   0                                $ Crossing plane
  100 so  200.0                             $ Universe bound

c ************************************************************************
c      Data Cards
c ************************************************************************
c Adjoint source is in cell number 1. The cell is made out of
c parallelepiped with given dimensions. Points are chosen uniformly
c  within the parallelepiped.
c
SDEF  PAR=2  ERG=d1  X=d2  Y=d3  Z=d4  CEL=1
c
c ************************************************************************
c ************ Energy Distribution 2100-6MV  ***********************
c ************  Group structure MCNP-MGXSNP   ***********************
c ************************************************************************
c
SI1 H 0.000 0.010  0.100  0.500  1.000  2.000  3.000  4.000  5.000
      6.000
SP1 D 0.000000000  3.12689E-10  9.90001E-10  3.00098E-09  5.29621E-09
      7.76637E-09  9.74813E-09  1.15586E-08  1.33190E-08  1.49516E-08
c
c ************************************************************************
c ************** Where to pick starting points ********************
c ************************************************************************
SI2 -11.0 -2.0            $ X-range for Adjoint source
SP2  0.0  1.0             $ uniform probability over the X-range
SI3  0.1  8.0             $ Y-range for Adjoint source
SP3  0.0  1.0             $ uniform probability over the Y-range
SI4 -4.0  4.0             $ Z-range for Adjoint source
SP4  0.0  1.0             $ uniform probability over the Z-range
c
c ************************************************************************
c *************** Materials ***************************************
c ************************************************************************
c WATER for gamma-ray transport (by mass fraction)
c ************************************************************************
c
 M1   1000 -0.11190                $ elemental H mass fraction
      8000 -0.88810                $ elemental O mass fraction
c
c ************************************************************************
c ******************** Problem FMESH4 Tally  ********************
c ******************** Need to have EMESH    ********************
```

```
c ******************** to run Adjoint problem **********************
c *******************************************************************
c
FC4 Adjoint-MCNP-MGXSNP - Adjoint Source RtEye(-7.0,4.0,0.0) R=3.5 cm
FMESH4:P GEOM=xyz
          ORIGIN=-25 0 -25
          IMESH=25.   IINTS=100
          JMESH=.5    JINTS=1
          KMESH=25.   KINTS=100
          OUT=ik
          EMESH = 6.000
c
c *******************************************************************
c ****************  NJOY Dose Conversion factors    ***************
c ****************  For MCNP-MGXSNP group structure  ***************
c *******************************************************************
c
 E0  0.010  0.100  0.500  1.000  2.000  3.000  4.000  5.000  6.000
 EM0 0.000000  0.007698  0.133707  0.235028  0.303138  0.166534
     0.093532  0.048771  0.011591
c
c *******************************************************************
c PHYS:P EMCPF IDES NOCOH ISPN NODOP
c To turn off electron production and the bremsstrahlung photons
c use IDES=1 default =0 --> thick target bremsstrahlung. To turn
c off coherent scattering NOCOH=1; photo nuclear collision ISPN=0
c Doppler energy broadening NODOP=1
c *******************************************************************
c
CUT:P J 6.000
MODE P
c SSW -3
MGOPT A 12
c PRINT 100 40 110 150 160 161 162
NPS 250000000
PRINT
```

D.4. Adjoint model for left eye (Sphere)

```
Adjoint-MCNP-MGXSNP - Adjoint Source LtEye(7.0,4.0,0.0) R=3.5 cm
c ********************************************************************
c     Cells  - 50.0 x 50.0 x 50.0 Water Box
c ********************************************************************
  1   1 -1.0  -1 -2     imp:p=1   $ Adjoint source  Lt Eye
  2   1 -1.0  -2 #1     imp:p=1   $ 50.0x50.0x50.0 Water box
  3   0 #2  -100        imp:p=0   $ outside water box inside universe
  4   0 +100            imp:p=0   $ Outside universe -void

c ********************************************************************
c     Surfaces
c ********************************************************************
c
  1   S   7.0 4.0 0.0 3.5                  $ Adjoint Source Lt Eye
  2   RPP -25.0 25.0 0.0 50.0 -25.0 25.0   $ Water box 50.0x50.0x50.0
  3   PY   0                               $ Crossing plane
  100 so  200.0                            $ Universe bound

c ********************************************************************
c     Data Cards
c ********************************************************************
c Adjoint source is in cell number 1. The cell is made out of
c parallelepiped with given dimensions. Points are chosen uniformly
c  within the parallelepiped.
c
SDEF  PAR=2  ERG=d1  X=d2  Y=d3  Z=d4  CEL=1
c
c ********************************************************************
c ************  Energy Distribution 2100-6MV  **********************
c ************  Group structure MCNP-MGXSNP   **********************
c ********************************************************************
c
SI1 H 0.000 0.010  0.100  0.500  1.000  2.000  3.000  4.000  5.000
      6.000
SP1 D 0.000000000  3.12689E-10  9.90001E-10  3.00098E-09  5.29621E-09
      7.76637E-09  9.74813E-09  1.15586E-08  1.33190E-08  1.49516E-08
c
c ********************************************************************
c *************** Where to pick starting points ********************
c ********************************************************************
SI2   3.0  11.0              $ X-range for Adjoint source
SP2   0.0   1.0              $ uniform probability over the X-range
SI3   0.1   8.0              $ Y-range for Adjoint source
SP3   0.0   1.0              $ uniform probability over the Y-range
SI4  -4.0   4.0              $ Z-range for Adjoint source
SP4   0.0   1.0              $ uniform probability over the Z-range
c
c ********************************************************************
c *************** Materials ****************************************
c ********************************************************************
c WATER for gamma-ray transport (by mass fraction)
c ********************************************************************
c
 M1   1000 -0.11190               $ elemental H mass fraction
      8000 -0.88810               $ elemental O mass fraction
c
c ********************************************************************
c ******************** Problem FMESH4 Tally *********************
c ******************** Need to have EMESH   *********************
```

```
c ******************** to run Adjoint problem **********************
c *******************************************************************
c
FC4 Adjoint-MCNP-MGXSNP - Adjoint Source LtEye(7.0,4.0,0.0) R=3.5 cm
FMESH4:P GEOM=xyz
          ORIGIN=-25 0 -25
          IMESH=25.   IINTS=100
          JMESH=.5    JINTS=1
          KMESH=25.   KINTS=100
          OUT=ik
          EMESH = 6.000
c
c *******************************************************************
c ****************  NJOY Dose Conversion factors    ****************
c ****************  For MCNP-MGXSNP group structure  ****************
c *******************************************************************
c
 E0  0.010  0.100  0.500  1.000  2.000  3.000  4.000  5.000  6.000
 EM0 0.000000  0.007698  0.133707  0.235028  0.303138  0.166534
     0.093532  0.048771  0.011591
c
c *******************************************************************
c PHYS:P EMCPF IDES NOCOH ISPN NODOP
c To turn off electron production and the bremsstrahlung photons
c use IDES=1 default =0 --> thick target bremsstrahlung. To turn
c off coherent scattering NOCOH=1; photo nuclear collision ISPN=0
c Doppler energy broadening NODOP=1
c *******************************************************************
c
CUT:P J 6.000
MODE P
c SSW -3
MGOPT A 12
c PRINT 100 40 110 150 160 161 162
NPS 250000000
PRINT
```

146

D.5. Adjoint model for brain (made out of three boxes)

```
Adjoint-MCNP-MGXSNP - Adjoint Source Brain - made of three boxes
c **********************************************************************
c      Cells  - 50.0 x 50.0 x 50.0 Water Box
c **********************************************************************
  1   1 -1.0 (-1:-4:-5) -2 imp:p=1   $ Adjoint source  Lt Eye
  2   1 -1.0  -2 #1         imp:p=1   $ 50.0x50.0x50.0 Water box
  3   0 #2  -100            imp:p=0   $ outside box inside universe
  4   0 +100                imp:p=0   $ Outside universe -void


c **********************************************************************
c      Surfaces
c **********************************************************************
c
  1   RPP -10.0 10.0 17.0 29.5 -9.0   1.0  $ Adjoint Source - Box 1
  2   RPP -25.0 25.0  0.0 50.0 -25.0 25.0  $ Water box 50.0x50.0x50.0
  3   PY   0                               $ Crossing plane
  4   RPP -10.0 10.0 21.0 28.5   1.0  8.0  $ Adjoint Source - Box 2
  5   RPP -10.0 10.0  3.5 31.0   8.0 15.0  $ Adjoint Source - Box 3
 100  so  200.0                            $ Universe bound


c **********************************************************************
c      Data Cards
c **********************************************************************
c Adjoint source is in cell number 1. The cell is made out of
c parallelepiped with given dimensions. Points are chosen uniformly
c  within the parallelepiped.
c
SDEF  PAR=2  ERG=d1  X=d2  Y=d3  Z=d4  CEL=1
c
c **********************************************************************
c ************  Energy Distribution 2100-6MV  **********************
c ************   Group structure MCNP-MGXSNP   *********************
c **********************************************************************
c
SI1 H 0.000 0.010  0.100  0.500  1.000  2.000  3.000  4.000  5.000
      6.000
SP1 D 0.000000000  3.12689E-10  9.90001E-10  3.00098E-09  5.29621E-09
      7.76637E-09  9.74813E-09  1.15586E-08  1.33190E-08  1.49516E-08
c
c **********************************************************************
c *************** Where to pick starting points ********************
c **********************************************************************
SI2 -10.0 10.0               $ X-range for Adjoint source
SP2   0.0  1.0               $ uniform probability over the X-range
SI3   3.5 31.0               $ Y-range for Adjoint source
SP3   0.0  1.0               $ uniform probability over the Y-range
SI4  -9.0 15.0               $ Z-range for Adjoint source
SP4   0.0  1.0               $ uniform probability over the Z-range
c
c **********************************************************************
c *************** Materials ****************************************
c **********************************************************************
c WATER for gamma-ray transport (by mass fraction)
c **********************************************************************
c
 M1   1000 -0.11190               $ elemental H mass fraction
      8000 -0.88810               $ elemental O mass fraction
c
c **********************************************************************
```

```
c ********************  Problem FMESH4 Tally  **********************
c ********************   Need to have EMESH   **********************
c ******************** to run Adjoint problem **********************
c ****************************************************************
c
FC4 Adjoint-MCNP-MGXSNP - Adjoint Source Brain - made of three boxes
FMESH4:P GEOM=xyz
          ORIGIN=-25 0 -25
          IMESH=25.   IINTS=100
          JMESH=.5    JINTS=1
          KMESH=25.   KINTS=100
          OUT=ik
          EMESH = 6.000
c
c ****************************************************************
c ****************  NJOY Dose Conversion factors    ***************
c ****************  For MCNP-MGXSNP group structure  ***************
c ****************************************************************
c
 E0   0.010  0.100  0.500  1.000  2.000  3.000  4.000  5.000  6.000
 EM0 0.000000  0.007698  0.133707  0.235028  0.303138  0.166534
     0.093532  0.048771  0.011591
c
c ****************************************************************
c PHYS:P EMCPF IDES NOCOH ISPN NODOP
c To turn off electron production and the bremsstrahlung photons
c use IDES=1 default =0 --> thick target bremsstrahlung. To turn
c off coherent scattering NOCOH=1; photo nuclear collision ISPN=0
c Doppler energy broadening NODOP=1
c ****************************************************************
c
CUT:P J 6.000
MODE P
c SSW -3
MGOPT A 12
c PRINT 100 40 110 150 160 161 162
NPS 250000000
PRINT
```

VITA

Mat Mustafa Al-Tamimi was born in Kuwait City, Kuwait to Abdel Jawad and Samira Al-Tamimi. He is the second of six siblings: Aminah, Imad, Rula, Mobin and Tasneem. He attended Jareer Middle School in Kuwait and continued to Abdula Al-Saleem High School in the same city. He came to the United States to pursue higher education. He attended Hillsborough Community College for two year as a pre-engineering major. After completing all the needed pre-engineering credits he attended the University of South Florida in Tampa for one semester. He transferred to New Jersey Institute of Technology in Newark New Jersey and completed a Bachelor degree in Electrical Engineering with concentration in communication in 1991. He returned to school in 1997 to complete graduate studies in Nuclear Engineering. During his studies he worked as a graduate assistant at the University of Tennessee Radiological Safety Office. He earned his Master of Science in Nuclear Engineering with concentration in Radiological Engineering from the University of Tennessee at the end of 1999. He then pursued another graduate degree in the field of Medical Physics at the University of Kentucky at Lexington. He served as a physics tutor in the physics department at the University of Kentucky for two semesters. He also completed a medical physics internship at the Marshfield Clinic in Marshfield Wisconsin. He completed his Medical Physics graduate studies and earned a Master of Science in Radiological Medical Physics from the University of Kentucky in 2001. In 2001 he began to work as a medical physicist working for RadPhys Medical Physics consultant serving primarily Baptist Hospital in Knoxville. In 2014 he received his Doctorate degree from the University of Tennessee Nuclear Engineering Department.